Small angle light scattering apparatus for analysis of single micrometric particles in microfluidic flows

David Dannhauser

Advisor
Paolo A. Netti

FEDERICO II UNIVERSITY OF NAPLES

SMALL ANGLE LIGHT SCATTERING APPARATUS FOR ANALYSIS OF SINGLE MICROMETRIC PARTICLES IN MICROFLUIDIC FLOWS

A THESIS SUBMITTED IN PARTIAL FULFILMENT OF THE REQUIREMENT
FOR THE DEGREE OF DOCTOR OF PHILOSOPHY IN
MATERIALS AND STRUCTURES ENGINEERING

AUTHOR
David Dannhauser

COORDINATOR
Professor Giuseppe Mensitieri

TUTOR
Filippo Causa

ADVISOR
Professor Paolo A. Netti

UNIVERSITÀ DEGLI STUDI DI NAPOLI FEDERICO II

FACOLTÀ DI INGEGNERIA

Dipartimento di Ingegneria Chimica, dei Materiali e della Produzione Industriale D.I.C.MA.P.I

2. April 2013

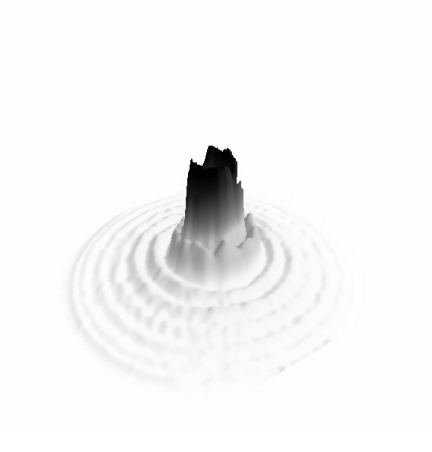

Affidavit

I hereby declare by oath that I have written this paper myself. Any ideas and concepts taken from other sources either directly or indirectly have been referred to as such. The paper has neither in the same nor similar form been handed in to an examination board, nor has it been published.

Place, Date

Signature

Table of Contents

List of Figures

List of Tables

Acknowledgments

I would like to express my deepest gratitude to all who have supported me during this work.

In particular I would like to thank Prof. *Paolo A. Netti* for allowing me to work in his working group.

Without the great support of my wife *Gaia*, all of my research activities wouldn't be possible, therefore I want to especially thank you.

The encouragement, guidance and support, from my tutor *Filippo Causa* and *Giovanni Romeo* enabled me to develop an understanding of the subject. Without there guidance writing this thesis would not have been such a satisfying and successful experience for me.

The discussions and co-operations with all of my colleagues have contributed substantially to this work, particularly those of my working group, *Maurizio Ventre, Carlo Natale, Costantino Casale, Raffaele Vecchione, Daniela Guarnieri, Maria Iannone and Anna Aliberti.*

Finally, I would like to show my gratitude to my *family* and *friends* for their continuous and unconditional support of all my undertakings, scholastic or otherwise.

Abstract

The fast characterization of micrometric particle is becoming of increasing importance. The measurement of shape and the index of refraction of a particle allows very accurate characterization of the analysed material. A CCD-camera based small angle light scattering (SALS) apparatus has been developed to characterize single micrometric particles. The measured scattering vector spans the range 2x10^{-2} - 6.8x10^{1} μm^{-1}. The incident laser light is collimated to a spot of about 50 μm in diameter at the sample position with a divergence lower than 0.045 rad. Such a small collimated laser beam distinguishes this system from previous small angle light scattering instruments described in literature and opens the possibility to perform SALS in quiescent and in-flow conditions in small microfluidic channels. By properly designing the micro-channel and using a viscoelastic liquid as the suspending medium, it is able to realize a precise 3D focusing of the target particles. The forward scattering emitted from the particle is collected by a lens with high numerical aperture. Further, at the focal point of that lens a homemade beam stop blocks the incident light. Finally, a second lens maps the scattered light on the CCD sensor, allowing for the collection of far field images on short distances. Measurements with mono-disperse polystyrene particles, having nominal radii of 0.95, 1.64, 2.08, 2.90, 3.04, and 4.01 μm, both in quiescent and in-flow conditions have been realized. Experiments in-flow conditions allow the measurement of the single particle scattering profile. Results are validated by comparison with calculations based on the Lorenz-Mie theory. Measurements of real multiplexed particle solutions, with particles down to 1 μm in radius confirmed the possibility to use this SALS apparatus. Moreover, initial analyses of microgel particle structures in quiescent conditions over time have been carried out. This analysis can be extended for more complex systems, like multi-shell, or non spherical particles in terms of single particle characterization.

Chapter 1

INTRODUCTION

This study is focused on the development of a novel small angle light scattering (SALS) apparatus, which is able to characterize single micrometric particles in micro-channel flows. The detectable wave number range thereby has to be greater than established spans for SALS instruments in literature and the detection stage has to be able to detect size changes in the sub-micrometric range. The main attention is given to demonstrate the feasibility to characterize precisely single particles in microfluidic flows.

To reach this target, the use of light scattering patterns to characterize flowing particles is chosen. Such patterns gives the by far most complete optical characterization of micrometric particle. Therefore, light scattering is one of the most powerful tools to validate micrometric particle nowadays. The first measurements of single micrometric particles was published by *Gucker* and *Egan* in 1961. Above all others *Gucker et al.* measured the intensity of a single spheres of dioctyl phthalate at different scattering angles. [18] Whereby, the scattering of a homogenous sphere has already been mathematically understood more then 100 years before by *Alfred Clebsch.* [12] In fact the solution of the scattering problem in its modern form, was first published by *Ludvig Lorenz* in 1890, but is nowadays mainly known by the later publication from *Gustav Mie* as the Mie scattering solution. Thereby the Lorenz-Mie scattering solution for a single micrometric particle refers to an ideal spherical and dielectrically homogenous particle. [31] The scattering pattern of such a particle refers directly to the particle radius, refractive index and absorption coefficient. [60]

The first Lorenz-Mie scattering measurements of micrometric polystyrene latex (PSL) particles was published by *Philips et al.* nearly 10 years after *Gucker.* Since that time, PSL particles are used as standards for a wide range of light scattering applications. [45]

The simplest application of single particle scattering is the counting and sizing at a fixed scattering angle. For this purpose gas suspended particles flowing through a small illuminated aperture one at a time. The collection of

the resulting light flashes provides information about the density and size of particles. [7] A fundamental problem hereby is the inaccuracy of the system by unknown refractive index of the target particle.
Indeed, there are nowadays several well established and routinely used light scattering setups for the classification of micrometric particles, which are divided in static light scattering (SLS) products [43] and dynamic light scattering (DLS) ones [2, 15, 6]. The most direct and effective approach to improve such light scattering system is the use of a multi-element sensor, such as the pixel array of a charged coupled device (CCD) camera, to collect the signal from many different scattering angles simultaneously. [11, 59]
In fact, there is a rapid development on SALS techniques in the last years, which is essentially related to the progress in the CCD sensor technology. [51] Modern SALS devices can typically cover a range of scattering vectors going from $2x10^{-2}$ to $2x10^{1}\mu m^{-1}$ which corresponds to 0.1° until 10° for the visible wavelengths of light. [51]
However, a SALS apparatus of *Norman et al.* has recently shown the formation and subsequent size distribution of multilamellar vescicles of diblock copolymers in a flow stream. [42] Also *Quirantes* and co-workers showed the applicability of SLS with spherical core shell particles as a tool for particle sizing. [49] Beside, the paper of *Karlsson et al.* is a good reference for the use of a simulation algorithm for SLS at non-spherical particle. His group simulates the scattering of blood cells with different simulation algorithm and compared the out coming results. [27] Another attempt is going in the direction of three-zone annular filters. Each annular ring on the sensor area corresponds to a specific angle of scattered light. [35, 64] Moreover, a big variety of techniques for the focusing and collecting of scattered light is present in literature. [33] Unfortunately, due to the difficulty in focusing a laser beam in a micro-channel, with diameters smaller than 100 μm, the implementation of SALS as detection tool in microfluidic devices has been limited until now. [47]
Indeed, the SALS apparatus described in this PhD thesis overcome that issue and is able to analyse single particle flowing in a micrometric channel. For instance, the use of a optical spatial filter for a so called cleaning and shrinking of the incident beam is therefore assistant. [5, 44] Unrewarding a spatial filter is not obligatory necessary to use in such a setup. The use of a spatial filter depends mainly on the quality, intensity and of course the diameter of the used incident beam. However, the spatial filter has a quite simple principle, which gets very tricky when one try to use it at the border of optical laws. Diffraction in particular is the main criteria, which one has to have in his mind for the proper working of a focused beam spot. [24, 39, 52, 41] The Fresnel and Fraunhofer diffraction are therefore necessary to be understood and minded. [21, 40, 38] Detailed description here fore can be looked up in chapter 2.
Too cut the matter short, in general the smaller, one focus a beam diameter,

the bigger is the divergence of the outgoing beam which results out of optical laws. [8] Therefore the use of pinholes or pinhole arrays is widely common. [61] But not only the beam diameter is a crucial factor, also the illumination of a lens or pinhole has to be uniform to ensure a small spot diameter at the target plane of the apparatus. [26] Pinhole optics is generally easy to handle, but also has their limits one should be aware. [5, 65, 46] Nonetheless, the correct illumination of a lens also the use of the best fitting lens material and shape is from particular importance and can reduce aberration, coma and several other optical effects. Therefore, it should be mention the use of achromatic doublet lenses instant of normal plano-convex lenses, helps significantly to reduce the spot size. [53] Furthermore, as much similar the refractive indices between particle and surrounding medium, as smaller is the scattered light intensity and of course conversely. [16]

Without the use of a beam stop, all the incident light is transmitted directly on the sensor and thereby reduce the overall sensitivity or even destroy the sensor of the camera. It is quite difficult to find proper information about the application of beam stop in this field of research, but some of the papers which roughly describe a beam stop were found in the literature. [58, 25, 17, 29, 30] For such reason a self designed beam stop is developed. In fact, a beam which has a small beam diameter and also a quite small divergence is needed. To do so, the finding of the optimal correlation between spot size and numerical aperture of the laser beam has to be found. Therefore several optical simulation programs exists, which can help to calculate the best arrangement between optical lens diameter, focal length, numerical aperture and spot size. There are some papers in the literature that mention this problem, but no golden rule to calculate the necessary optical parameters in a proper way exists at the moment. Often microscope objectives are implemented to minimize the spot size of a laser beam with a resulting large divergence, which makes this approach not viable for the target of this work. [48, 14, 34]

Surprisingly, a theoretical and experimental investigation of the factors affecting the beam waist size at the focal point is reported recently. [8] For instance, is shown in literature that by optimizing the layout of the optical path of the laser, the beam waist at the focal point can be as small as few micrometers. Based on this result, focusing a laser beam within a micrometric channel should therefore be possible, thus benefit the system to perform in-flow single particle detection using the SALS technique.

However, the best light scattering setup will not work precise, if the target particles do not pass the centre of the laser beam. Therefore the focusing of the target particle in the middle of the incident light at a defined hight in the apparatus is crucial for detailed analyses of the scattering pattern.

In fact, by the use of viscoelastic liquids as suspending medium, *D'Avino* and co-workers showed the ability to determine particle migration towards the centre of a cylindrical tube and hence realize a precise 3D focusing of tar-

get particle. [13] The apporach from D'Avino has a by far easier production geometry compared to other published 3D focusing techniques in literature. [63, 9, 55, 32]
In the following chapters will be summarized the theory behind light scattering with main focus on the Lorenz-Mie theory. Further the precise explanation of the developed SALS apparatus with essential theory behind is outlined. Moreover, the calibration of the system as well as the first results in quiescent and in-flow are shown in this study. Future aspects and technical limitations concerning the SALS apparatus conclude this work in the end.

Chapter 2

THEORY of LIGHT SCATTERING

2.1 Definition

Light is defined as visible electromagnetic radiation, with a wavelength λ ranging from $\sim$400 (violet) to $\sim$750 nm (red) and a frequency f between 8×10^4 and 4×10^{14} Hz. Moreover is this wavelength band only an extremely narrow portion of the electromagnetic spectrum, which covers a range greater than 10^{20}. The ratio of velocity of light $c = f\lambda$ in vacuum (3.0×10^8 m/sec) to the velocity of light in a particular material V_p is the so called ***index of refraction*** m of a material. This index varies slightly with used wavelength (see equation 2.7). For non-absorbing materials, the *index of refraction* m is given by:

$$m = \frac{c}{V_p}, \tag{2.1}$$

which is described, as the absolute index of refraction and is always greater than 1. Though, for absorbing materials (having appreciable electrical conductivity) is expressed as a *complex index of refraction* and given by the following equation:

$$m = n_r + i\kappa, \tag{2.2}$$

where n_r is the real part and κ the imaginary part of the index of refraction. The imaginary part is related to the absorption of a particle. Indeed, is the imaginary part equal to zero for non-absorbing particles. It is noted that the value of κ is never exactly zero for any material, though particles with a value approaching zero are termed non-absorbing. The commonly used *absorption coefficient* A of a material is related to the complex part of the index of refraction with the following relation:

$$A = \frac{4\pi k}{\lambda}. \tag{2.3}$$

Moreover, for particles in a two-phase system, a *relative index of refraction* m_r is used, which is defined as the ratio of the velocity of light in ambient medium V_m to the velocity in a particle V_p:

$$m_r = \frac{V_m}{V_p} = \frac{m_p}{m_m}. \tag{2.4}$$

However, the refractive index of air is practically equal to the one of vacuum. Particles suspended in liquids have an index of refraction greater or lower than 1. For instance, by light scattering measurements in liquid the avoiding of air bubbles is fundamental to measure correct particle sizes, since each air bubble increase immediately the light intensity on the detector of the system. [23]

2.2 Scattering by small particles

Scattering is observed, when light interacts with the electrons bound in the particle. In fact, when a light beam illuminates a particle having a dielectric constant different from 1, light will be absorbed or scattered, or even both, depending on the wavelength of light and the optical properties of the particle. The general scattering behaviour of a particle in vacuum or ambient medium illustrate figure 2.1, where a sphere scatters in all directions.

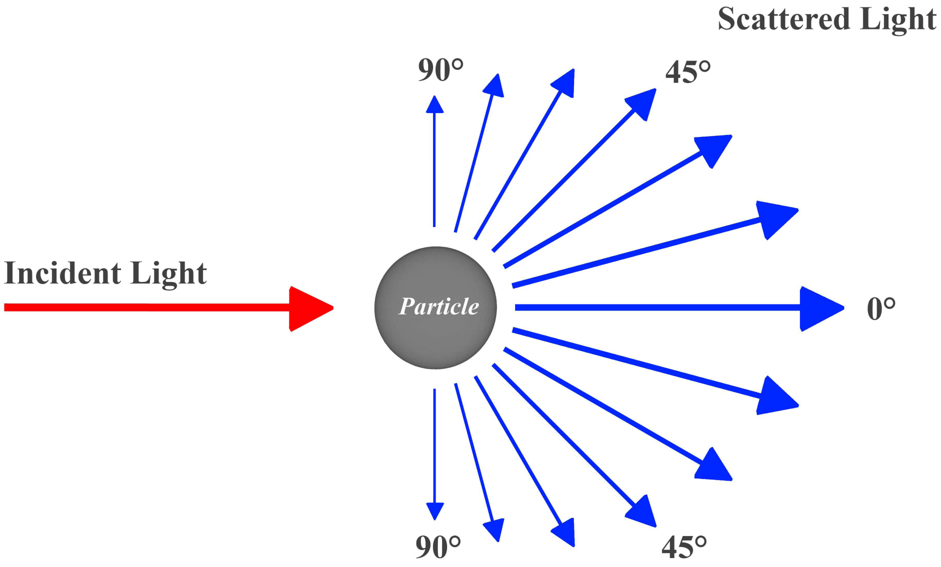

Figure 2.1: Scattering of incident light by a particle in vacuum or ambient medium.

Depending on whether the frequency of scattered light to be detected is the same as that of the incident light, a light scattering experiment is described by elastic *(ELS)*, quasi-elastic *(QELS)*, or inelastic light scattering *(IELS)*. The majority of light scattered by a particle is emitted at the identical frequency of the incident light, a process which is referred to ELS. In this context only the ELS is from importance, where the scattering signal to be detected is the time-averaged light intensity. [62]
The net result of the absorption and scattered caused by the particle is known as the *extinction* of the incident light which is given by:

$$Extinction = Absorption + Scattering. \tag{2.5}$$

The schematic figure 2.1 of a scattering sphere is showing only the forward- and side-scattering rays of light. The here fore used definition is done by the scattering angle θ, which is measured from the direction fo the incident beam to the scattered beam. Light that deviates only slightly from its incident direction has a small scattering angle and is said to be forward-scattering ($\theta = 0°$). Back-scattering ($\theta = 180°$) which would go back in the direction of the incident light is not shown in figure 2.1, and also negligible for the calculations. Side-scattering ($\theta = 90°$) is mentioned to be light reflected perpendicular to the incident beam. [23]

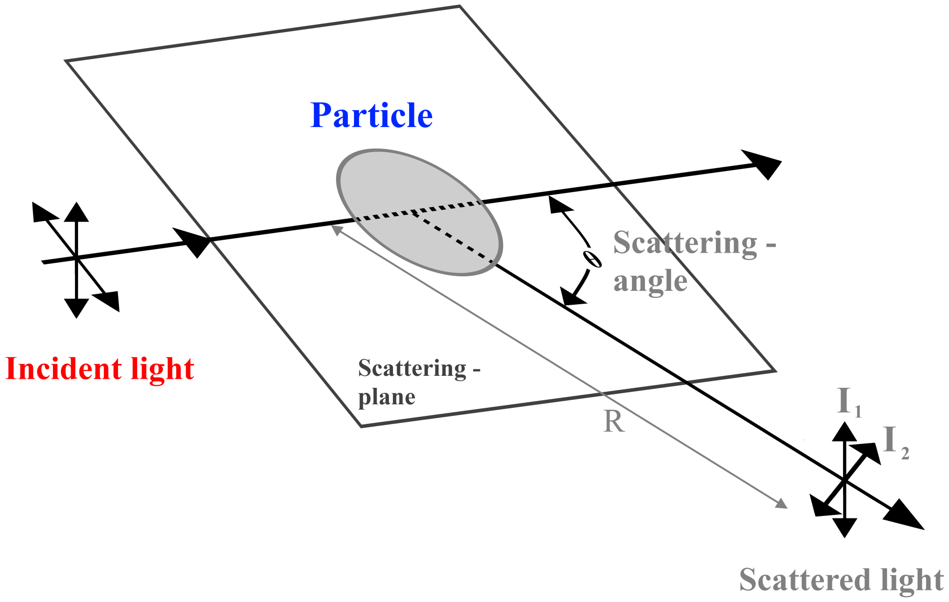

Figure 2.2: Diagram showing scattering angle θ, scattering plane, distance between particle and observation point R, and the polarization components of scattered light.

In fact, the absorbed incident light is transferred through thermal degradation or lost through a radiative decay producing fluorescence depending on the electronic structure of the material. Indeed, many particle exhibit strong absorption in the infrared and ultraviolet regions of light, which strongly reduces the scattering intensity. Therefore, the most light scattering measurements are performed by using visible wavelengths of light. [62]
Moreover, the intensity of the scattered light, depends on the polarizability of the sphere. The polarizability on his side depends on the molecular weight of a sphere. Beside the molecular weight, light scattering also has a direct dependence on the particle size. The figure 2.2 illustrate the plane formed by the incident beam and the direction of observation (scattered beam), which is called the scattering plane. [23]
In almost all light scattering experiments, a collimated light source at a distance much larger than the dimension of the particles, is used to illuminate the sample. Therefore, the scattering intensity is detected at a far field (the distance R, between the detector and particle is much larger than the dimension of the particle) [62]
There are several light scattering theories to describe the scattering patterns of particles in literature.

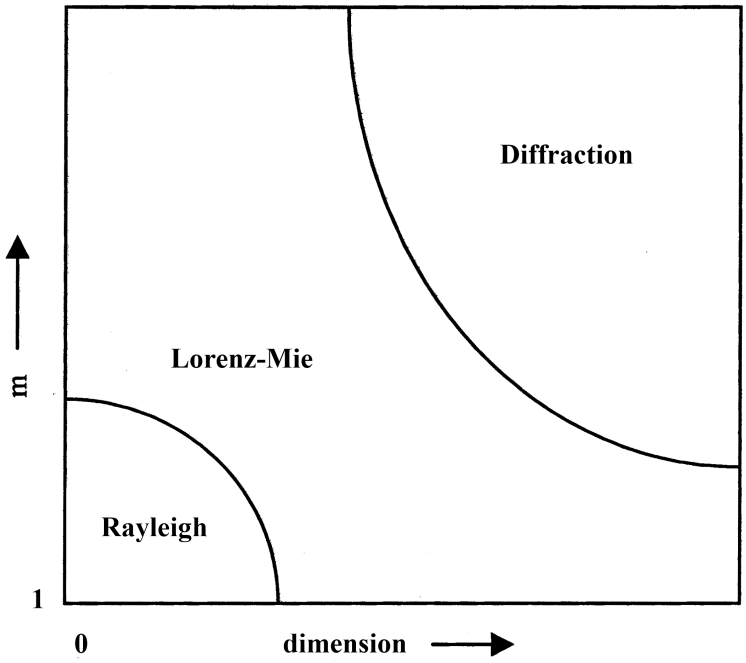

Figure 2.3: The diagram show an overview of the scattering theories mentioned in this chapter according to there application ranges. [62]

The most known theoretical frameworks therefore are the *Rayleigh theory*, *Lorenz-Mie theory* and *Geometrical optic theory.* The geometrical optic theory is only valid for particles, which are much larger then the wavelength of light. The diffraction of pinholes is described by the geometric optic scattering theory, which is from significant interest for the alignment procedure of a light scattering apparatus. More informations therefore, are shown in section 2.5.

2.3 Rayleigh theory

The classical light scattering theory also called Rayleigh theory was derived by *Lord Rayleigh* and applies only to small non-absorbing particle. Small in this context means, particle sizes small compared to the wavelength of used light. As a rule of thumb, for particle diameters smaller then 0.05 μm the Rayleigh scattering theory should be used. For bigger particle sizes the more complex Lorenz-Mie theory is utilised. Indeed, scattering of light is in each case governed by the ratio of the particle size to λ of the radiation. Therefore, this ratio which is called (dimensionless) *size parameter* x is given by:

$$x = k \cdot a = \frac{2\pi m_m a}{\lambda}, \tag{2.6}$$

where $k = 2\pi/\lambda$ is the ***wave-number*** and m_m the index of refraction for the ambient medium. Furthermore is the factor π used to simplify the light scattering equations, by making x equal to the ratio of the circumference of the particle to the wavelength. [19] The term a express the particle radius. Moreover, is the *relative scattering wavelength* λ defined as:

$$\lambda = \frac{\lambda_0}{m_m}, \tag{2.7}$$

where λ_0 is the already mentioned vacuum wavelength. In fact, by using this relationship the scattered light gets depending on the incident wavelength used in a light scattering setup. [19]
However, for small particles the instantaneous electromagnetic field of the incident filed of the incident light is uniform over the entire particle, creating a dipole that oscillates in synchronization with the energy in all directions. (see figure 2.4)

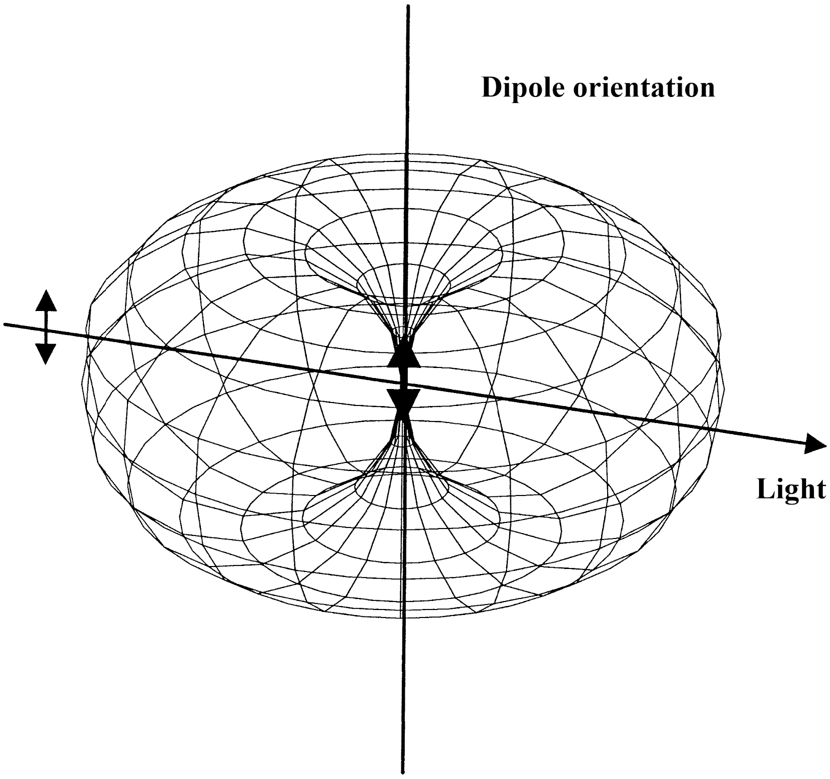

Figure 2.4: Scattering form a dipole. [62]

The intensity and scattering pattern therefore are known as ***Rayleigh scattering*** I_θ and for un-polarized illumination given by:

$$I_\theta = \frac{I_0 \pi^4 d^6}{8R^2\lambda^4}\left[\frac{m^2-1}{m^2+2}\right]^2 (1+\cos^2\theta), \tag{2.8}$$

where I_0 is the incident light intensity. Moreover formula 2.8 indicates that the intensity of the scattered light at any angle is proportional to the factor d^6/λ^4. In fact the Rayleigh scattering is therefore strongly dependent on the particle volume squared and as a result independent to the particle shape. [23]

Indeed, for the particle shape independence of the Rayleigh scattering theory, the use of the more complex Lorenz-Mie theory has to be taken under consideration. The following section is summarizing the main formulas of that complex particle scattering theory.

2.4 Lorenz-Mie theory

The Lorenz-Mie scattering theory has no size limitations and converges to the limit of geometric optics for large particles. Moreover, it also may used for describing most spherical particle scattering systems, including Rayleigh scattering. [19]

Indeed, the understanding of the Lorenz-Mie theory is not an easy task and the derivation of the equations is somewhat elaborate. By considering a plane electromagnetic wave in vacuum with a wavelength λ, incident on a sphere of radius a with a complex refractive index m. The interaction of this wave with the sphere causes the sphere to radiate electromagnetic waves of itself. These waves are not isotropic in general. By expanding this outgoing wave using vector spherical harmonics. The idea is the same as for expanding a scalar field in spherical harmonics, but now for a vector field. Like with spherical harmonics, this involves Legendre polynomials and Bessel functions. The expansion coefficients are written as a_n and b_n, where n is the expansion index going from $n = 1$ to $n \to \infty$. These a_n and b_n (the outgoing wave) are called the scattering coefficients. [3]

However, it is an analytical solution of the **Maxwell vector wave equations**[1] for the scattering of electromagnetic radiation by spherical particles. The theory is a solution for the scattering from a spherical, homogeneous, isotropic and non-magnetic particle of any radius in a non-absorbing medium. The Mie equations become increasingly complicated for particles with a size greater than the wavelength of light used for the scattering. [4]

Because of difficulties in preparing stable dispersions with a sufficiently narrow size distribution, it needed nearly 40 years after the publication of the Mie paper published by *Gustav Mie*, for measuring high-resolution wavelength spectra of light attenuation. It was also the fast improvement in the computing power due to the advent of computers, that made possible the prediction and subsequent verification of some consequences of the Lorenz-Mie theory, such as the existence of optical resonances, only 70 years after the theory was published. [54]

In short, the solution of the Maxwell vector wave equations (Second-order partial differential equation that describes the propagation of electromagnetic waves through a medium or in a vacuum. [1]) in the Lorenz-Mie theory is obtained as follows.

The incident plane vector wave and the scattered spherical wave are expressed in spherical coordinates, which entails expansion of the waves into infinite series of vector spherical harmonics. The expansion coefficients of the scattered wave series are determined from the boundary conditions linking the electric and magnetic fields of the incident and scattered waves at

---

[1] The Maxwell equations for the macroscopic electromagnetic field, which describe the electric field, magnetic induction, electric displacement and magnetic field of matter are used to define how the fields vary in space due to the sources. [4]

the sphere boundary. This leads to the scattering matrix, a function of the scattering angle, for the sphere. Therefore, relates the incident and scattered **Stokes parameters**[2]. By using the non zero terms of the matrix, it is possible to calculate the scattering intensities for polarized (parallel or perpendicular) and un-polarized incident light. [4]
However, to calculate the scattering intensity, the complex scattering amplitudes S_1 and S_2 have to be expressed by implying the scattering coefficients a_n and b_n. The coefficients inside the sphere (c_n and d_n) are hereby from no interest and not considered. For further informations about the internal coefficients the reader is referred to the textbook of *Craig F. Bohren and Donald R. Huffman* entitled, Absorption and Scattering of Light by Small Particles. [4]
For knowing how the various observable quantities vary with the size and optical properties of the sphere and the nature of the surrounding medium, the explicit expressions for the scattering coefficients a_n and b_n has to be expressed. This *scattering coefficients* a_n and b_n are described by the scattering field of a spherical sphere like:

$$a_n = \frac{\mu m^2 j_n(mx)[xj_n(x)]' - \mu_1 j_n(x)[mxj_n(mx)]'}{\mu m^2 j_n(mx)[xh_n^{(1)}(x)]' - \mu_1 h_n^{(1)}(x)[mxj_n(mx)]'}, \tag{2.9}$$

$$b_n = \frac{\mu_1 j_n(mx)[xj_n(x)]' - \mu j_n(x)[mxj_n(mx)]'}{\mu_1 j_n(mx)[xh_n^{(1)}(x)]' - \mu h_n^{(1)}(x)[mxj_n(mx)]'}, \tag{2.10}$$

with the already mentioned size parameter x and the relative refractive index m. Furthermore, μ is the magnetic permeability of the medium and μ_1 of the sphere. The function $j_n(z)$ and $h_n^{(1)} = j_n(z) + iy_n(z)$ (Spherical Hankel function of first kind) are Bessel functions of first order with $n = 1$ and of the given arguments, $z = x$ or mx, respectively. Primes in this context, mean derivatives with respect to the argument.
Moreover the functions $\pi_n(\cos\theta)$ and $\tau_n(\cos\theta)$ describe the angular scattering patterns of the spherical harmonics and so forth describe the complex scattering amplitudes S_1 and S_2. The *angular scattering functions* $\pi_n(\cos\theta)$ and $\tau_n(\cos\theta)$ expressed in terms of Legendre polynomials are:

$$\pi_n = \frac{2n-1}{n-1}\cos\theta\ \pi_{n-1} - \frac{n}{n-1}\pi_{n-2}, \tag{2.11}$$

$$\tau_n = n\cos\theta\ \tau_n - (n+1)\tau_{n-1}. \tag{2.12}$$

---

[2] The stokes parameters are a set of values that describe the polarization state of electromagnetic radiation, in terms of its total intensity, degree of polarization, and shape parameters. [4]

Accordingly, the complex *scattering amplitudes* S_1 and S_2, which describe scattering patterns of the target particle are hereby given by the equations:

$$S_1(\cos\theta) = \sum_{n=1}^{\infty} \frac{2n+1}{n(n+1)}(a_n\pi_n + b_n\tau_n), \tag{2.13}$$

$$S_2(\cos\theta) = \sum_{n=1}^{\infty} \frac{2n+1}{n(n+1)}(a_n\tau_n + b_n\pi_n). \tag{2.14}$$

By summing the both amplitudes, it is possible to calculate the ***Lorenz-Mie scattering intensity*** I_θ for a *un-polarized incident* light with the following equation:

$$I_\theta = \frac{I_0(|S_1|^2 + |S_2|^2)}{2k^2R^2}, \tag{2.15}$$

where R is the distance from the target plane to the sensor of a light scattering apparatus and I_0 the corresponding incident light. The equations for polarized light are not mentioned in this work. For more profound information and in this context not mentioned formulas about the Lorenz-Mie theory, the reader is invited to take a look in the textbook published by *Craig F. Bohren and Donald R. Huffman* entitled, Absorption and Scattering of Light by Small Particles. [4]
For better understand how such a scattering of a particle according to the Lorenz-Mie theory could look like. Figure 2.5, illustrate the radial plot of the scattering profile from a latex particle with radius 2 μm. The forward scattering lobe has a significant higher intensity compared to the rest of the scattering pattern. It can be proved that the spatial distribution is not randomly.
It is obviously, that this particle has significant minima and maxima in the wave-vector range from 0° to 45°. The position of this peaks are depending on all factors previously mention. Therefore demonstrate figure 2.5 impressive the scattering behaviour of a PSL particle.
However, for the alignment of the SALS apparatus the use of the Fraunhofer diffraction has to be understood. Therefore the following section will give a brief overview about this scattering theory.

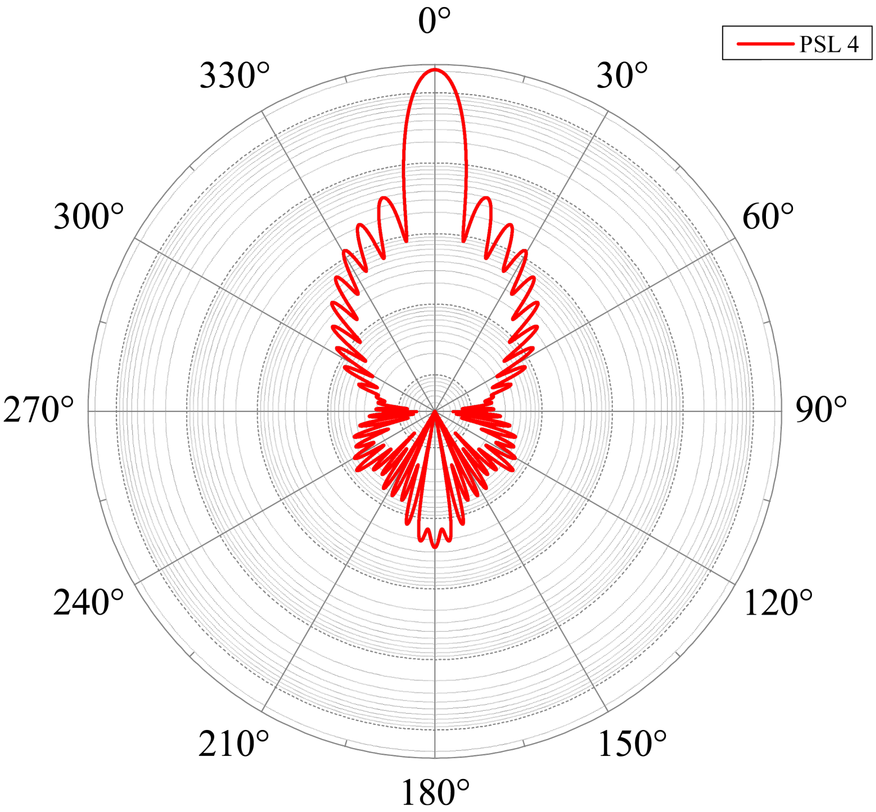

Figure 2.5: The polar plot of a PSL particle with radius 2 μm is plotted. 0° is the forward direction of the incident light.

2.5 Fraunhofer diffraction

Diffraction in general is defined by small deviation from ray propagation, according to the theory of geometric optics. [4] In general, the geometrical optics is considered to be a good approximation if all dimensions are much larger than the wavelength.

Deviation occurs if an obstacle or angular aperture, is placed in the incident beam and the scattering angle is assumed to be small. At very large distances a certain angular intensity distribution rise by the **Huygens principle**[3] and is named, the Fraunhofer diffraction pattern. The intensity distribution depends only on the form and size of the angular aperture or slit and is independent of its composition. Indeed, the diffraction pattern is independent on

---

[3] The Huygens principle is a method of analysis applied to problems of wave propagation both in the far- as also in the near-field of diffraction. [4]

the polarization of the incident light. This limitation overcomes the already mentioned Lorenz-Mie scattering theory. [56]
However, for a constant scattering angle θ the intensity I_θ of the so called **airy disk**[4], which is also named airy diffraction pattern is given as subsequent:

$$I_\theta = I_0 \left[\frac{2J_1(ka\sin(\theta)}{ka\sin(\theta)}\right]^2, \tag{2.16}$$

where J_1 presents the **Bessel function of zero order**[5], k the already mentioned wave-number and a the radius of the pinhole. [22]

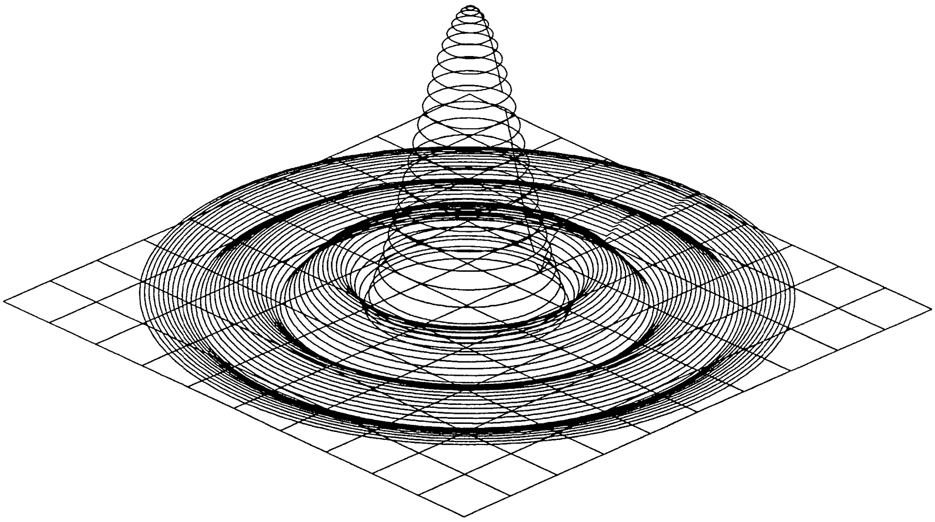

Figure 2.6: The theoretical diffraction pattern (absolute electromagnetic field distribution) of a circular disk for the azimuthal angle ranging from 0° to 360° and scattering angle spanning from 0° to 3.5°. [62]

The resulting intensity distribution is consisting of a central maximum and dark and bright rings. The bright region in the centre, is known as the airy disk which together with the series of concentric bright rings around is called the Airy pattern. The *first dark ring* u is calculated to be at:

$$u = \frac{2\pi a \sin\theta}{\lambda} = 3.83 \tag{2.17}$$

However, the intensity distribution for a pinhole with radius of 5 μm calcu-

---

[4] The airy disk is named after an English mathematician and astronomer, *George Biddell Airy.* [31]

[5] The Bessel function of zero order is a solutions of Bessel's differential equation. [4]

lated with the Fraunhofer diffraction theory is illustrated in figure 2.7. The first minima in figure 2.7 is according to the formula 2.17 at an angle of 4.42°.

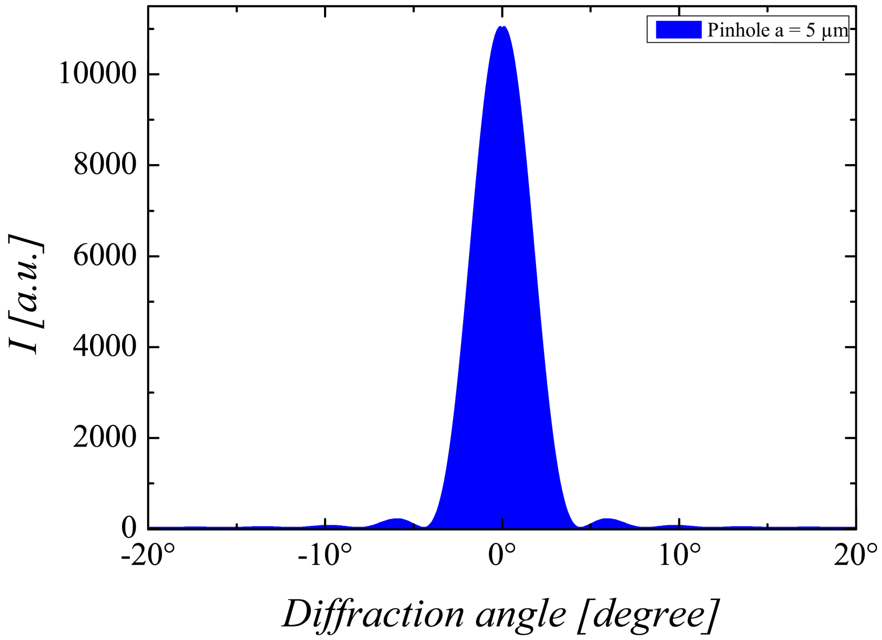

Figure 2.7: Diffraction pattern of a pinhole with radius of 5 μm.

The simple calculation of the diffraction pattern enables the use as fitting parameter. The chapter 4 is going in detail about the implementation of such a fitting procedure for the calibration of the SALS apparatus.

Chapter 3

EXPERIMENTAL SETUP

3.1 Introduction

The accuracy of a light scattering apparatus is mainly limited due to physical limitations in optics. Moreover reduce apparatus factors like stray light, instrument noise or lens aberration the efficiency of a system. The main focus during the development of a new SALS apparatus, is the minimization of this factors. In fact, there are several possibilities to built a SALS apparatus in literature (see in chapter 1).

The apparatus should be able to measure particle radii in the range from 1 up to 4 μm in quiescent and in-flow conditions by collecting the scattering angle up to 35 degree for each particle. An accuracy of ± 50 nm for the particle radius and ± 0.01 for the real part of the index of refraction is required. According to the specifications needed, the development of a new apparatus is necessary. For precise planning of the necessary auxiliary parts a 3D-CAD program is used. This commercial software named ***Solidworks***[1] is a very useful tool to plan the overall size and to predict overlapping of possible mechanical parts from the apparatus. Optical parts necessary to build up the system, are mainly from this two suppliers: ***Edmund Optics***[2] and ***Thorlabs***[3].

Beside mechanical simulation also optical simulation are from relevant interest for the proper working of the system. The here fore used software is named ***Zemax***[4]. This commercial software is specialist to simulate the trajectory of optical rays according to the used lenses. Indeed, the exact lens specifications are mandatory.

However, with the use of this optical and mechanical simulation software it is possible to chose the best fitting optical and mechanical parts for the SALS

---

[1] Dassault Systèmes SolidWorks Corporation, Waltham (MA), USA

[2] Edmund Optics Incorporated, Barrington (NJ), USA

[3] Thorlabs Incorporated, Newton (NJ), USA

[4] Radiant Zemax LLC, Redmond (WA), USA

apparatus. A list of all components used for building up the here elaborated SALS apparatus can be read in the appendix A (see table A.2) of this work. In any way, the developed apparatus is divided in different parts. The light source with beam expander is generating the incident beam of the apparatus. Followed by the optical focusing part, which includes the focusing of the incident beam in an optical fibre as well as the collimation of the out coming beam. Further the microfluidic focusing used for in-flow measurements of target particles in a homemade microfluidic device and the a rectangular glass capillary for quiescent conditions is mention in one part of this chapter. The most complex stage of the apparatus is the collecting part, where the scattered light of the target particle is collected and mapped on the detector. The data processing and analysis is mention in chapter 4.
Before each specific part of the SALS apparatus is explained in detail, a short overview should picture out the functionality of the new SALS apparatus (shown in figure 3.1).

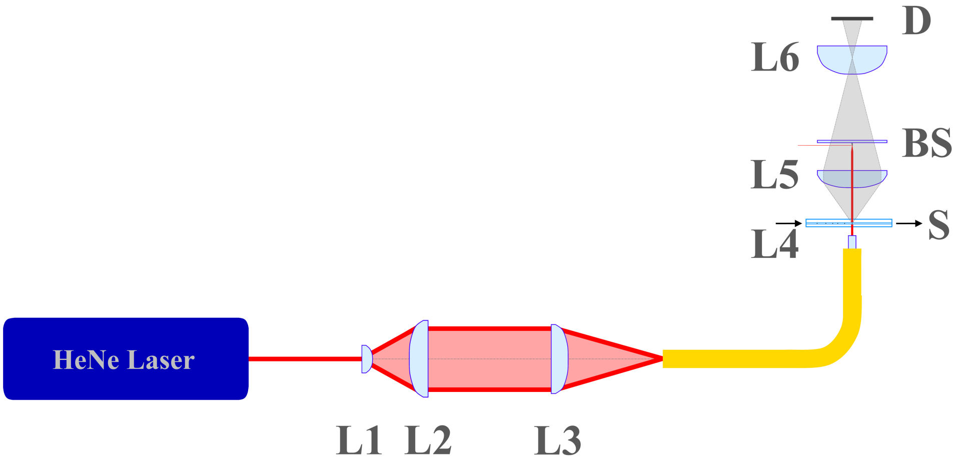

Figure 3.1: Schematic diagram of the experimental setup. *L1* & *L2* are lenses of the beam expander, while *L3* is focusing the incident laser light in an optical fibre. *L4* indicates the collimation lens at the end of the optical fibre. *S* show the position of the target sample. *L5* & *L6* are the lenses of the collimation stage, which collect and map the scattered laser light on the detector *D*. *BS* indicates the homemade beam stop, which blocks the incident light.

The novel SALS apparatus uses a HeNe laser source, which gets magnified by 20 times with a commercial beam expander. The expanded beam is focused in an optical fibre by an achromatic lens. The laser light is afterwards collimated to a small beam diameter, before it passes the microfluidic device, where the target particle is passing the incident beam. The scattered light coming from the target particle is collected by a series of lenses. In between this lenses a homemade beam stop is blocking the incident light. All the not blocked scattered light in with a certain wave-vector range is mapped on the sensor of a cooled CCD-camera by the last lens of the collimation stage. Finally, the collected data is recorded by a program and post-preceded with a homemade ***Matlab***[5] routine.

The scattering vector for the here expressed SALS apparatus spans from $2x10^{-2}$ up to $6.8x10^{1}\mu m^{-1}$, corresponding to scattering angles of 0.1° unitl 31°.

3.2 Optical focusing & collimation

3.2.1 Incident beam

The schematic figure 3.2 represent the parts involved in the incident beam part of the SALS apparatus, which are the incident laser source followed by a beam expander.

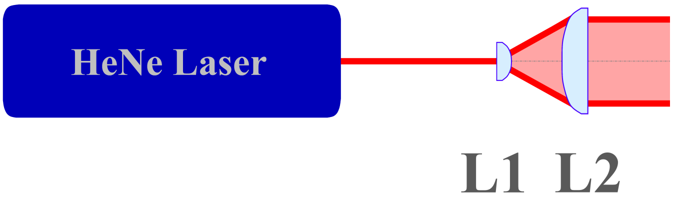

Figure 3.2: Schematic diagram of the incident light source and the used beam expander.

The referring light source *(MELLES GRIOT - 05LHP151)* for the SALS apparatus, is a 5 mW linear polarized (500:1) HeNe laser, operating at a wavelength of 632.8 nm with a beam waist diameter $1/e^2 = 0.80$ mm and full angle divergence $2\alpha = 1.00$ mrad. This kind of laser source is widely used for setting up light scattering instruments and principle research activities. The HeNe laser is known for its TEM00[6] specification, which is crucial for a precise focusing of light. Additionally it has to be known that a HeNe laser, consists of a Gaussian intensity profile.

The diameter of the beam is characterized as a circular region having a radius twice the standard deviation (2σ). Most of the light power is within

---

[5] The MathWorks Inc., Natick (MA), USA

[6] TEM modes (Transverse Electro Magnetic) neither electric nor magnetic field in the direction of propagation. [4]

this region and the intensity at the radius 2σ from the centre falls off to 0.135 of the maximum intensity. Indeed therefore it is important to use a homogeneous beam intensity profile for the incident laser beam of the apparatus and to reduce the beam divergence to a minimum. [62] The laser source is attached on a working desk *(MELLES GRIOT - 07OBH509)*, with a special laser holder for alignment and fixation *(THORLABS - C1502/M)*. The output of the laser is directly aligned in a beam expander *(L1, L2 - EDMUND OPTICS - NT55-579)* which enlarges the beam waist 20 times. This expander is connected to an adjustable kinetic mount *(EDMUND OPTICS - NT58-872)* for precise alignment.

An alignment collinear to the incident beam vertical and horizontal has to be preciously realized for the beam expander. With a small misalignment of the expander the intensity of the incident laser will be unevenly, which afterwards results in problems for the following stages.

A series of mirrors *(THORLABS - KM200-E02)* manage the adjustment of the expanded laser light in all terms of degree of freedom, before a lens focuses the beam in the optical fibre. Indeed, with the use of two mirrors, the incident light coming from the beam expander is redirected in such a way, that it passes perfectly in the centre of the focusing lens of the optical fibre. A misalignment of one of the mirrors ends up from a lower intensity in the optical fibre until diffraction of the Gaussian beam.

It is necessary to say that the second mirror is mounted on a XY-stage *(THORLABS - DT12XY/M)* for a better and more precise alignment of the laser beam. In fact, the bigger someone expand a laser beam the smaller afterwards the beam can be focused. By knowing this simple optical rule and the specifications of the optical fibre, calculations showed that a magnification of 20 times bring the best arrangement for the focusing in an optical fibre. But not only is this optical rule crucial, furthermore the light which should be focused by a lens should illuminated around 66% of the lens diameter to minimize the effect of spherical aberration. [8]

The use of mounting posts with pedestal base adapter from the P-series of *Thorlabs* in the size of one inch as well as half an inch for the connection to the working desk are not explicit mentioned in this work.

3.2.2 Optical focusing

The optical focusing and collimation part of the SALS apparatus is schematically shown in figure 3.3, where the focusing lens *L3* followed by the optical fibre is illustrated. At the output of the optical fibre the lens *L4* is placed, which collimate the incident beam to the smallest possible beam diameter and divergence at the target particle plane.

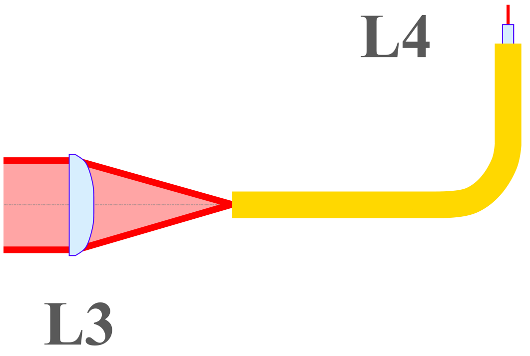

Figure 3.3: Schematic diagram of the optical focusing and collimation part. *L3* represent the focusing lens, while in yellow the optical fibre is indicated. Moreover, illustrate *L4* the collimation of the incident laser beam at the optical fibre outcome.

According to preliminary simulations, the use of an achromatic lens *(L3 - EDMUND OPTICS - NT47-712-INK)* with a given focal length of 125 mm and a diameter of 18 mm achieve the best focusing results. An achromatic lens has the enormous advantage that aberration of light is strongly minimized. Moreover use this special kind of lens black inked edges, which additionally reduce reflections in the lens itself and therefore the overall noise of the SALS apparatus. Furthermore has to be mention that in front of the focusing lens an iris diaphragm *(THORLABS - SM1D12)* is placed (not shown in figure 3.3) which let pass a certain beam diameter of maximum 12 mm. The diffraction generated by the diaphragm itself, is negligible small and can be ignored.

The previous mentioned rule of minimal 66% of an optical lens to reduce spherical aberration is completely fulfilled in this case. Additionally is the intensity of light very high and homogeneous, due to the fact of Gaussian intensity distribution of the expanded incident light. In fact the cut part of light has a significant lower intensity compared with the passing one. In addition to the diaphragm is an absorptive neutral density filter *(THORLABS - NE10B)* placed before *L*3 (not shown in figure 3.3). This filter has an optical density of 1, which is used to reduce the laser intensity of the overall system. Indeed without this filter a too high light intensity would be focused, which can result in damages at the optical fibre as well as too high intensity levels at the sensor of the CCD-camera.

Beside, a Z-stage *(THORLABS - SM1Z)* is used for the fine adjustment of the distance among the optical single mode fibre *(THORLABS - P1-630A-FC-1)* entrance and *L3*. A misalignment at this point is dramatically dropping down the overall intensity of the incident laser beam. The optical fibre cable itself is connected with a fibre coupler *(THORLABS - SM1FCA)* placed in a XY-stage *(THORLABS - ST1XY-S/M)*, which makes it possible to align precise the fibre inlet to the focal point of *L3*. The entrance of the optical single mode fibre is thereby tilted by 8°, to reduce backscattering affects in the focusing system.

3.2.3 Collimation

All steps until now, are necessary to change the beam diameter of the incident laser in such a way to collimate the laser beam in a certain small size. Depending on the final beam size, this task can get very tricky to handle. The divergence of the laser beam coming from the optical fibre is depending on the entering laser light angle. Therefore the use of the previous chosen achromatic lens with a long focal length reduces additionally the divergence at the outlet of the fibre. Additional attention is hereby given to the critical angle of the used single mode fibre, which can lead to a dramatically intensity drop, when reached.
Indeed, the out coming numerical aperture (NA) of the used optical fibre is in the range of 0.10 and 0.14. A similar value for the inlet of the optical fibre should be taken in consideration. Whereby, the best results can be reached, by fine tuning of the several distances and angles, with the use of a laser power & energy-meter *(THORLABS - PM100D)*, which measures the absolute light intensity at a given point. In addition is the *numerical aperture* NA defined as followed:

$$NA = m_m sin(\theta), \tag{3.1}$$

where m_m is the index of refraction of the surrounding ambient and θ the half angle of the maximum cone of light that exit or enter a lens. According to this facts the use of a glass ball gives an optimal solution. In figure 3.4, is the impressive way of collimation from the incident laser light in the range of sub-millimetres shown. The glass ball is hereby directly bound on the end of an optical single mode fibre.
Glass balls have the advantage of their very small focal length. The difficulty hereby is the placing of the glass ball close to the exit of the optical fibre. Further is the radius of the glass ball very critical to be chosen. The radius of a glass ball is comparable with the radius of the curvature of a conventional lens (see figure 3.10). Whereby, the very difficult placing of the lens exactly at the outlet of the fibre makes the use complicated. A dis-alignment of some micrometers hereby, diffract the out coming light on the side.

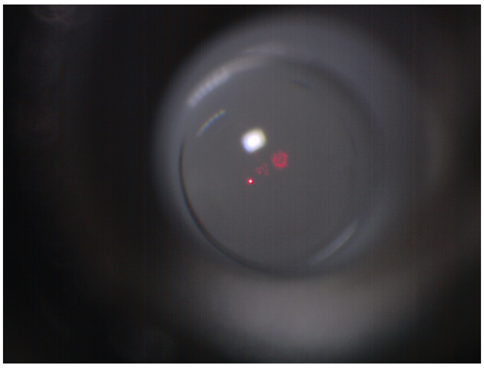

Figure 3.4: A glass ball with a radius of 1 mm is bond on a single mode fibre, which shows in an impressive way the collimation of incident red laser light.

Therefore, the use of a gradient-index (GRIN) lens *(L4 - EDMUND OPTICS - NT64-515)* with a working distance of zero, directly bond to the exit of the optical fibre is preferred. A transparent UV cured adhesive *(NORLAND PRODUCTS - NOA61)* is used to bound *L4* on the outlet of the optical fibre. In fact, with a diameter of 0.5 mm and a length of 1.15 mm is this lens not at all easy to handle. Though, the placing of the *L4* at the centre of the exit of the optical fibre is easier to realize by additionally better collimation results for the incident laser beam. The image of figure 3.5, shows how such a GRIN lens is bound on the exit of an optical single mode fibre.

Figure 3.5: The GRIN lens (*L4*) bound on the optical outlet of the single mode fibre.

Indeed, there are also commercial available collimating modules on the market, to collimate the out coming light of an optical fibre for instance an adjustable aspheric FC collimator *(THORLABS - CFC-2X-B)*. The minimal working distance of such system limit the usability. Moreover has such systems a minimum working distance between the position of collimating lens and final target particle plane S, given by the mounting part. All in all the best solution is the use of the so called GRIN-lens.

For the SALS apparatus, the end of the optical fibre is connected with a homemade fibre holder, which on his side is placed in an adjustable kinematic Mount *(EDMUND OPTICS - NT58-872)* to adjust preciously the position of the GRIN lens. A divergence of less than 45 mrad at the output of $L4$ is realized with such a lens system, which ensures the quasi collimation of the incident light to a waist diameter of maximal 50 μm at S. Therefore, the collimated laser beam diameter at S distinguishes this SALS apparatus from others in the literature and enables the precise single particle characterization at low scattering wave-vectors.

The intensity distribution of the incident beam at different distances from the GRIN lens is shown in figure 3.6. Here the half beam shape starting from 0° (1 pixel) is represented with a pixel pitch[7] of 7.5 μm *(IMPERX*[8] *- IGV-B0620)*.

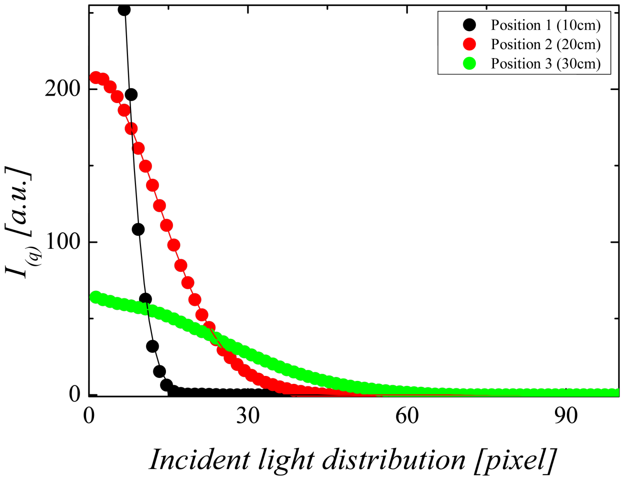

Figure 3.6: The Gaussian beam distribution of the incident laser beam at distances of 10, 20 and 30 cm after the optical fibre exit is plotted. The hereby used CCD-camera has a pixel pitch of 7.5 μm.

---

[7] The pixel pitch is the relative distance from one pixel centre to another, which is the ideal case the pixel size.

[8] IMPERX, Boca Raton (FL), USA

The incident beam distributions are recorded at distances of 10, 20 and 30 cm after the exit of the optical fibre. By calculating the beam divergence and knowing the distance from S to $L4$, the spot size diameter in the homemade micro-channel is calculated.

3.3 Sample device

The adequate working of a single particle detecting SALS apparatus is strongly depend on the ability to measure each target particle at once separated from each other. In general, there are two ways to measure such target particles. According to the state of the particle during the measurement procedure, a distinction in quiescent and in-flow is done.

3.3.1 Quiescent - device

One way, is the measuring of single particles in quiescent conditions. Therefore the observation of single particles is done without any external forces on the target particle solution (H_2O). The strong diluted solution is placed at S by a microslide *(VITROCOM - W3520-050)* with an inner rectangular size of 0.2 x 4.0 mm. Both ends of this rectangular slides are sealed to predict dynamic liquid drifts during the time interval of measurement. By adjusting the position of the microslide with a XY- and Z-stage *(THORLABS - DT12XY/M & SM1Z)*, a positioning of single target particles in the centre of the incident laser beam is realized.

Quiescent measurements allow to measure very accurate the scattering pattern of single particle. Moreover gives the measurement of the sum of equal particle the opportunity to measure the scattering characteristic of a single particle with increased scattering intensity. Additionally is the measurement over longer time intervals possible, which further increase the final scattering result. In fact is the quiescent measurement procedure very useful to characterize particle with low scattering intensity.

Additionally is the measurement of structural sample changing over time possible, i.e. microgel can be observed in such conditions. Indeed, the quiescent condition opportunity opens the possibility for precise characterization of material properties for single particles and therefore is fundamental for the prove of workability of the overall SALS apparatus.

On the other hand is the main focus of this work, the development of a SALS apparatus, which is able to characterize particle in-flow.

3.3.2 In-flow - device

Inflow measurement requires the accurate single line focusing of the target particles, to allow the incident laser light to efficiently interrogate them one at a time. [37] The suspension of particle used for such predictions has to be strongly diluted and free from agglomerates.

3D focusing condition can be achieved by viscoelastic induced migration of spheres in pressure driven flows of simple cylindrical micro-channels. This technique avoid complex and expensive microfluidic devices. By using a non-Newtonian liquid, the presence of both elastic stresses and shear thinning behaviour promotes and influences the cross-migration dynamics and the equilibrium radial distribution. Both the magnitude and the direction of migration is tuned by varying the rheological characteristics[9] of the suspending liquid.

Inertia is in this context from no relevance. The focusing of the target particles comes from purely elastic effects. In fact by selecting an elastic, but viscose liquid, a single equilibrium position coincident with the channel centreline exists, leading to a 3D focusing mechanism in a straight channel.

The migration dynamics of a particle in viscoelastic liquids flowing in a channel at low Deborah numbers[10] is described by a single *dimensionless number* Θ, which is given by:

$$\Theta = \frac{1}{2} De (1 + C\frac{\Psi_2}{\Psi_1})\beta^2 \frac{L}{R}, \tag{3.2}$$

with the *Deborah number De*:

$$De = \frac{\lambda_t Q}{2\pi r_c^3} = \dot{\gamma}\lambda_t, \tag{3.3}$$

where the ratio Ψ_2/Ψ_1 describing the fluid rheology, while the relaxation time λ_t and flow rate Q (angular velocity) is included in De. The geometrical properties of the channel are L the length of the glass capillary with inner radius r_c and the *blockage ratio* β given as:

$$\beta = \frac{a}{r_c}, \tag{3.4}$$

with a the radius of the particle flowing in the channel. The *flow rate* Q is hereby given by:

$$Q = \frac{\pi r_c^4}{8\eta} \frac{\Delta_p}{L}, \tag{3.5}$$

where η is the viscosity of the used liquid and Δp the relative pressure gradient from a pressure pump. Indeed, the flow in the microfluidic channel is generated only by the use of a pressure pump with adjusted working pressure (see section 4.1). The adjustable Δ_p of the pressure pump is the main

---

[9] Rheological properties of materials is the quantitative and qualitative relationships between deformations and stresses and their derivatives.

[10] Deborah number is equivalent to the *Weissenberg number* and described as the ratio of fluid and flow characteristic times.

parameter to regulate Q and therefore also $\dot{\gamma}$. According to Q the *shear rate* $\dot{\gamma}$ in the microfluidic tube is calculated with the following formula:

$$\dot{\gamma} = \frac{4Q}{\pi r_c^3}. \tag{3.6}$$

By increasing $\dot{\gamma}$ the viscosity and normal stress coefficients decrease, which results in shear thinning. The successful 3D focusing for particles flowing in a round channel is achievable when the final assumption is fulfilled:

$$\Theta > -\ln(3.5\beta) \simeq 1. \tag{3.7}$$

for β values of particle between $0.01 \leq \beta \leq 0.3$ and $De \ll 1$. [50] The values used for the SALS apparatus are given in section 4.1.

Indeed, the microfluidic device of the SALS apparatus is specifically designed to induce particle migration towards the central axis of the channel and hence to realize a precise 3D focusing of the target particle. For this aim a solution of 0.4% polyethylene oxide (PEO[11]) in H_2O by weight is the viscoelastic suspending medium.

Indeed, due to the presence of normal stress differences, it is well-known that viscoelastic liquids induce particle migration in a certain range of shear rate.[13] By adjusting the applied Q to get a $\dot{\gamma}$ of about 100 $\sec^{-1}$ optimal particle focusing with this liquid is possible.

The used microfluidic device is made of high quality Poly-methyl-methacrylate (PMMA from *GOODFELLOW*[12] *- 3.0 & 0.5 mm (ME303032BA, ME303006GB))*, which provides high transparency. Figure 3.7 shows the design of the device, which is realized by micro-milling technique.

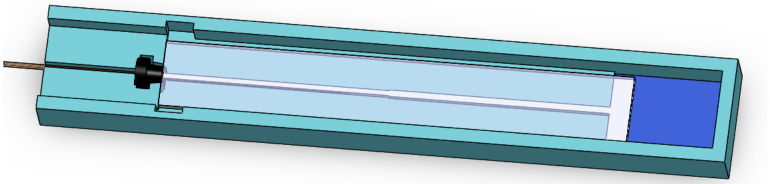

Figure 3.7: 3D view of the homemade microfluidic-device. The tube entering the device on the left side is a glass capillary with inner diameter of 75 μm. A rubber conic ferrule holds this capillary in space and closes the channel to avoid liquid leakage. After the ferrule the microfluidic channel has a width of 381 μm until the middle of the device. Afterwards the channel enlarge to a width of 508 μm. The depth of the channel is held constant by around 400 μm according to the production accuracy. The top of the channel is closed by bonding with a coverslide PMMA of 0.5 mm.

---

[11] PEO with M_w = 4 MDa, from Sigma-Aldrich

[12] Goodfellow Cambridge Ltd., Huntingdon (CAM), England

The device has an open groove on one side, in which a round glass capillary *(UNIFIBRE (MOLEX*[13]*) - TSP075375)* with inner radius r_c of 37.5 μm is placed. The end of this capillary is hold in place with a soft ferrule *(NANOPORT*[14] *- Ferrule 6-32 FB-360/510 µm)*; this ferrule additionally seals the microfluidic channel.

The inside focused target particle leave the glass capillary at the entrance of the rectangular measurement channel. The target particle are reaching the homemade microfluidic device exactly at the centre of the rectangular measurement channel entrance and keep flowing on.

The channel is build with a width of 381 μm and hight of 400 μm until the middle of the device. Afterwards the channel width enlarges to 508 μm until the end, where a reservoir collects all the out coming liquids. The relative target particle position in the microfluidic device is adjusted by XY- and Z-stage *(THORLABS - DT12XY/M* & *SM1Z)* to match exactly the centre of the incident beam.

The quiescent and in-flow device is placed directly on the top of a peltier element at the temperature module of the apparatus.

3.3.3 Temperature control module

The accurate measuring of target particle requires constant ambient temperature. Therefore a peltier element *(EURECA*[15] *- TEC1R-17-22-9.5-23/78-B)* is implemented directly under the target particle plane of the SALS apparatus. A peltier element transfers heat from one side of the device to the other, by consumption of electrical energy. By alternating the current, the element heat or cool, which a controller *(MINCO*[16] *- TC0806-RS232)* with automatic feedback loop regulates. Figure 3.8 shows the peltier element implemented in the apparatus. The peltier is embedded in a homemade peltier holder, which is placed on top of the Z-stage of the microfluidic device (see section 3.7). A cover plate close the temperature system and moreover fix the microfluidic device in place. This peltier element in particular is produced with a central hole of 9.5 mm, through which the incident light directly passes to the quiescent or in-flow device. The automatic feedback loop of the controller measures automatically every second the actual peltier temperature with a PT1000[17] resistance thermometer (RS COMPONENTS[18] - Cat. no. 362-9907). Temperatures from 15.5°C up to 42°C are achievable with this system. In fact, the heat transfer to the bottom of the peltier holder limits the minimum obtainable temperature.

---

[13] Molex, Lisle (IL), USA

[14] IDEX Health & Science, Oak Harbor (WA), USA

[15] EURECA Messtechnik GmbH, Cologne (K), Germany

[16] Minco EC AG, Wil (SG), Switzerland

[17] A PT1000 measures the temperature by correlating the resistance with temperature.

[18] RS Components GmbH, Moerfelden-Walldorf (HE), Germany

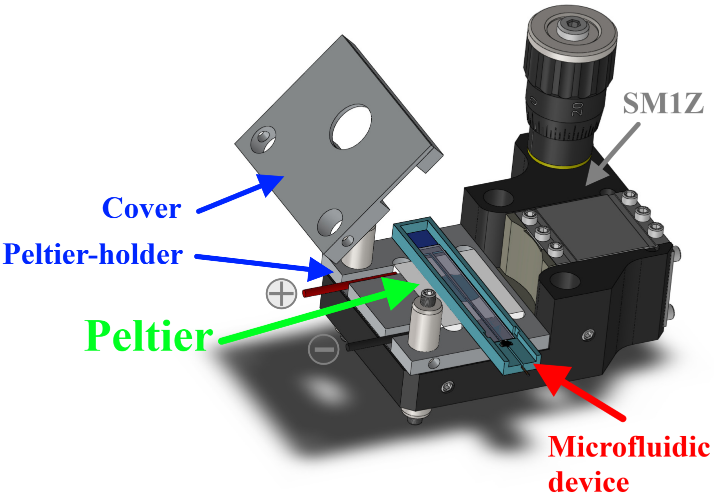

Figure 3.8: A schematic 3D side view of the temperature control unit of the SALS apparatus. The Cover is detached for easier visualization of the peltier element.

3.4 Detection system

The most complex part of the apparatus is the collection system for scattered light. In general, as bigger the wave-vector a system can collect, as better a particle can be characterized. Several different simulations with the previous mentioned optical simulation software is used to optimize this part of the apparatus. The main point hereby is to bring the scattering pattern in a reproducible way to the sensor of the camera. The schematic diagram of the scattering pattern detection stage is shown in figure 3.9.
There are two already in the introduction mentioned works in literature, which elaborated on such a problem. One is the work from *Jan van Heiningen* with his dissertation, describing the calculation of the spot size on the detector by the use of a *"ultrasmall angle light scattering apparatus"* and there design optimizations. [57] The other very interesting paper is coming from *Fabio Ferri*, who describes the use of a CCD-camera for the measurement of low angle light scattering. [15] The purpose of the here shown detection system (figure 3.9) is to decrease the distance between sample and detector to a minimum, by obtaining far field condition.
The meaning of the indications rs and r' need some previous knowledge of theory and will therefore be explained in section 3.4.3. However, to calculate the perfect lens distances as well as the position of the beam stop some formulas are necessary. The sections 3.4.1 & 3.4.2 will summarize the most important ones.

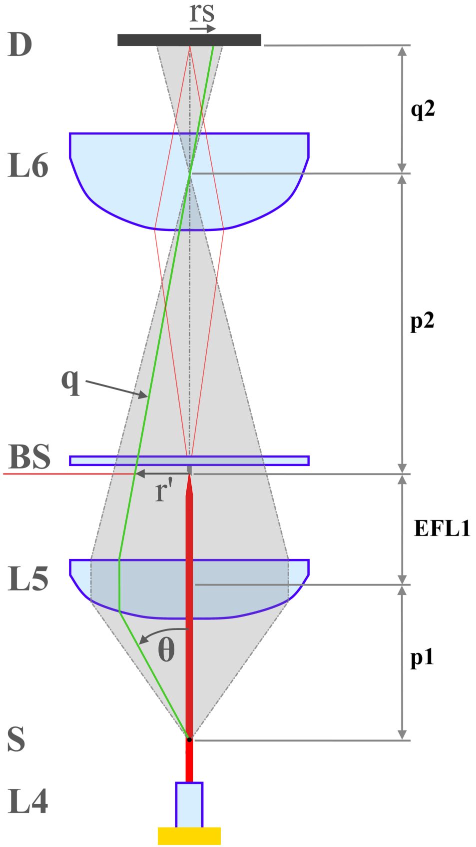

Figure 3.9: Schematic overview of the scattering pattern detection system. *L4* indicates the GRIN lens at the end of the optical fibre. *S* is mentioning the target sample in the microfluidic device. Additionally is the lens for the scattering pattern collection *L5* and mapping *L6* shown. The beam stop *BS* is indicating the reflection of the incident beam, while the green ray of light is illustrating one single wave-vector q coming from the target particle. The indication rs with r' show the radius of the scattered ray on the detector for the given scattering angle.

3.4.1 Lens position

Before simulation of the best fitting lens distances as well as the positions are calculated, a research of possible optical lenses was done. This part is looking trivial, but is crucial for reaching the best possible scattering collection result. Hence the first lens, which collect the light scattered by the target particle has to have a very high NA. Indeed the diameter of this lens is not from prior significance.

According to calculations with a homemade Matlab routine appendix C

(SpotSizeCCDchip.m) the best fitting lenses are computed. Here only the end results of the simulation process with the final chosen lens couple is shown. All the length between the lenses as well as the beam stop are related to figure 3.9.
To start the calculations the parameters from the used lenses have to be known. The scattering pattern collecting lens, is an aspheric lens *(L5 - EDMUND OPTICS - NT67-245)* with NA = 0.85. Indeed, with a higher NA the distance $p1$ between S and *L5* can be further reduced. Whereby a more close position from *L5* to S increase automatically the acceptable scattering angle the lens can collect, but hence also several alignment problems. The minimal distance *L5* can not overcome the effective focal length (EFL) of the used lens. In fact, smaller distances can not be focused to a point.
Also the overall length of the collection stage has to be mention during this calculations. The more close the position of *L5* comes to the focal length, the more far away the collected light will be focused, which increase the overall length of the system. Indeed considerable hereby is also that, with distances of p_1 close to EFL_1 the system gets more sensitive to dis-alignments of particles at the target particle plane. A compromise between smallest possible distance between S and *L5* and maximal collecting scattering angle has to be found.
The lenses *L5* & *L6* have the following specifications described subsequently:

Specifications:	**Value *L5***	**Value *L6***	**Dimension**
Diameter - ***D***	25.00	25.40	[mm]
Numerical aperture - ***NA***	0.83	0.50	
Clear aperture - ***CA***	90	90	[%]
Effective focal length - ***EFL***	15.09	25.43	[mm]
Radius - ***R***	10.09	13.10	[mm]
Centre thickness - ***CT***	11.00	11.70	[mm]
Edge thickness - ***ET***	1.64	1.80	[mm]
Substrate	1.668	1.515	[nm]

Table 3.1: Table with the specifications for the aspherical lens *L5 (EDMUND OPTICS - NT67-245)* and plano-convex lens *L6 (THORLABS - LA1951-A)* according to a wavelength of 632.8 nm.

The value of EFL in this context is different from the given one of the supplier, according to an adaptation, by the used laser wavelength for the SALS apparatus. The precise *EFL* values can be calculated by:

$$EFL_n = \frac{R_n}{m_n - 1}, \tag{3.8}$$

where the suffix n for EFL, the *radius* R and the *index of refraction* m depends on the used lens. According to *L5* a EFL_1 of 15.0939 mm is cal-

culated. For *L6* the EFL_2 is 25.4324 mm. Both values are similar to the nominal ones from the seller. Based on the values in table 3.1, the calculation fo the distances p_1, q_1, p_2, q_2 as well as the according magnification of M_1 and M_2 of the two lenses is calculated. Each distance is consolidated from the principal plane H of the according lens.
The figure 3.10 summarize the main parameters of a plano-convex lens to clarify the used terms for the following formulas.

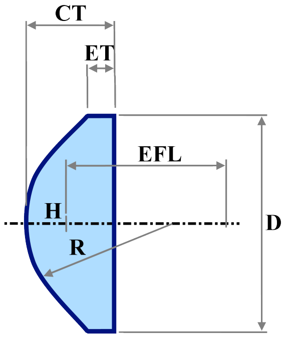

Figure 3.10: Schematic figure of a plano-convex lens.

Indeed is the collection system very sensitive to the position of each lens, therefore the *principal plane* H inside the lenses has to be calculated and is described like:

$$H_n = \frac{EFL_n CT_n (N_n - 1)}{N_n - R_n}, \tag{3.9}$$

where CT is the *centre thickness*. The resulting values for the principal planes are $H_1 = 6.5928$ mm and $H_2 = 7.7223$ mm. The position, where the principal plane crosses the optical axes of a lens is named principal point of the lens. Indeed, for a theoretical lens it is assumed that the refraction happens only at the principal plane. [3]
Anyway, the main focus of the calculation is to have a small p_1 value. Therefore, p_1 is chosen to be **16,86 mm**. Starting with this value the distance q_1 can be calculated by the given formula:

$$q_1 = \frac{p_1 EFL_1}{p_1 - EFL_1} = 144.0973\ [mm]. \tag{3.10}$$

This length q_1 is the distance between the principal planes of *L5* and *L6*. In fact, this length is mainly depending on the pre-defined p_1 and therefore main factor for the overall length of the scattering collection stage. Moreover, the length p_2 is calculated in the following way:

$$p_2 = q_1 - EFL_1 = 129.0034\ [mm]. \tag{3.11}$$

The length is showing the correct position of *BS* in the scattering pattern collection system. Detailed information about the used homemade beam stop can be read in section 3.4.2. Furthermore, the last length q_2 between *L6* and the *D* is calculated by the following relationship:

$$q_2 = \frac{p_2 EFL_2}{p_2 - EFL_2} = 31.6775\ [mm], \tag{3.12}$$

The *overall length* of the collecting system l_{col} is given by:

$$l_{col} = p_1 + q_1 + q_2 = 192.635\ [mm], \tag{3.13}$$

This value seems to be a good compromise between compact size and maximum able wave-vector range for the given lenses. However, by considering all the mentioned difficulties it is not simple to implement all optical parts in the SALS apparatus. Additional specifications of the system are the *magnification* of each lens. The following formula gives the relationship therefore:

$$M_n = \frac{q_n}{p_n}, \tag{3.14}$$

where for *L5* a value of $M_1 = 8.5467$ and $M_2 = 0.24556$ for *L6* is realized. Indeed a bigger magnification leads automatically to a bigger spot size of the lens. Therefore the spot size of *L5* is very big, which mainly effect the overall spot size on *D*. In consideration of the higher wave-vector range which is collected by a bigger magnification of *L5* the bigger overall spot size could be beard.

In fact one important point of the collection system has been neglected until now. The beam stop which is fundamental for the correct working of the SALS apparatus. The next section will outline the main problems according the *BS* and how they could be solved during the development of the apparatus.

3.4.2 Beam stop

The main criteria of a beam stop (*BS*) is to be as small as possible, but on the other side to block, reflect or diminish as much as possible the incident light. There are different options to handle this problem. Beside the blocking also the possibility of reflecting the light out of the collection system is widely used. There is only few information in literature about the use and structure of *BS*, some authors described a *BS* are already mention in chapter 3.1. By variation of different *BS* structures, sizes as well as positions in the system, a final configuration is found. The more promising approach is the light reflecting one. Therefore a small mirror, with a relative cut off angle of 45° is placed exactly at the focal point of *L5*. Figure 3.11, shows a schematic view on the working principle of the *BS* of the SALS system.

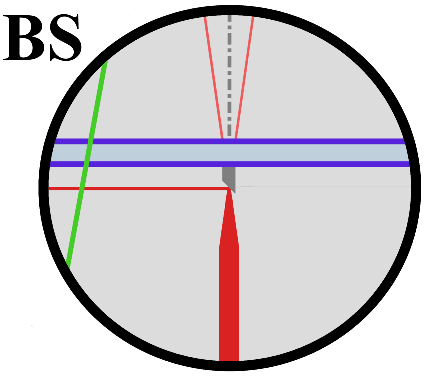

Figure 3.11: Zoom on *BS*, from the schematic figure 3.9. The green line indicates one wave-vector of a particle. In the upper part of the figure is the incident light without *BS* influence indicated by 2 red lines. The *BS* itself (in grey) is shown at the centre bound on the glass target (blue lines).

The *BS* position depends on the incident beam diameter. For instance, a very small incident beam is focused after the focal point of *L5*. For calculating the minimum angle the SALS system can collect, the accurate incident beam diameter entering *L5* has to be known.

Indeed the measuring of this value is quite tricky, therefore an assumption based on the beam divergence, mentioned in figure 3.6 plus the distance l_b between S and H_1 of *L5* is used. The here fore calculated *incident beam diameter* D_1 at the principal plane of *L5* is:

$$D_1 = 2l_b \tan(\theta_b) + D_0 = 0.808\ [mm], \tag{3.15}$$

with a given half beam divergence θ_b. For the diameter D_0 the beam diameter at the sample plane is considered. Therefore a length l_b equal to p_1 is used. By knowing D_1 the further calculation of the *BS* size is assumed. Considerable at this context is the knowing of the scattering intensity of the target particles at very low scattering angles, which can ensue in saturation problems with the used sensor of the detecting camera. Furthermore is the calculation of the beam diameter based on a perfect Gaussian beam shape, which is very tricky to realize at this point.

All in all is the use of a bigger *BS* diameter D_{BS} convenient. A value of 200% the calculated *BS* diameter is required for reflecting the main amount of the incident light out of the detection system.

By knowing D_1 the calculation of the *minimal scattering angle* θ_{min} at the sensor area of D is estimated. The formula therefore is:

$$\theta_{min} = \arctan\left\{\frac{\frac{D_{BS}}{2}}{EFL_1}\right\} = 0.0661\ [rad], \tag{3.16}$$

Therefore also the *maximum scattering angle* θ_{max} at D is calculated with the formula:

$$\theta_{max} = \arctan\left\{\frac{\frac{D_{L5}}{2}}{p_1}\right\} = 0.6456\ [rad], \tag{3.17}$$

which is mainly depending on the scattered light entering *L5*, which is defined as D_{L5}. In consideration here fore has to be the *CA* of 90% and blocking of light by the lens holding equipment.

For instance also the *wave-vector* q for the minimum and maximum scattering angle is predicted with the following relationship:

$$q = \frac{2\pi m_m}{\lambda}\sin(\theta) = 13.2225 \cdot \sin(\theta), \tag{3.18}$$

with m_m the index of refraction is 1.33169 (H_2O at $\lambda = 632.8$ nm[20]). In fact with this apparatus specific factor of 13.2225, each wave-vector value can be pre-calculated. A theoretical wave-vector span starting from 0.8733 to 7.9557 μm^{-1}, which corresponds to a scattering angle ranging from 3.78° to 36.99° is calculated. The for the apparatus used *BS* is shown in picture 3.12.

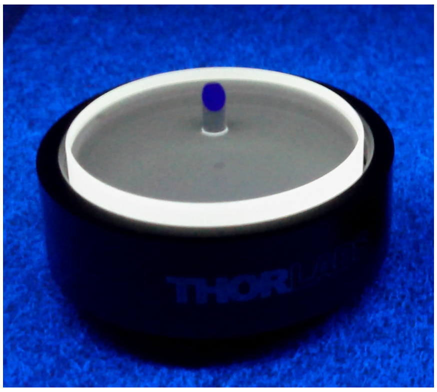

Figure 3.12: Picture of the for the SALS apparatus used *BS*. A glass rod of radius 1 mm with a 45° cut is bound on a glass target.

The *BS* system is existing of a glass target *(EDMUND OPTICS - NT49-141)* where a commercial glass rod *(EDMUND OPTICS - NT54-092)* of 2 mm diameter with an optical cut of 45° is glued on. The cut area is reflective coated and the rod itself is glued on a special glass target by a highly transparent optical glue *(THORLABS - NOA61)* which is also used for the bounding of *L4* on the outlet of the optical fibre.

The glass target is chosen for the wave length of a HeNe laser and therefore should not add additionally scattering or refection behaviours to the system. Experiments with smaller *BS* diameters have been done, during the development of the apparatus. By using a *BS* with a diameter of 1 mm, the minimal measurable wave-vector is reaching 0.4375 μm^{-1}, which corresponds to an angle of 1.89°. As a matter of fact is the main problem at this wave-vector range the saturation of the sensor according to higher particle scattering intensities passing through to *BS* (see figure 2.5 for the dependence of forward scattering). A better collimation of $L4$ would may give the opportunity to measure smaller wave-vectors. In fact, the *BS* size and shape as well as the dynamic range of the used CCD-camera is restricting the minimal measurable wave-vector range.

In should be noted, that the lenses *L5*, *L6* as well as also *BS* are all placed in translating lens mounts *(THORLABS - LM1XY/M)* for fine adjustment of the XY-position. Indeed also the hight of *L6* has a precise adjustability. Several additional lens tubes and a vertical holder for the whole detection stage are not mention in this context.

3.4.3 Mapping & detector

Concluding the scattering pattern detection system, the already mentioned plano-convex lens *L6* after the *BS* maps the scattered light on the sensor of the cooled CCD-camera *(HAMAMATSU PHOTONICS K.K.*[19] *- C11440-22CU (ORCA-Flash4.0)).* The use of a CCD-camera enables hereby the possibility to measure different wave-vectors simultaneously, which is a big advantage compared to photo-multiplier used as standard detector.

The camera has a pixel pitch of 6.5 μm, a maximal sensor size of 2048x2048 pixel and is operating at a sensor temperature of minus 10°C. The before explained two lens collecting system, allows obtaining far field images on short distances. Therefore, each speckle corresponding to the same magnitude of the scattering wave-vector $q \equiv |q|$ but different azimuthal orientations are collected by rings. Each of this ring is further used to analyse the scattering pattern. [10]

In particular is the length q_2 which maps the scattered light on the pixels of the CCD-camera from great interest. A small focusing of the lens would, need a bigger sensor size, which in general is limited. On the other side a too strong focusing reduces the length, and thereby can end up in problems with the mechanically feasibility to bring the sensor close enough to *L6*.

In fact, most of the commercial available cameras have a minimum distance between the sensor chip and the border of the chassis. The calculation of 3.12 accomplish the specifications of the used D, when the chassis of the camera is open.

However, according to the chosen frame rate of the CCD camera, each frame is saved as a picture. The frame rate hereby is depending on the exposure time and read out velocity of the camera. The section 4.2 is going in more detail about the analysis of such frames.

---

[19] HAMAMATSU PHOTONICS K.K., Hamamatsu City (SP), Japan

By referring to the green ray in figure 3.9, the light scattered at an angle θ is mapped by *L5* into a ring of radius r' placed in the focal plane of *L5*. Furthermore by following the ray the ring is mapped by *L6* on the sensor area of D, given by the *radius* rs, which is calculated in the following way:

$$rs = q_2 \frac{p_1}{q_1} \theta. \tag{3.19}$$

Important hereby is that the formula 3.19 is expressed to be only dependent from EFL_1, EFL_2 and p_1. Indeed all calculations necessary for the calculation of the wave-vector are dependent of p_1, because EFL_1 and EFL_2 are fixed parameters for a given lens. This brings the advantage of using this formula in a fitting procedure, depending only on p_1.

In fact the previous section 2.5, mentioned this fitting possibility. By using formula 2.16, and expressing θ only depending on the parameters EFL_1, EFL_2 and p_1, the scattering pattern of a pinhole placed at S can be analysed. The new formula here fore with the *fitted scattering intensity* If_θ is given as:

$$If_\theta = I_0 \left[\frac{2J_1(ka\sin(\frac{EFL_1(EFL_1+EFL_2)-(EFL_2\,p_1)}{EFL_1 EFL_2(-EFL_1+p_1)})rs}{ka\sin(\frac{EFL_1(EFL_1+EFL_2)-(EFL_2\,p_1)}{EFL_1 EFL_2(-EFL_1+p_1)})rs} \right]^2. \tag{3.20}$$

The fitting procedure, is in this case only depending on p_1 and the real position of a pinhole can be calculated. All not mentioned parameters in formula 3.20 are given. The section 4.3 shows graphically such a fitting result. The whole fitting procedure can be read in the homemade Matlab routine at the appendix C *(Auswertungssoftware.m)*. This fitting procedure is only useful for the calibration of the collection stage of the system. Analysis of particles causes according to their complexness calculations based on theoretical predictions of the Lorenz-Mie theory.

Chapter 4

ACQUISITION and DATA PROCESSING

4.1 Sample preparation & acquisition

First measurements for the developed SALS apparatus are proceeded in quiescent (multi-particle scattering) and flow (single particle) conditions. The target particles are made of polystyrene latex (**PSL**). This particle are widely used for the calibration and testing of light scattering systems, because of their perfectly spherical shape (see section 5.19) and minimal absorption for visible wavelengths. It can be assumed that the complex refractive index of the PSL particle is $n = \mathbf{1.58722 + 0.000001}i$ for $\lambda = 632.8$ nm (**sample medium**). [28]
The PSL particle (POLYSCIENCE[1] & SIGMA-ALDRICH[2]) measured with the SALS apparatus are listed in table 4.1, with radii and σ *(SD)*. Particles

Particle	Nominal radius	SD	*Supplier*	*Cat. number*
PSL 8	4.010	0.049	*Sigma-Aldrich*	*84192-5ML-F*
PSL 6	3.042	0.041	*Sigma-Aldrich*	*89756-5ML-F*
PSL 5	2.895	0.088	*Polyscience*	*15716-5*
PSL 4	2.078	0.031	*Sigma-Aldrich*	*81494-5ML-F*
PSL 3	1.644	0.041	*Polyscience*	*17139-5*
PSL 2	0.947	0.022	*Sigma-Aldrich*	*80177-5ML-F*

Table 4.1: Table of nominal radii from *Sigma-Adlrich* and *Polyscince* particle. All values are given in μm.

---

[1] Polysciences Incorporated, Warrington (PA), USA

[2] Sigma-Aldrich Corporation, St. Louis (MO), USA

measured in quiescent conditions are strongly diluted in pure H_2O with a index of refraction $n = \mathbf{1.33169}$ **(ambient medium)**. [20] The stock solution from the supplier is diluted between 5x10^4 and 2x10^5 times according the particle size. Particle solutions are prepared on the same day of the experiment and stored at room temperature. Indeed, all measurements are proceeded at room temperature. The particle solution are filled in microslides (see section 3.3.1) 30 minutes before the measurement. Both sides of the microslide are sealed to predict leakage of solution. The slide itself, is around 10 minutes before the final measurement placed at the target particle plane. The laser source is turned on, for short adjusting of the target particle in the centre of the incident beam by the use of a XY-stage. After the adjustment, the laser source is blocked for around 3 minutes to prevent thermal effects in the slide, before the measurement is started.
The exposure time (ET) of the CCD-camera changes according to the measured particle size from 1 up to 100 ms. Since ET of 100 ms are only necessary for PSL 8 measurements for the relative high scattering intensity, a density filter of 2 *(THORLABS - NE20B)* is used only during this measurements to predict saturation. Thus made the use of higher ET necessary. Preliminary tests showed consistent intensity patterns if the saturation or noise level of the camera is avoided, which linearly shift up with increasing the ET. The laser intensity is alternated before each measurement to measure the highest possible particle intensities without saturation.
For in-flow measurements PEO is used as ambient medium solution (see section 3.3.2). The refractive index of the 0.4 % PEO solution was measured with a refractometer *(ANTON PAAR*[3] *- Abbemat 200)* and showed similar values compared to H_2O. Indeed all in-flow calculations for the ambient medium are proceeded with the refractive index of H_2O.
The 3D focusing of the target particle is obtained by a flow rate of 0.153 mm^3/min and shear rate of 61 sec^{-1} with De of 0.0061. According to this values Θ is only valid for particle size bigger than PSL 4 (see section 3.3.2). Nonetheless a 3D focusing of all target particle is achievable.
The PEO-particle solution is filled in round glass cuvette and slowly mixed *(BIOSAN*[4] *- Bio RS-24)* for minimum one hour before placed in the pressure pump (DOLOMITE[5] - Mitos P-Pump). Directly after the cuvette is placed in the pump the measurement is started.
However, for each frame the camera collects, one image file is saved on the computer. In fact, between 6x10^3 - 10x10^3 frames are saved for one measurement. Finally, to get the scattering pattern from a measured particle the data has to be analysed, which is described in section 4.2.

---

[3] Anton Paar GmbH - Graz (ST), Austria

[4] Medical-Biological, Research & Technologies, Riga (LV), Lithuania

[5] Dolomite Microfluidics, Charlestown (MA), USA

4.2 Data processing

Data processing of a measured particle, is divided in two parts. First, images of interest are selected, processed and saved as one file for each particle. Second, the chosen data file is analysed by a homemade Matlab routine.

4.2.1 Data selection

For quiescent and in-flow measurement is a different data selection necessary. Due to the quasi idle state of a particle during the quiescent condition, all measured frames can be proceeded for the data analysis. A representative amount of 200 frames is selected and stacked for the analysis. Indeed, for in-flow measurements the scattering profile depends on the relative position from the particle to the incident laser beam centre. Only frames, in which the measured particle is lasting in the centre of the incident light are considered for analysis. This requires the manual selection of the frame with the highest scattering intensity for each particle measured. Once the frame with the highest intensity is determined, the frames before and after are stacked together for analysis.
The intensity for each pixel of the selected stack of frames is averaged (shown in figure 4.1) and saved in one final image.

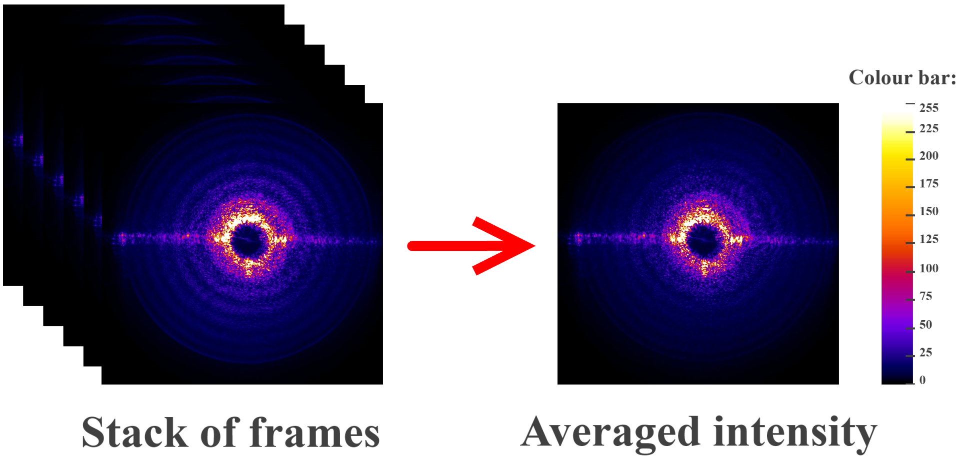

Figure 4.1: The stacked images are averaged pixel by pixel to one final image of the measured particle. The intensity distribution is shown in according to the colour bar.

Thus averaging of image files reduce the thermal noise of the CCD camera. The next step is the subtraction of the background noise and stray light of the apparatus.

Background subtraction

The background intensity is collected as described in section 4.2.1, by a representative amount of frames (50 - 100), in which no particle or different obstacle is measured. This stack of frames is averaged (see figure 4.1) and used as background intensity image.
Indeed, for higher accuracy the background subtraction file is produced for each particle measurement new. The intensity of each pixel from the image of interest and the background image is subtracted. This subtraction of the background is important for an appropriate signal analysis. Figure 4.2 shows the principle behind.

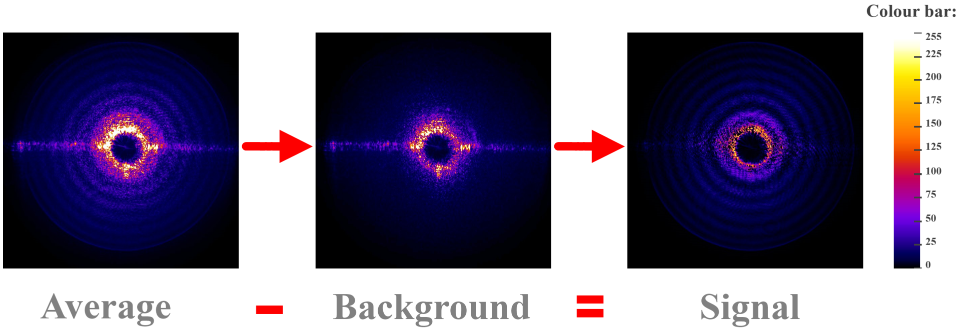

Figure 4.2: The averaged intensity image is subtracted by the background intensity image to reach the real scattering intensity profile of the measured particle. The intensity distribution is shown according to the colour bar.

The scattering profile of the measured particle in figure 4.2 appears more visible than before. Indeed, the user may not recognize a significant difference of the image before and after the subtraction, figure 4.3 shows the background subtraction of a particle in more detail. The corresponds among scattering pattern of the analysed image and wave-vector in figure 4.3 is neglected in this moment. Explanation here fore is given in section 4.2.2.
In the upper part, of the figure the pure scattering intensity ***(Pure signal)*** measured for a PSL 4 particle (nominal radius = 2.078 μm) with green full circles and the corresponding background signal without particles ***(**H_2O**)*** with empty blue stars is shown.
After the background subtraction procedure, the intensity profile, shown with black open circles, reflects a much more defined scattering pattern ***(PSL 4*** μ***m)*** over the whole wave-vector range. A comparison with the theoretical predicted Lorenz-Mie theory ***(Mie theory)*** is shown as red line in figure 4.3 The Lorenz-Mie theory confirms the accuracy of the measurements in the entire meaningful wave-vector range and the importance of the background subtraction.

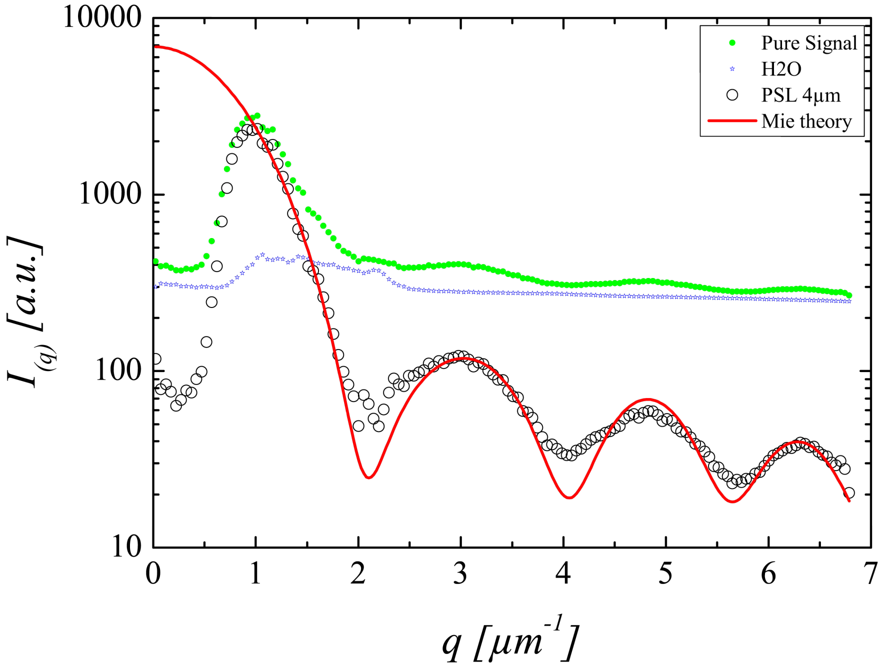

Figure 4.3: Intensity profiles as function of wave-vector. Small solid circles indicate the pure raw data *(Pure Signal)* from a polystyrene particle with a nominal radius of 2.078 μm. Below the curve the background signal *(H2O)* of a glass capillary filled with H_2O is reported with small blue stars. By subtracting the background signal from the pure signal curve, the particle signal appears well-defined and is shown by big empty black circles *(PSL 4 μm)*. The theoretical prediction from the Lorenz-Mie theory corresponding to a particle radius of 2 μm is shown by the solid red curve *(Mie theory)*.

4.2.2 Data analysis

The image file with the averaged intensity profile of a measured particle is analysed by a homemade Matlab routine in appendix C (*Auswertungssoftware.m*). The graphically user interface of this program loads the selected data as a contour plot for the user, where to user is able to manually or automatically select the centre of the imported pattern. The centre of the scattering profile is the pixel on the sensor D, which has a scattering angle of exactly 0° (*'zero pixel'*).

The accurate measurement of the centre of a scattering profile is a very tricky task. Hence, the centre of the measurement doesn't have to be exactly the centre of the blocked light through the beam stop. Small dis-alignments of the sample itself, as well as parts of the collecting system causes different

centre position. It is convenient to check the position of the centre for each measurement to ensure best possible results. In-fact, by perfect calibration of detection system to sample, only ones the zero pixel is calculated.
After the manual or automatic selection of the wave-vector equal to zero, the programs start to analysis the intensity profile of the image. Hereby growing rings (masks) with the width of one pixel starting from the zero pixel until the border of the pixel array are used to average the wave-vector value for each pixel distance of the centre. Thereby, each ring of pixel is averaged over the amount of pixel in the ring. The resulting values, show the scattering profile of a target particle according to the pixel size of the detector. Figure 4.4 illustrated this concept in a more practicable way, by a representative amount of rings.

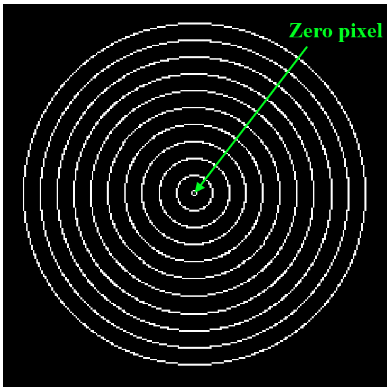

Figure 4.4: Rings in white indicate the mask used for each wave-vector value. The central pixel also named zero pixel is indicated in green. Only every tenth ring is printed for easier visibility.

In general is the use of this rings indicated in figure 4.5. The scattering intensity pattern is shown in the background of the picture, while a certain amount of pixel rings (red) is overlayed. This pixel rings are centred with the wave-vector of zero. As a consequence the scattering intensity according the scattering pattern is highlighted in green at the bottom of the figure. This profile is a schematic graph symmetric to the zero pixel. The symmetry is shown for easier recognition for the user and not implemented in the Matlab routine. Moreover is the position of the representative pixel rings (red rings) on the scattering intensity profile (green line) indicated with white dashed arrows.
The blocked amount of scattered light by BS is easy to recognize by the low intensity profile starting from the zero pixel until the first significant maxima. The relationship between pixel size and scattering wave-vector is from significant interest for the analyses of a particle. By using the formula 3.18 & 3.19 and setting rs equal to the pixel size of D, the measured scattering

pattern is referred to the wave-vector. This corresponding wave-vector value for each pixel can be calculated by inserting formula 3.19 solved for θ in formula 3.18, given as:

$$q_{pix} = \frac{2\pi m_m}{\lambda} \sin\left\{\frac{rs}{q_2 \frac{p_1}{q_1}}\right\}. \tag{4.1}$$

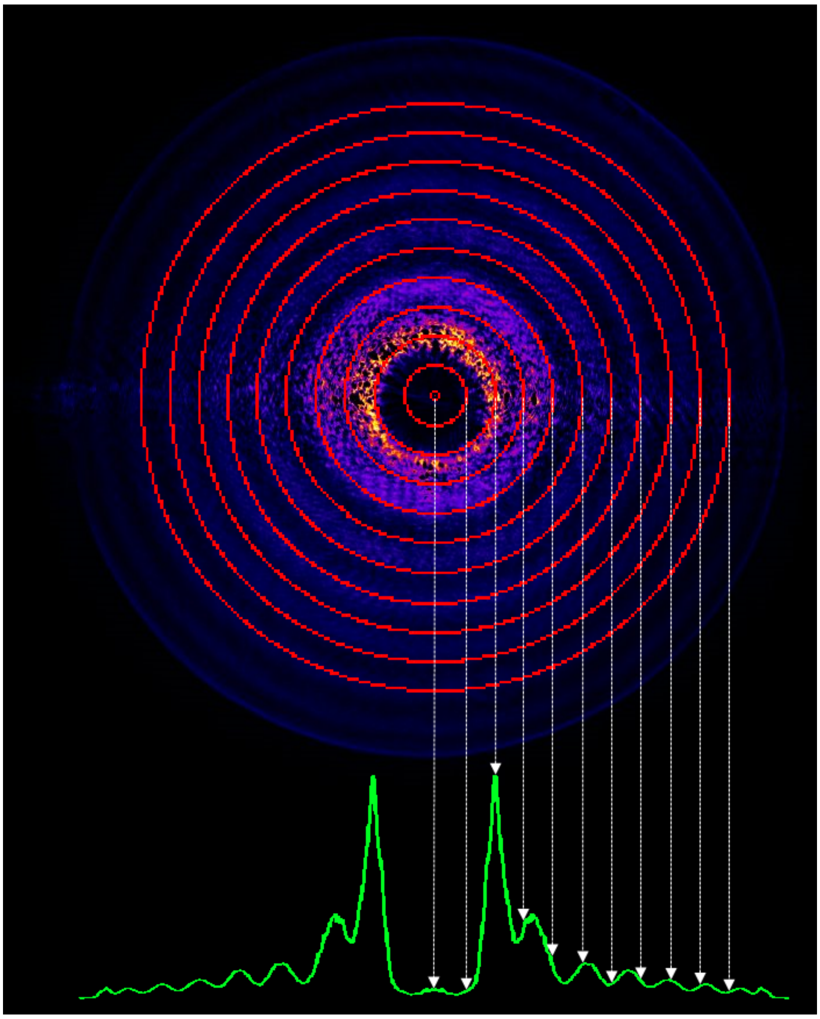

Figure 4.5: The measured scattering intensity is overlayed by a mask of rings indicated in red, for the calculation of the wave-vector. The scattering profile for the whole pixel range is plotted in green, where the corresponding values for the shown rings are indicated with dashed arrows in white. A representative amount of rings is used to indicating the analysis procedure.

Figure 4.5 plot the scattering profile according to the pixel. Indeed, typically the scattering intensity profile for a particle is plotted over the measured

wave-vector range. In addition figure 4.6 illustrate the theoretical predicted Lorenz-Mie scattering profile compared with the previous result. As a matter of fact is an automatic fitting procedure due to the complexity and amount of parameters of the Lorenz-Mie theory impossible to implement.
The overlay of pre-calculated Lorenz-Mie theory is considered as best way, to analyse the scattering profile for a measured particle. Therefore, according to all the parameters of the SALS apparatus the user chose the particle radius, as well as the refractive indices and the Matlab routine automatically overlay the corresponding theory.
By varying the radius and/or index of refraction of the particle, the best matching fit of theory and measurement can be found. For instance the overlay of the theoretical predicted Lorenz-Mie theory on the previous mentioned particle scattering profile (PSL 4 μm) is illustrated in figure 4.6. The ordinate is plotted by the logarithm of base 10.

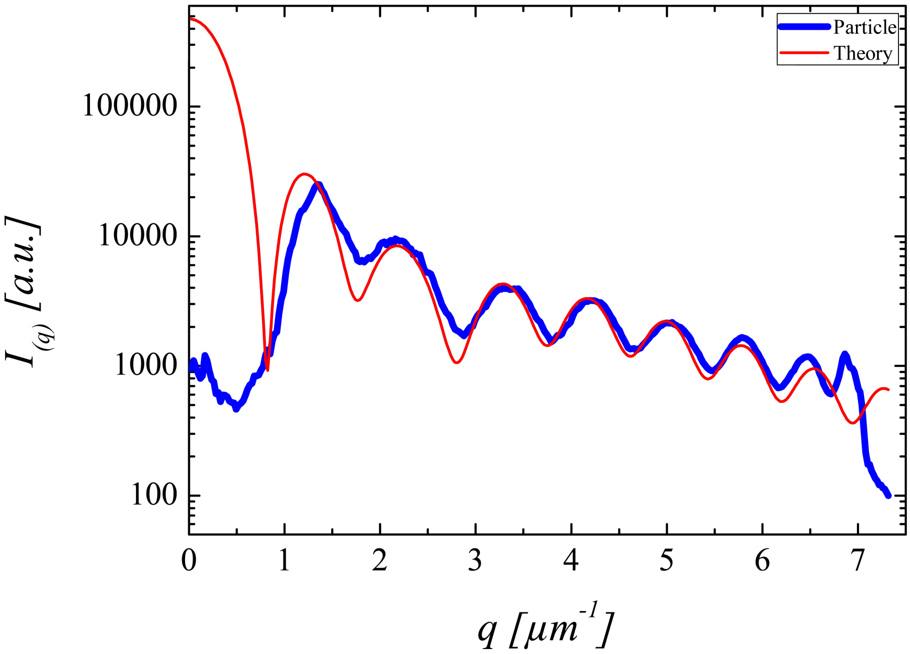

Figure 4.6: The scattering profile is plotted over the wave-vector range of the SALS apparatus in blue, while the according theoretical predicted Lorenz-Mie theory is overlayed in red. The scattering data is the same already shown in figure 4.5.

As a result of finding the best fitting radius for the analysed particle scattering pattern, all parameters are saved in a corresponding file on the computer. Moreover should give a screen-shot of the used Matlab routine a small overview of the parameters the user can additionally select. For more informations regarding the Matlab routine, the reader is referred to the appendix C of this work *Auswertungssoftware.m*.

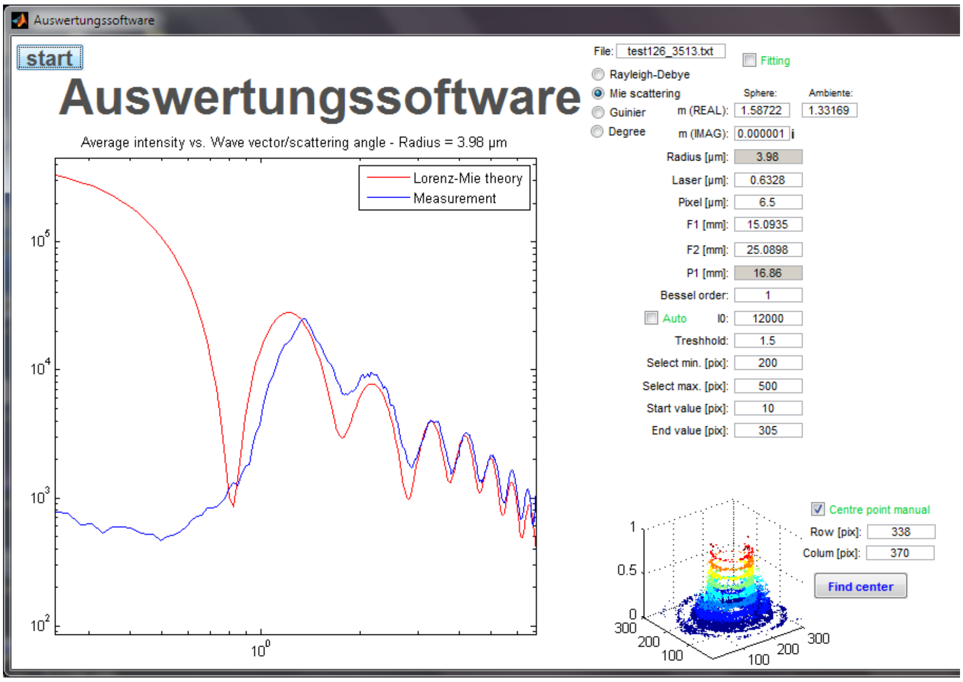

File: test126_3513.txt
☐ Fitting
○ Rayleigh-Debye
● Mie scattering
○ Guinier
○ Degree
Sphere: / Ambiente:
m (REAL): 1.58722 / 1.33169
m (IMAG): 0.000001 i
Radius [µm]: 3.98
Laser [µm]: 0.6328
Pixel [µm]: 6.5
F1 [mm]: 15.0935
F2 [mm]: 25.0898
P1 [mm]: 16.86
Bessel order: 1
☐ Auto I0: 12000
Treshhold: 1.5
Select min. [pix]: 200
Select max. [pix]: 500
Start value [pix]: 10
End value [pix]: 305
☑ Centre point manual
Row [pix]: 338
Colum [pix]: 370

Figure 4.7: Screen-shot of the Matlab routine used to analyse a measured particle with the SALS system. The abscissa and ordinate are plotted with the logarithmic scale of base 10.

4.3 Calibration

For the correct working of the SALS apparatus a calibration of the optical stage is unavoidable. Therefore the relative position of *L4, L5, L6, S, BS,* and *D* are from significant interest. Indeed, a dis-alignment of only one of the mentioned parts causes deformation of the scatting profile, and therefore diminish the usability of the system. A schematic overview of all the included parts is shown in figure 4.8.

A common way, to align a light scattering apparatus is, by the analyses of far field patterns from different pinhole radii. The circular aperture of a pinhole, has a very simple scattering profile, and therefore also gives the possibility to predict possible dis-alignment causes. Section 3.4.3 show the use of the Fraunhofer diffraction theory to describe the scattering profile of a circular aperture. In particular, by using formula 3.20, with given pinhole aperture radius, the calibration of the SALS apparatus is achievable. Pinhole radii of

5 and 10 μm *(EDMUND OPTICS - NT56-276 & NT56-279)* are evaluated by the homemade Matlab routine in appendix C - (*Auswertungssoftware.m*).

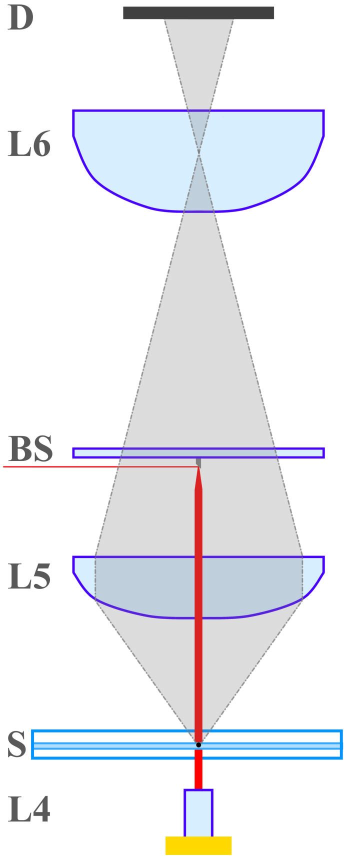

Figure 4.8: A schematic overview, from the parts influencing the calibration. Where *L4* is the collimation lens from the optical fibre. *S* the sample plane. *L5 & L6* are the lenses of the detection stage, while *BS* indicates the beam stop and *D* the detector of the SALS apparatus.

The pinhole aperture position has to be exactly at the target particle plane *S*. The chosen pinholes have a thickness of 12.5 μm. Essentially, the pinholes can be assumed to be without thickness. Any tilting, vibration or movement of the pinhole during the measurement must be predicted. The resulting scattering pattern is collected and analysed like previously described for quiescent measurement (see section 4.2.2). Figure 4.9 shows the scattering profile of a 5 μm pinhole (P5). The abscissa and ordinate are plotted with logarithmic scale of base 10.

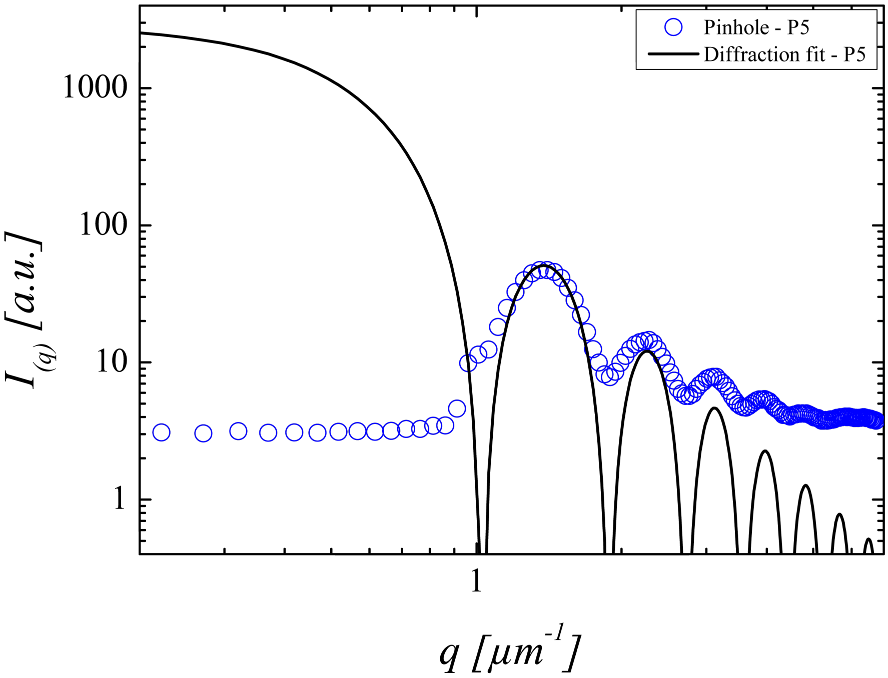

Figure 4.9: A pinhole with radius 5 μm is used to calibrate the SALS apparatus. The measured scattering profile is shown with blue circles. Only one out of two data-points is shown for easier visualization. The theoretical predicted Fraunhofer diffraction pattern is illustrated with a black curve.

The lowest measurable wave-vector $q \approx 5\mu m^{-1}$ is set by the *BS* dimension. The dynamic range of the CCD camera sets the lowest measurable intensity. Indeed it is able to distinguish the first five maxima in the scattered pattern, while the intensity of higher order peaks is in the noise level of the camera. The final agreement among the measured maxima and minima with the theoretically predicted positions suggests the alignment of the system.
For a pinhole with aperture radius of 10 μm the first minima of the theoretical prediction is not detectable with the SALS apparatus, due to the wave-vector range blocked by *BS*. Figure 4.10 shows the pattern scattered by a pinhole with aperture radius of 10 μm (P10).
Indeed precise calibration of a light scattering apparatus is difficult to realize, when the first minima and maxima of the scattered pattern is not detected. Nevertheless, by starting from the second maxima, the scattering pattern is distinguished with the SALS apparatus. After seven maxima the scattering intensity reaches the level of noise. Agreement of the measurable peaks of the pinhole with the theoretically predicted Fraunhofer diffraction theory is given.

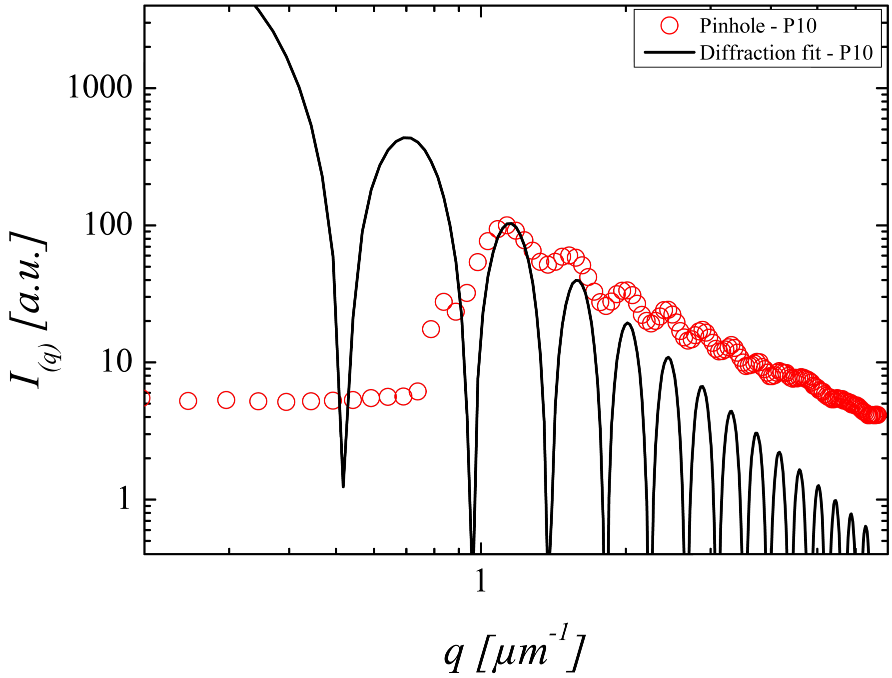

Figure 4.10: A pinhole with radius 10 μm is used to calibrate the SALS apparatus. The measured scattering pattern is shown with red circles. Only one out of two data-points is shown for easier visualization. The theoretical predicted Fraunhofer diffraction pattern is illustrated with a black line.

The measuring of two different aperture radii, with one radius completely detectable at the first five maxima is needed to precisely confirm the alignment of the SALS apparatus. The good agreement of the pattern scattered from the pinholes of 5 and 10 μm with the predicted theory, confirms the alignment of the apparatus.
However, the scattering pattern of a pinhole is collected and analysed equal to a particle in quiescent conditions (see in section 4.2.1 & 4.2.2). In fact, due to the implementation of a fitting procedure, the Matlab routine automatic fits the scattering profile according to the parameters chosen from the user. The parameter of interest is thereby p_1, which shows the relative position of the pinhole to the rest of the detection system. By reaching a fitting value equal to the previous decided value of p_1 by the software, the system is aligned.
Moreover, show the result of the fitting procedure not only the value of p_1, which can be smaller or bigger than the theoretical chosen value, but also gives a graphical feedback of the fit. This graphical results indicates the fitting accuracy in each part of the scattering profile. Thus information is

very helpful to find possible misalignments in the system. Each part of the detection system influence the final scattering pattern in a different way. All in all is the fine adjustment of the SALS apparatus a very tricky and time consuming task, which is mainly a matter of practice and difficult to quantify in this short context.

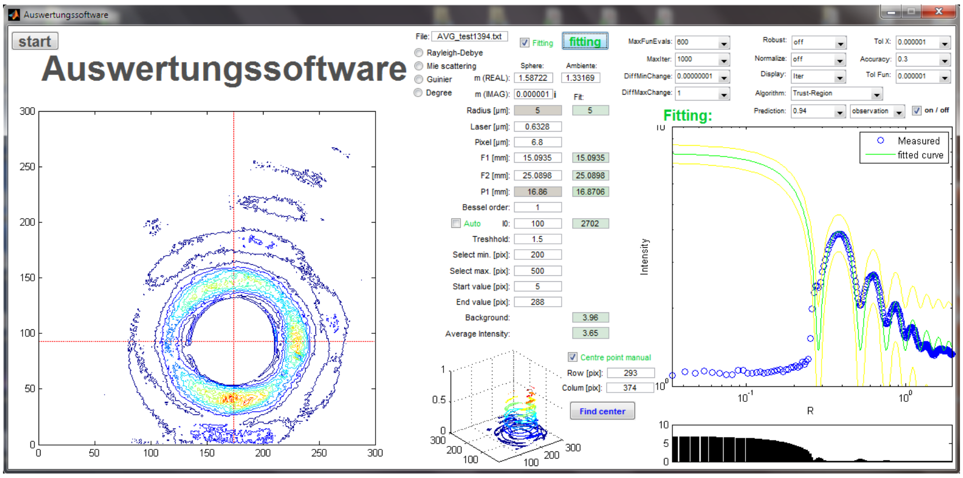

File: AVG_test1394.txt

☑ Fitting

Sphere: Ambiente:

m (REAL): 1.58722 1.33169

m (IMAG): 0.000001 i

Fit:

Radius [µm]: 5 5

Laser [µm]: 0.6328

Pixel [µm]: 6.8

F1 [mm]: 15.0935 15.0935

F2 [mm]: 25.0898 25.0898

P1 [mm]: 16.86 16.8706

Bessel order: 1

☐ Auto I0: 100 2702

Treshhold: 1.5

Select min. [pix]: 200

Select max. [pix]: 500

Start value [pix]: 5

End value [pix]: 288

Background: 3.96

Average Intensity: 3.65

☑ Centre point manual

Row [pix]: 293

Colum [pix]: 374

MaxFunEvals: 600

MaxIter: 1000

DiffMinChange: 0.00000001

DiffMaxChange: 1

Robust: off

Normalize: off

Display: Iter

Algorithm: Trust-Region

Prediction: 0.94 observation ☑ on / off

Tol X: 0.000001

Accuracy: 0.3

Tol Fun: 0.000001

Figure 4.11: Screen-shot of the Matlab routine for fitting a scattering pattern loaded from a pinhole with a radius of 5 μm.

Agreement for all pinhole patterns complete the calibration procedure and measurements with particles can be started.

Chapter 5

RESULTS

Mono-disperse polystyrene particles of different sizes have been measured in quiescent and flow conditions. This chapter is mentioning results from both particle measurement types and the relevance among them. Moreover technical limits of the SALS apparatus are demonstrated during this chapter.

5.1 Quiescent measurements

Measurements of PSL particle with different radii are compared with theoretical predictions of the Lorenz-Mie theory. An overview of all measured particles is given in table 4.1.
Given results are normalized to an exposure time of 1 ms and their corresponding theoretical predicted Lorenz-Mie theory overlayed by a red curve. The particle preparation and data processing step is discussed in the previous chapter 4.
The measured scattering Intensity is plotted against the wave-vector in logarithmic scale with base 10. Linear plot for the abscissa highlight the oscillation of the scattering profile in more detail. In addition indicate consistent scaling of all shown quiescent measurements the relative scattering intensity differences of each particle fraction. Each figure show three separate measurements of one particle size, whereby one representative measurement is highlighted with bigger black circles. Moreover, constant ambient temperature ensure optimal measurement conditions.

PSL 8 in quiescent condition

Figure 5.1 shows the scattering profile of the biggest measured particle (PSL 8) with a nominal radius of 4.01 μm. The scattering profile for the given wave-vector range shows seven minima and maxima. All of this peak positions agree very good with the pre-calculated Lorenz-Mie theory. The less distinct minima of the scattering profile is due to polydispersity of particles,

when more than one particle is measured. Moreover influence the finite pixel size of the detector a more accurate measurement of the minima. It is expected that the height of the first peak is less pronounced due to the stray light subtraction of the beam stop. The following four peaks of the measured PSL 8 particle match the predicted Lorenz-Mie theory very accurate.
At wave-vector larger than 5 μm^{-1} a lightly change of the slope direction for the next two peak heights is recognized. In general is this wave-vector range (for PSL with radius 4 μm) more sensitive to polarization changes of the incident light. In particular matches the slope of a parallel polarized incident light in this case more precise the scattering profile of the measured particle. In fact, figure 5.1 shows only the un-polarized theoretical Lorenz-Mie theory. The average particle radius show a very good agreement to the nominal value of the supplier with 4.0083 μm. The small measured target particle radius difference of 0.0017 μm highlight in this context the accuracy of the developed SALS apparatus.

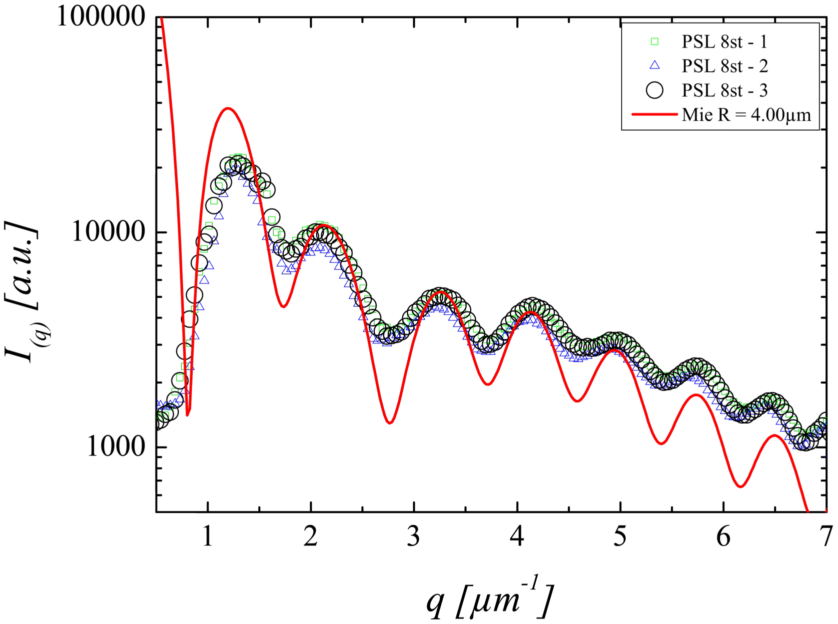

Figure 5.1: SALS measurement of PSL 8 particles in quiescent condition. One representative measurement **(PSL 8st - 3)** is highlighted with big black circles, while the theoretical predicted Lorenz-Mie theory is indicated by a red curve **(Mie R = 4.00μm)**. The radius of the calculated theory is given in the legend of the graph. The measurements are normalized to an exposure time of 1 ms. Only one out of two data-points is shown for easier visualization.

PSL 6 in quiescent condition

The scattering profiles for PSL 6 particles measured in quiescent condition are illustrated in figure 5.2. A significant height difference of the first measured maxima compared to the theoretical predicted Lorenz-Mie theory is measured. Indeed it is expected that the stray light of the beam stop subtraction causes the opposite effect. Therefore the absolute height of the first peak should be less pronounced.
The following two scattering peak heights agree good with theory, while the last two are with significantly lower intensity. All minima and maxima agree according the wave-vector position. The slope difference for the last two peaks is related to a possible polarization shift of the scattered light and effects from the detection system itself.

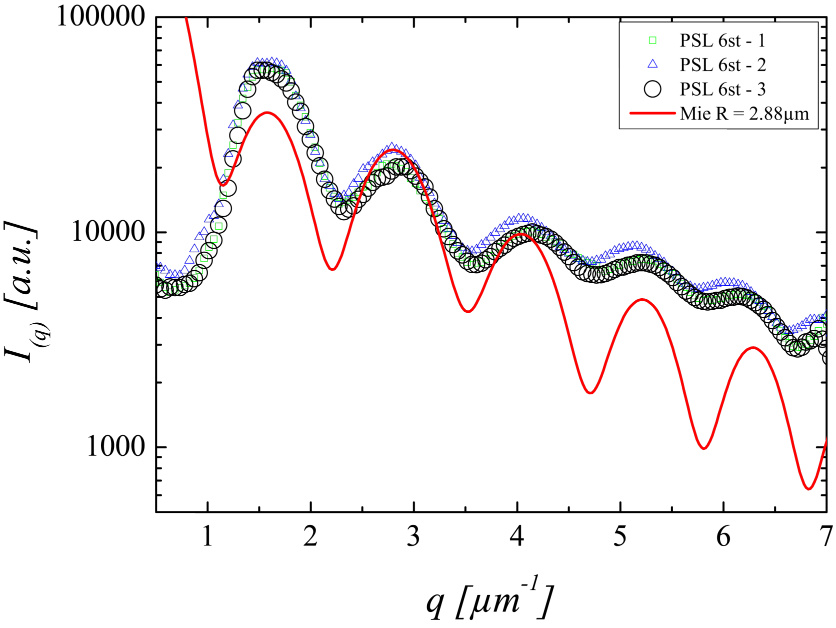

Figure 5.2: SALS measurement of PSL 6 particles in quiescent condition. One representative measurement **(PSL 6st - 3)** is highlighted with big black circles, while the theoretical predicted Lorenz-Mie theory is indicated by a red curve **(Mie R = 2.88μm)**. The radius of the calculated theory is given in the legend of the graph. The measurements are normalized to an exposure time of 1 ms. Only one out of two data-points is shown for easier visualization.

Additionally, illustrate the PSL 6 particle measurement a significant higher polydispersity compared to other results. This effect is mainly recognized by less profound scattering minima. A measured particle radius of 2.883 μm for PSL 6 particle hereby differs clearly from the nominal value of the particle supplier. In general demonstrate the theoretical PSL scattering profile a different oscillation behaviour compared to other measured particle sizes. For a theoretical radius of 3.00 μm, the first peak height is lower than the second one. This particular difference is not present at other particle sizes. Moreover effect small size changes significantly the wave-vector profile from 1 up to 3 μm^{-1}. Nevertheless, a size difference of 0.159 μm is reported for the PSL 6 measurements. Additional size analysis for PSL 6 particles are shown in section 5.3.

PSL 5 in quiescent condition

PSL 5 particle show a very good agreement with the predicted Lorenz-Mie theory. Figure 5.3 show PSL 5 particles with theory.

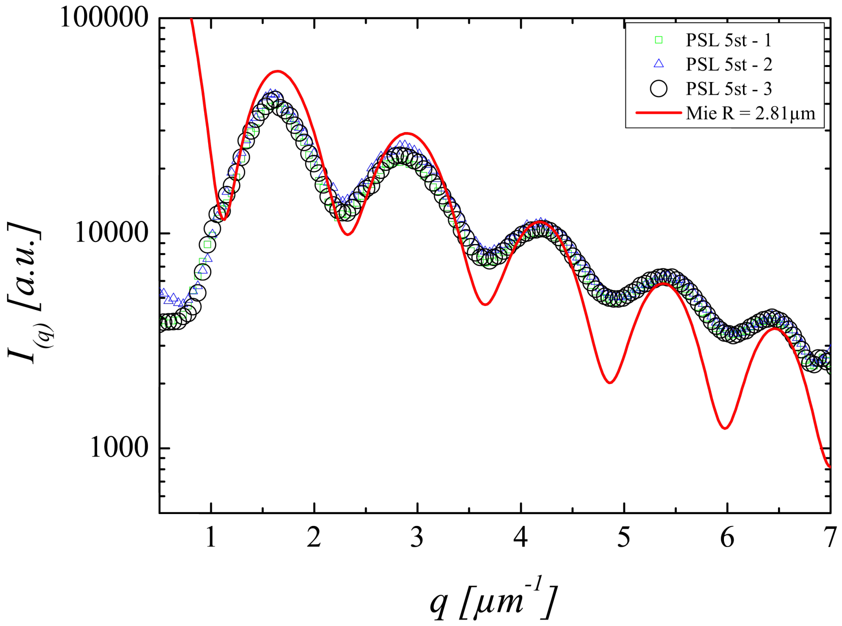

Figure 5.3: SALS measurement of PSL 5 particles in quiescent condition. One representative measurement **(PSL 5st - 3)** is highlighted with big black circles, while the theoretical predicted Lorenz-Mie theory is indicated by a red curve **(Mie R = 2.81μm)**. The radius of the calculated theory is given in the legend of the graph. The measurements are normalized to an exposure time of 1 ms. Only one out of two data-points is shown for easier visualization.

All peak positions fit the theory while a small slope discrepancy is recognized. The scattering profile minima are less profound for higher wave-vector ranges, which is due to possible polydispersity of the measured particles. Moreover is the absolute scattering intensity height at wave-vectors ranging from 1 up 3 $\mu\mathrm{m}^{-1}$ smaller compared to theoretical predictions. The fact of a constant slope discrepancy is reducible to possible mis-alignments of the SALS apparatus or in-accuracy of the background subtraction for this particle fraction.

PSL 5 particle have a similar particle radius compared to PSL 6 particle. The measured average radius for the shown measurements is 2.807 μm, which differs only 0.076 μm from the previous analysed particles.

Indeed, compared to PSL 6 particles is the agreement with theoretical predicted curve much better. The difference between measured particle radius and nominal one from the particle supplier is calculated to be 0.088 μm. Indeed is the standard deviation for PSL 5 particle the highest one of the quiescent tests. (see table 4.1)

PSL 4 in quiescent condition

Figure 5.4 represent the scattering profile of PSL 4 particles. All measured peak height correspond good to the theoretical predicted Lorenz-Mie theory. The first minima of the scattering profile is in a bigger wave-vector range compared to previous analysed particle sizes. Thus fact allow the first time, to mention the measurement of the real first minima of a particle scattering profile.

In fact the apparatus measure the shape and position of the first minima without difficulties. In general are the absolute minima values of the measurement less profound according to te presence of polydispersity. The effect of polarization is negligible small for this kind of particle size. The measured particle radius is calculated to be 2.02 μm, which differs with 0.058 μm from the value of the particle supplier. The scattering intensity in the wave-vector range 1.5 to 3 $\mu\mathrm{m}^{-1}$ is significant smaller compared to previous measurements.

Indeed is the influence of stray light from the beam stop more present for particle in the size range of 2 μm in radius due to the decreased scattering intensity coming from the illuminated particle. The small intensity fluctuations for the first minima and maxima are due to such effects. The figure 5.8b demonstrate this scattering intensity problem in more demonstrative way.

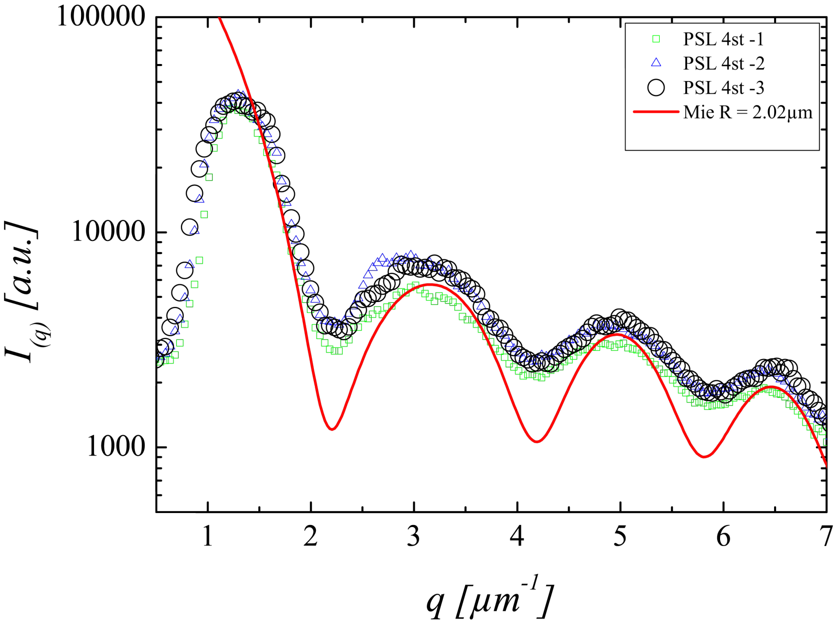

Figure 5.4: SALS measurement of PSL 4 particles in quiescent condition. One representative measurement **(PSL 4st - 3)** is highlighted with big black circles, while the theoretical predicted Lorenz-Mie theory is indicated by a red curve **(Mie R = 2.02μm)**. The radius of the calculated theory is given in the legend of the graph. The measurements are normalized to an exposure time of 1 ms. Only one out of two data-points is shown for easier visualization.

PSL 3 in quiescent condition

PSL 3 particle measurements in quiescent conditions are illustrated in figure 5.5. The resulting scattering profile agree with the predicted calculation. All maxima are measured correct in according to absolute height and position. The influence of the used beam stop is recognized by small variances for the first scattering minima.

As a matter of fact is the first minima near to the minimal wave-vector value the apparatus is able to detect. Moreover is the absolute value of the first minima highly sensitive to small changes of the particle radius and polarization effects. As a result from the comparison from the measured scattering profile with theoretical predictions, a radius of 1.523 μm is calculated. This value differs about 0.120 μm from the particle supplier. In fact is the standard deviation given from the supplier a little bit higher compared to previous particle measurements.

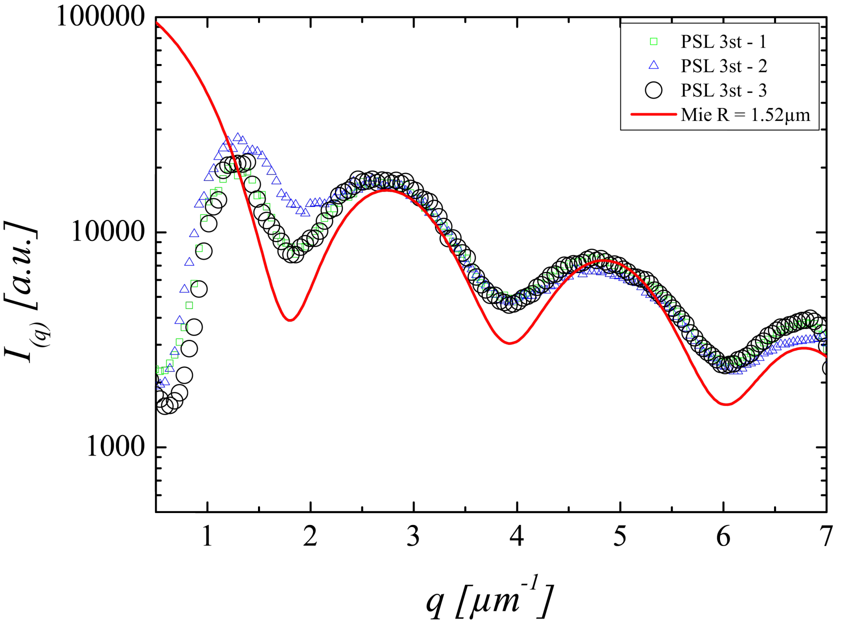

Figure 5.5: SALS measurement of PSL 3 particles in quiescent condition. One representative measurement **(PSL 3st - 3)** is highlighted with big black circles, while the theoretical predicted Lorenz-Mie theory is indicated by a red curve **(Mie R = 1.52μm)**. The radius of the calculated theory is given in the legend of the graph. The measurements are normalized to an exposure time of 1 ms. Only one out of two data-points is shown for easier visualization.

PSL 2 in quiescent condition

The final quiescent measurement is illustrated in figure 5.6 and demonstrate the scattering profiles of different PSL 2 particle. The particle scattering agree widely with the theoretical predictions of the Lorenz-Mie theory.

The first minima is less pronounced compared to the theory. Thus effect is clearly reduced to polydispersity effects of the measured particle radii and the already mentioned polarization effect. The second minima is at the upper edge of the wave-vector range from the SALS apparatus.

The correct measurement of the absolute scattering value for higher wave-vector ranges is difficult, due to the low scattering intensity. All in all is the resulting PSL 2 particle radius given to be 0.95 μm. This value differs only 3 nm from the value of the particle supplier. As a matter of fact change the measured particle radius negligible the shape of the scattering profile for small particle radii changes in the wave-vector range of the system.

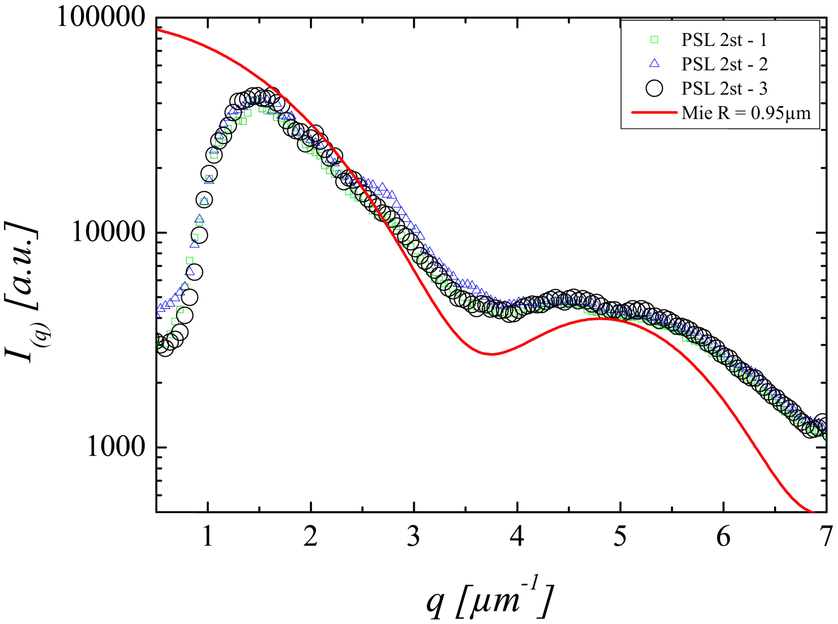

Figure 5.6: SALS measurement of PSL 2 particles in quiescent condition. One representative measurement **(PSL 2st - 3)** is highlighted with big black circles, while the theoretical predicted Lorenz-Mie theory is indicated by a red curve **(Mie R = 0.95μm)**. The radius of the calculated theory is given in the legend of the graph. The measurements are normalized to an exposure time of 1 ms. Only one out of two data-points is shown for easier visualization.

All particle sizes measured in quiescent conditions and the nominal radii from the particle supplier are summarizing in table 5.1.

Particle	**Nominal rad.**	***SD***	**Measured rad.**	***SD***	**Diff.**
PSL 8	4.010	0.049	4.008	0.018	**0.002**
PSL 6	3.042	0.041	2.883	0.006	**0.159**
PSL 5	2.895	0.088	2.807	0.006	**0.088**
PSL 4	2.078	0.031	2.020	0.001	**0.058**
PSL 3	1.644	0.041	1.523	0.006	**0.120**
PSL 2	0.947	0.022	0.950	0.001	**0.003**

Table 5.1: Table of nominal radii from *Sigma-Adlrich* and *Polyscince* particles measured in quiescent condition. All values are given in μm.

The difference among radius size of particle supplier and apparatus is highlighted in the last column of table. Non surprisingly, show table 5.1 for PSL 6 measurement the highest difference between measured and nominal radius. This result is expected due to the more complex scattering pattern for this particle size. To conclude the quiescent measurements figure 5.7 summarize the values of table 5.1.

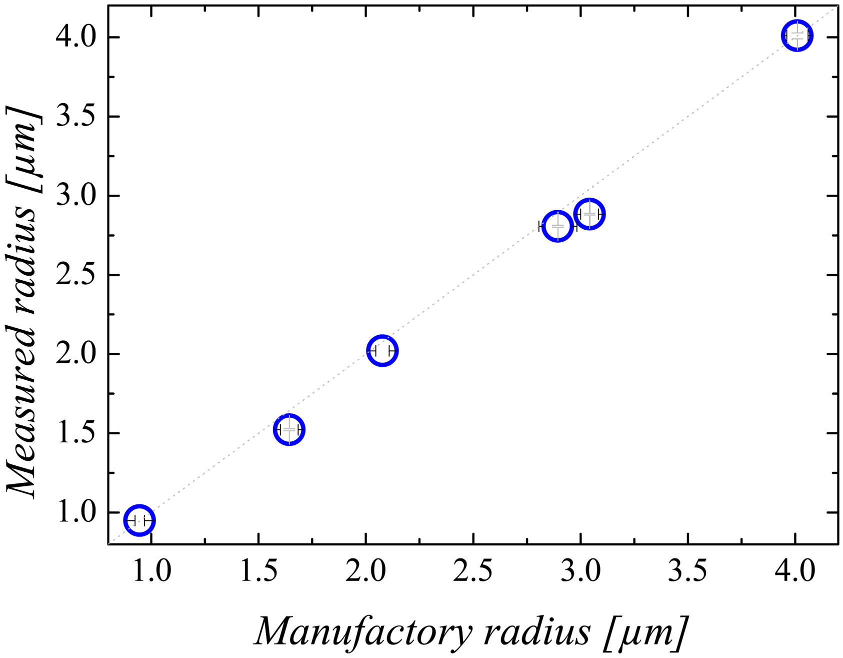

Figure 5.7: The nominal radius of the particle supplier is plotted versus the measured quiescent radius from the SALS apparatus. The dashed grey line indicates a co-incidence of 100%.

The dashed grey line indicates the perfect match among nominal and measured particle radius. All measurements of the SALS apparatus show a reliable result according to the dashed line of figure 5.7. In fact is the average difference between measured and nominal radius from the supplier smaller than 72 nm. Focusing on the relative intensity from one particle measurement to another is illustrated in the figure 5.8. The upper graph 5.8a shows all PSL measurement in quiescent conditions measured with the SALS apparatus, while in the graph below the theoretical predicted Lorenz-Mie theory is demonstrated. The theoretical curves are all calculated with the same incident laser intensity. In fact with both graphs a comparison of the relative curve intensities is possible.

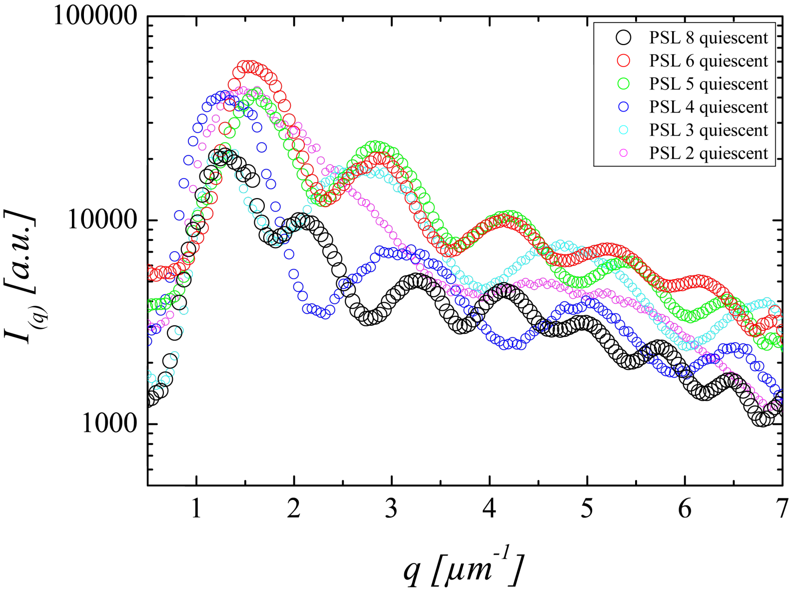

(a) PSL - quiescent measurements

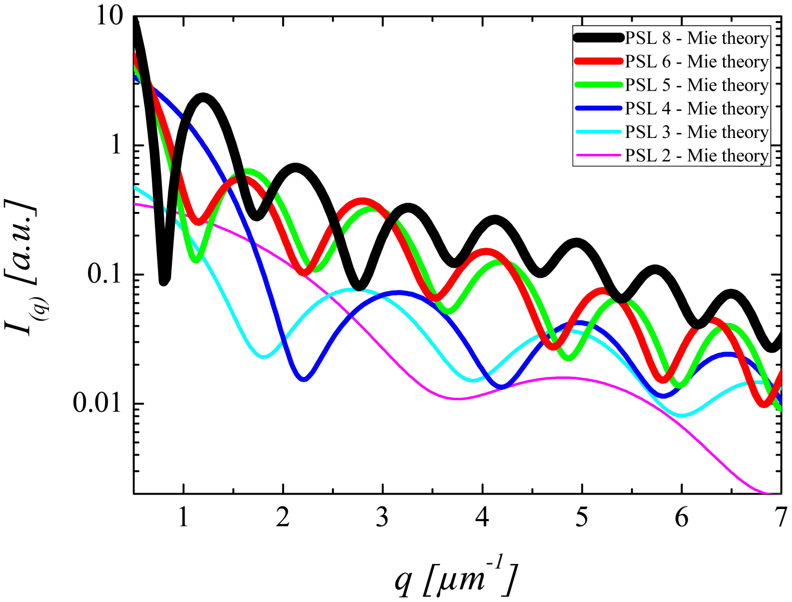

(b) PSL - Lorenz-Mie theory

Figure 5.8: All quiescent measured particles are plotted in graphic a, while the corresponding scattering profile for the theoretical predicted Lorenz-Mie theory is plotted in graph b. All quiescent measurement are normalized to an exposure time of 1 ms. The theoretical curves are calculated for a constant incident light. Only one out of two data-points is shown for easier visualization.

The relative intensity profile of PSL 2 particle is in general the lowest one, due to the smaller particle size. Indeed at the quiescent measurement of the SALS apparatus the intensity of PSL 2 is higher than a PSL 4 scattering profile. This suggests a possible multi-particle scattering during this measurements. In-flow measurements of PSL particle give more indications about the absolute scattering intensity of a single particle.

PSL 3 measurements show a higher scattering intensity compared to PSL 4. This may also be effected due to multi-particle scattering. The measurements of PSL 4, PSL 5 and PSL 6 agree with their relative intensity profile the theoretical predictions, while PSL 8 particles have a significant lower intensity pattern. As mention before, is PSL 8 the only particle size measured with a second density filter (see section 4.1). Due to this fact, is the curve shifted down.

All in all show the quiescent measurements a good agreement with the theoretical predicted Lorenz-Mie theory. All particle sizes are correct measured in size and index of refraction.

5.2 In-flow measurements

All previously in quiescent condition measured PSL particle sizes are now analysed in-flow. Moreover are solutions with mixed particle fractions analysed to prove the multiplex ability of the SALS apparatus. In contrast to quiescent conditions a different microfluidic device is used. The particles are solved in a PEO solution, a viscoelastic fluid to ensure 3D focusing to the centre of the incident beam. (see section 3.3.2)

All shown results are plotted in same conditions as previously for quiescent measurements except the starting scattering intensity, which is set to a lower value. The lower starting value is due to the overall lower scattering intensity for measurements in-flow. The particle preparation and data processing step is discussed in the previous chapter 4.

A pressure pump create a flow rate of 0.153 mm^3/min with a fixed pressure of 350 mbar for all measurements, while the only parameter changes during the different measurements is the exposure time and relative incident light intensity. As a consequence from the quiescent measurements is no additional density filter used for the in-flow measurements.

PSL 8 in-flow condition

The measurement of PSL 8 particles in-flow is first illustrated in figure 5.9. The scattering pattern of the particle shows a good agreement with the theoretical predicted Lorenz-Mie theory. All peaks are measured correct in their position and height. The first peak illustrate a little shift to the right. This effect is due to the presence of the beam stop, which may not be centred precisely enough and therefore generate in-correct background subtraction in

this wave-vector range. Surprisingly good is the absolute scattering intensity of the minima measured.
Indeed by excluding the first minima, indicate the scattering profile a perfect match among measured particle pattern and theory. At wave-vector ranges bigger than 6 μm^{-1} the measurement shows in-accuracy to the Lorenz-Mie theory, which is caused by stray light effects at the edge of the collection lens or the used microfluidic device.
The PSL 8 measurements result in a particle radius of 3.98 μm. Thus radius differs 0.015 μm from the nominal radius from the particle supplier. The measurement of PSL 8 illustrate high accuracy to the scattering profile of the theory, thus opens the ability of the SALS apparatus to characterize precise particle in-flow. In fact show this result the opportunity ot measure small changes of particle size or index of refraction.

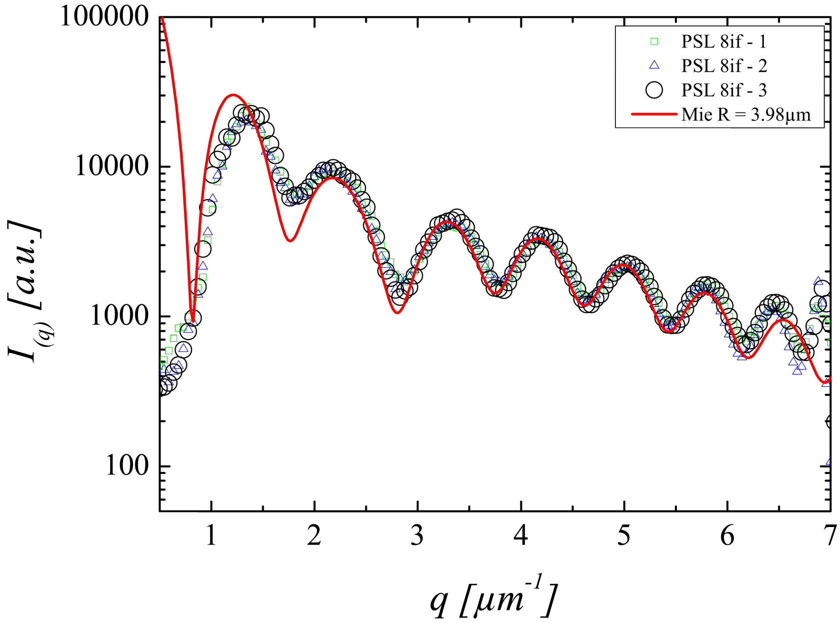

Figure 5.9: SALS measurement of PSL 8 particles in-flow condition. One representative measurement **(PSL 8if - 3)** is highlighted with big black circles, while the theoretical predicted Lorenz-Mie theory is indicated by a red curve **(Mie R = 3.98μm)**. The radius of the calculated theory is given in the legend of the graph. The measurements are normalized to an exposure time of 1 ms. Only one out of two data-points is shown for easier visualization.

PSL 7 in-flow condition

Figure 5.10 demonstrate a particle size which is not listed in table 4.1. In fact the particle size is the result of analyses from PSL 5 measurements. Due to impurity of the solution from the supplier, two different particle fraction are discovered in one solution. The amount of PSL 7 particle is very low compared to the real particle fraction.

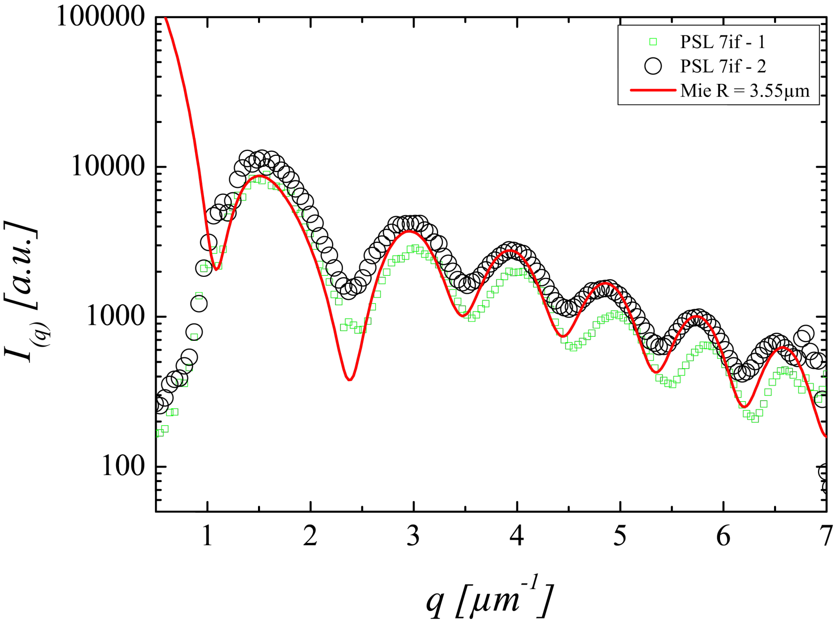

Figure 5.10: SALS measurement of PSL 7 particles in-flow condition. One representative measurement **(PSL 7if - 2)** is highlighted with big black circles, while the theoretical predicted Lorenz-Mie theory is indicated by a red curve **(Mie R = 3.55μm)**. The theoretical predicted Lorenz-Mie theory for the PSL 7if - 1 measurement is not plotted. The radius of the calculated theory is given in the legend of the graph. The measurements are normalized to an exposure time of 1 ms. Only one out of two data-points is shown for easier visualization.

However, due the rare presence of PSL 7 particle, only 2 representative scattering profiles are illustrated in graph 5.10. The first minima is in the wave-vector range close to the beam stop and therefore not precisely detected, while the following minima agree good with theory.
The peak heights of the PSL 7if - 2 particle agree perfect with the theoretical predicted Lorenz-Mie theory except for the first two peaks. The second particle (PSL 7if - 1) measured in this section is showing the polydispersity of

the analysed particle solution. The theoretical predicted Lorenz-Mie theory for this particle size is not illustrated in figure 5.13.

Nevertheless the PSL 7if - 1 particle size is calculated to have a radius of 3.25 μm while the radius of PSL 7if - 2 is given by 3.55 μm. This discrepancy is due to the polydispersity of the particle supplier and show the ability of the SALS apparatus to measure accurate unknown particle sizes.

For the proof of the existence of PSL 7 particles in the PSL 5 solution from the particle supplier additional measurement with an inverted microscope (OLYMPUS[1] - X81) are performed. This measurements identified efficient the existence of the PSL 7 particles. The picture 5.11 shows representative two different particle fractions in one sample.

The upper particle is measured to have a radius of radius of $\simeq 3.5$ μm, while the other measured particle below is measured with a radius of $\simeq 2.9$ μm.

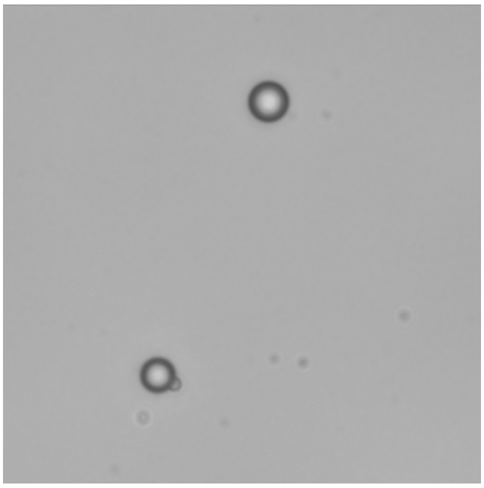

Figure 5.11: Picture of an inverted microscope from Olympus (X81) indicating the existence of PSL 5 and PSL 7 particle in one solution.

PSL 6 in-flow condition

The measurement of PSL 6 particles is illustrated in figure 5.12. The result show similarity to the quiescent measurement. The scattering intensity of the first peak is significant lower compared to the theoretical predicted Lorenz-Mie theory.

The following scattering pattern peaks match good the scattering profile of the theory. In fact, the last peak of the scattering profile is shifted to the left, thus effect is supposed by a systematic alignment errors at this wave-vector range of the SALS apparatus.

---

[1] Olympus Corporation, Shinjuku (TO), Japan

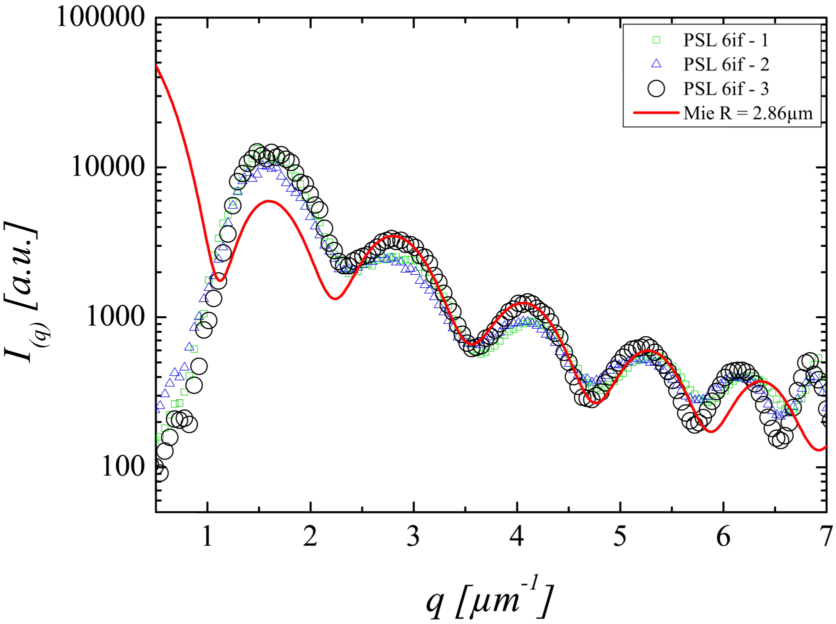

Figure 5.12: SALS measurement of PSL 6 particles in-flow condition. One representative measurement **(PSL 6if - 3)** is highlighted with big black circles, while the theoretical predicted Lorenz-Mie theory is indicated by a red curve **(Mie R = 2.86μm)**. The radius of the calculated theory is given in the legend of the graph. The measurements are normalized to an exposure time of 1 ms. Only one out of two data-points is shown for easier visualization.

No slope mismatch of scattering profile is recognized. All in all is the measured PSL 6 particle accurate recognized by the SALS apparatus. The resulting particle radius is given with 2.859 μm for the PSL 6 measurement. This value match the previous measured quiescent measurement more than the nominal value from the particle supplier.
Further analyses of the real particle size are necessary to validate the measured PSL 6 results. However, the given in-flow result differs with 0.147 μm from the nominal radius.

PSL 5 in-flow condition

Unsurprisingly good fit the PSL 5 measurement the theoretical predicted Lorenz-Mie theory, shown in figure 5.13. All peaks and minima from the scattering pattern agree perfect with theory. The first minima is not recognized precise, according to the mention beam stop presence in this wavevector range.

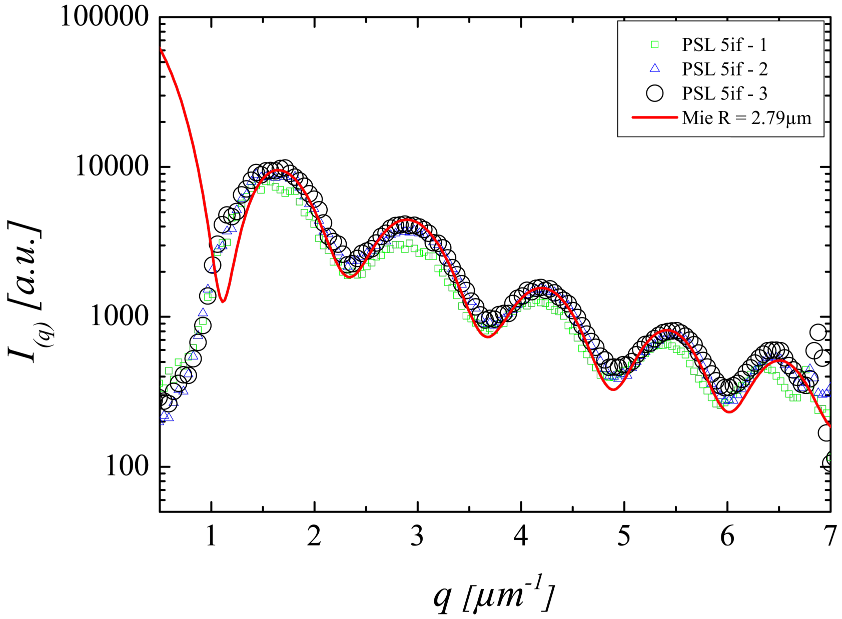

Figure 5.13: SALS measurement of PSL 5 particles in-flow condition. One representative measurement **(PSL 5if - 3)** is highlighted with big black circles, while the theoretical predicted Lorenz-Mie theory is indicated by a red curve **(Mie R = 2.79μm)**. The radius of the calculated theory is given in the legend of the graph. The measurements are normalized to an exposure time of 1 ms. Only one out of two data-points is shown for easier visualization.

The particle radius for the PSL 5 measurement is given with 2.72 μm which differs with about 0.175 μm from the nominal radius from the particle supplier. While in this solution of particle more than one size fraction is present the nominal value from the seller is taken with caution. As a matter of fact are PSL 5 (PSL 7) respectively PSL 3 particle from a different particle supplier.

PSL 4 in-flow condition

The scattering profile of PSL 4 particle measured in-flow is illustrated in figure 5.14. Due to the low scattering intensity the PSL 4 particle present during the measurement, the particle agree well the theoretical predictions. All scattering peaks are recognized, while one of the three measurements show a different scattering profile of the minima quantity. The surprising fact about the scattering values of this measurement (PSL 4if - 2) are the lower scattering intensity quantities compared to the theoretical predicted

Lorenz-Mie theory.

This is the first time such a behaviour is recognized during a SALS measurement with this system. A possible explanation for this effect is given by the polarization of the incident light, which may causes this intensity shift.

Note that the Lorenz-Mie prediction is plotted for an un-polarized incident laser light. Theoretical scattering predications show such effect for perpendicular polarized laser light. Section 6.4 describe the influence of incident laser light polarization in more detail. Moreover a problem with the background subtractions could cause such effects.

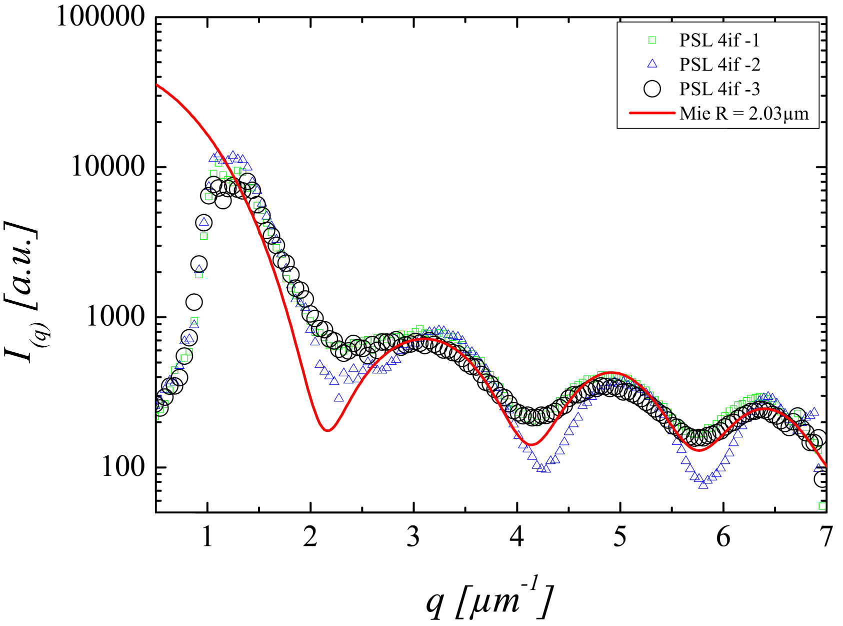

Figure 5.14: SALS measurement of PSL 4 particles in-flow condition. One representative measurement **(PSL 4if - 3)** is highlighted with big black circles, while the theoretical predicted Lorenz-Mie theory is indicated by a red curve **(Mie R = 2.03μm)**. The radius of the calculated theory is given in the legend of the graph. The measurements are normalized to an exposure time of 1 ms. Only one out of two data-points is shown for easier visualization.

The calculated particle radius for PSL 4 particle with 2.029 μm is again close to the nominal radius from the particle supplier. A difference of 0.054 μm agree not alone the nominal value, but also precise the quiescent measurement result.

PSL 3 in-flow condition

Measurements of PSL 3 particles in-flow are plotted in figure 5.15. The scattering profile of the measured particle is less accurate measured from the SALS apparatus compared to previous measurements. The particle size is detected, while the first minima is quantitative to high. Thus effect is due to the presence of the beam stop stray light.
Moreover show the scattering profile a small height discrepancy for the second peak. The peak positions as well the positions of the minima are recognized without any difficulty from the scattering profile from the SALS apparatus.

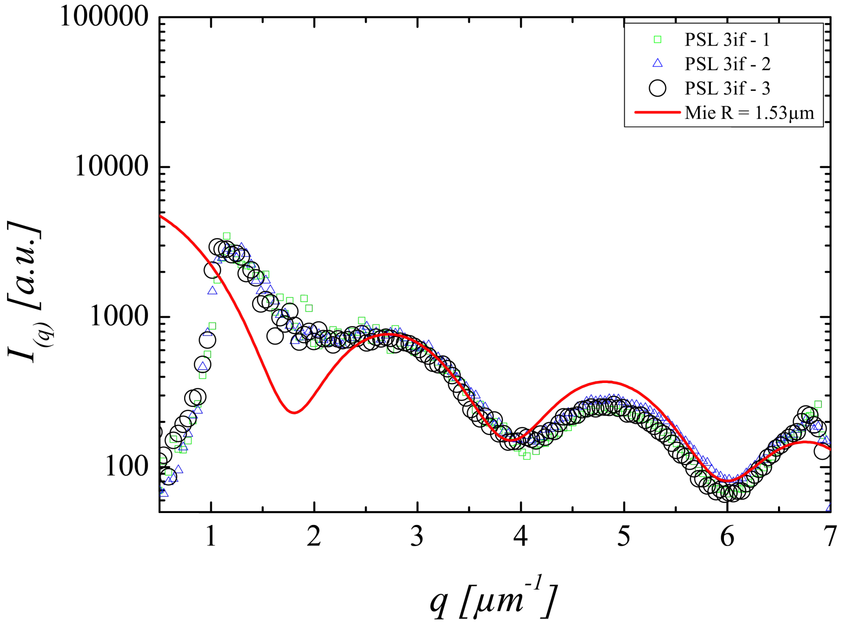

Figure 5.15: SALS measurement of PSL 3 particles in-flow condition. One representative measurement **(PSL 3if - 3)** is highlighted with big black circles, while the theoretical predicted Lorenz-Mie theory is indicated by a red curve **(Mie R = 1.53μm)**. The radius of the calculated theory is given in the legend of the graph. The measurements are normalized to an exposure time of 1 ms. Only one out of two data-points is shown for easier visualization.

Calculation for the PSL 3 particle size results in a radius of 1.530 μm. This value differs more then other measurements due to the particle supplier from the nominal radius. A difference of 0.114 μm is recognized. All in all agree the result more with the quiescent measurement.

PSL 2 in-flow condition

Concluding the in-flow measurements, the PSL 2 particle scattering profile is analysed by the SALS apparatus and demonstrated in figure 5.16. The result agree with the theoretical predictions from the Lorenz-Mie theory in the position of the peaks and slope of the scattering profile.
The only recognized minima is less pronounced in intensity quantity. This is due to possible stray light subtraction problems for this wave-vector range. The particle radius of PSL 2 is given with 0.9229 μm and therefore differs minimal from the nominal value from the particle supplier by 0.018 μm.

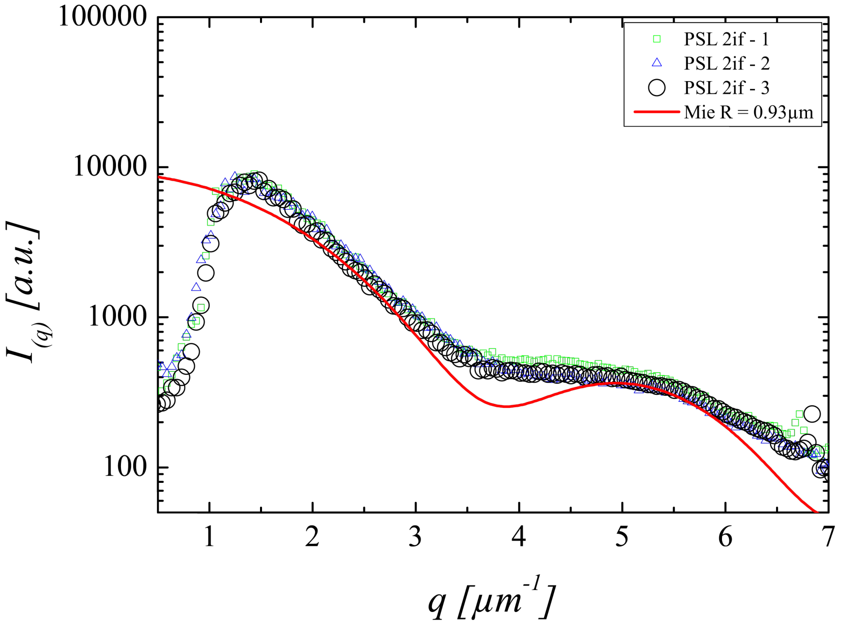

Figure 5.16: SALS measurement of PSL 2 particles in-flow condition. One representative measurement **(PSL 2if - 3)** is highlighted with big black circles, while the theoretical predicted Lorenz-Mie theory is indicated by a red curve **(Mie R = 0.93μm)**. The radius of the calculated theory is given in the legend of the graph. The measurements are normalized to an exposure time of 1 ms. Only one out of two data-points is shown for easier visualization.

The in-flow measurements highlight the possibility to use the SALS apparatus for more sophisticated applications, where detecting and distinguishing micrometric particles size in continuous microfluidic flows is required. Table 5.2 summaries all particle sizes measured in-flow conditions with the SALS apparatus and the nominal radii from the particle supplier.

Particle	**Nominal rad.**	***SD***	**Measured rad.**	***SD***	**Diff.**
PSL 8	4.010	0.049	3.995	0.025	**0.015**
PSL 7			3.433	0.168	
PSL 6	3.042	0.041	2.859	0.011	**0.147**
PSL 5	2.895	0.088	2.720	0.198	**0.175**
PSL 4	2.078	0.031	2.024	0.009	**0.054**
PSL 3	1.644	0.041	1.530	0.008	**0.114**
PSL 2	0.947	0.022	0.929	0.010	**0.018**

Table 5.2: Table of nominal radii from *Sigma-Adlrich* and *Polyscince* particles measured in-flow condition. The nominal radius of PSL 7 particle is not recorded by the supplier. All values are given in μm.

Table 5.2 and figure 5.17, indicate very well the problems during the measurement with PSL 5 and PSL 6 particles.

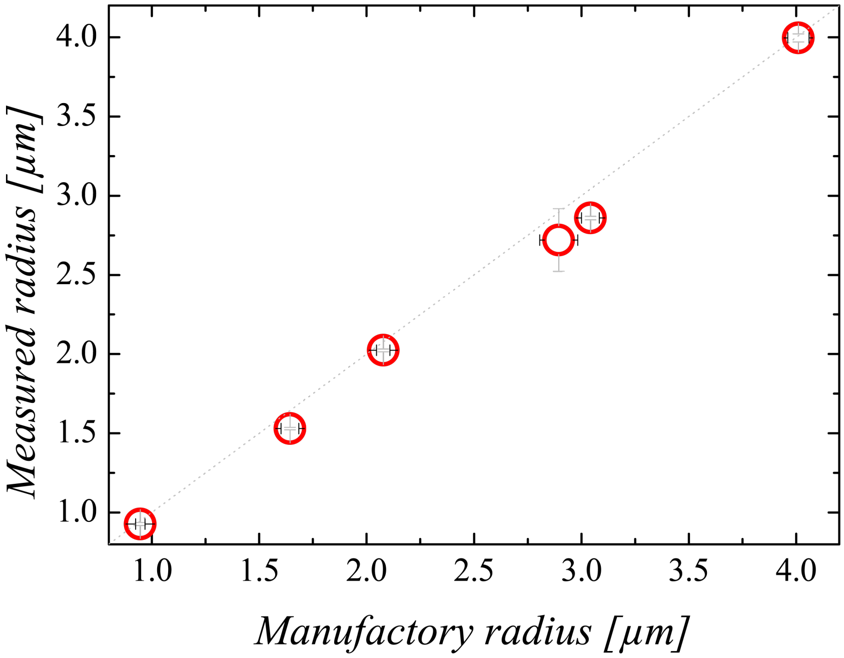

Figure 5.17: The nominal radius of the particle supplier is plotted versus the measured in-flow radius from the SALS apparatus. The dashed grey line indicates a coincidence of 100%.

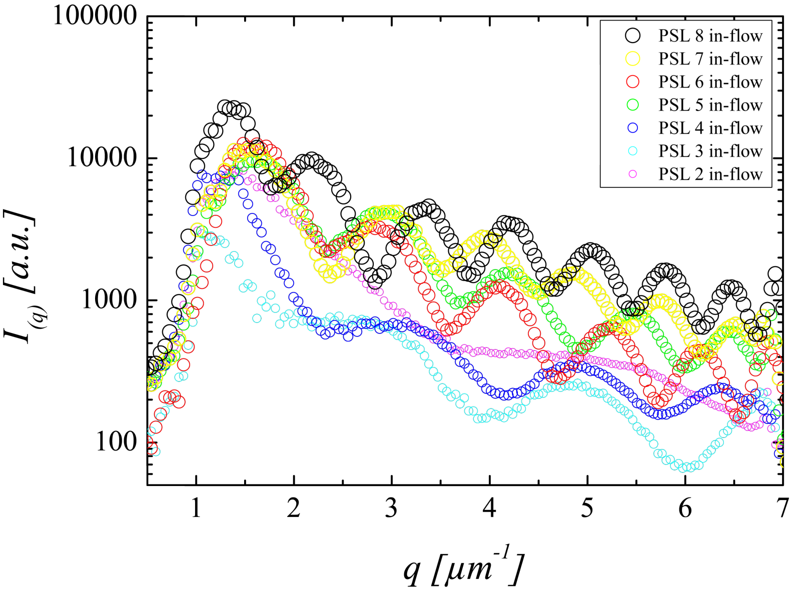

(a) PSL - in-flow measurements

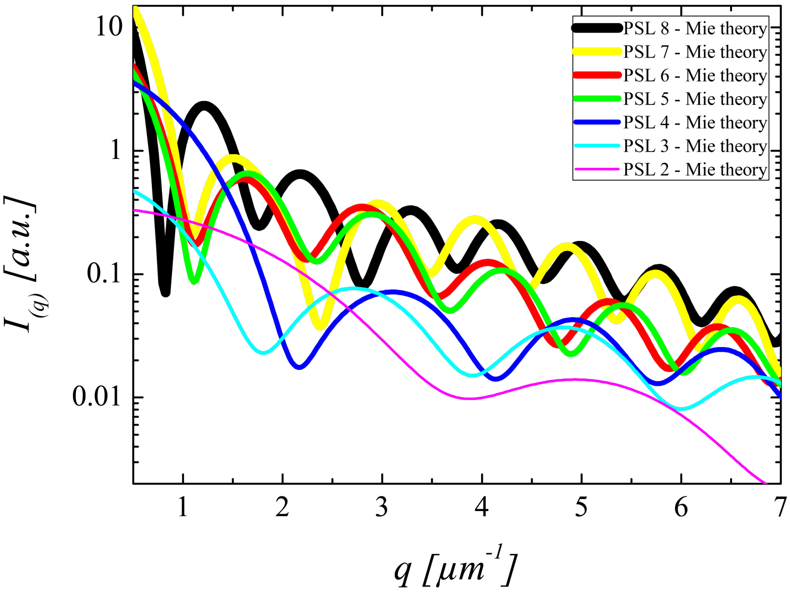

(b) PSL - Lorenz-Mie theory

Figure 5.18: All in-flow measured particles are plotted in graph a, while the corresponding scattering profile for the theoretical predicted Lorenz-Mie theory is plotted in graph b. All measurement are normalized to an exposure time of 1 ms. The Lorenz-Mie theory curves are calculated for a constant incident laser light power. Only one out of two data-points is shown for easier visualization.

Results in figure 5.17 demonstrate a significant higher standard deviation of PSL 5 & PSL 3 particles compared to the rest of the measurements. Due to the fact of measuring single particle, it is excluded that this inaccuracy is caused by the SALS apparatus.

Furthermore could be proved that the SALS apparatus measures particle in-flow at high accuracy without significant loss of precision. Due to the measurement of single particle is the scattering pattern more precise recognized in therms of absolute minima intensities compared to quiescent measurements.

Concluding the analyses of the measured in-flow particle one representative scattering profile for each size is plotted over the wave-vector range of the SALS apparatus. The resulting figure 5.18 illustrate on top the real measurement with the SALS apparatus, while below the theoretical predicted Lorenz-Mie scattering theory is demonstrated.

The absolute intensity height of all curves except PSL 2 agree with theory. This means a PSL 8 particle scatter in relation to a PSL 5 particle at a given wave-vector significant less or more according to the Lorenz-Mie predictions. The theoretical values are calculated for constant incident laser power, while during real measurement fluctuations of the incident light are possible. Moreover alternate the incident laser power with the pre-adjustment before each measurement (see section 4.1).

The absolute scattering intensity measured with PSL 2 particles differs from theory, by possible measurement of multi-particle at the same time. This aspect is difficult to recognize during a measurement, due to the significant low scattering intensity of PSL 2 particle. An average difference among measured and nominal radius from the particle supplier from around 0.087 μm is given. This average value is lightly higher compared to quiescent results, with a difference of 0.015 μm. All in all is the value mainly depending on the polydispersity from the particles.

In addition the measurement of mixed particle solution is tested with the apparatus. This final check is useful to understand the multiplex ability of the SALS apparatus. Therefore a PEO solution mixed with all previous measured particle sizes is prepared. This solution is used with the in-flow device of the system and measured equal to previous mentioned in-flow measurements. All particle fractions are separately recognized from the system over time. Moreover show the measurement results no difference to single particle fraction tests.

The 3D focusing channel used for all in-flow experiments limits the use of smaller or bigger particle size during such experiments. The blockage ratio β is hereby mention in particular (see section 3.3.2).

5.3 SEM measurements

Scanning electron microscope (SEM) measurements are used to control the real nominal particle radius from the particle supplier. Indeed the quiescent and in-flow measurements clearly detected differences from the suppliers. Only PSL particle from Sigma Aldrich are analysed. All in all, the measured particle radii agree with the values from Sigma Aldrich as well as from the SEM measurements with an accuracy of 5 %. In fact, measurement of the *Polyscience* particle are missing in table 5.3. Measurements here fore would further proof the accuracy of the SALS apparatus.

Particle	**Nom. r.**	**Static - r.**	**In-flow - r.**	**SEM - r.**
PSL 8	4.010	4.008	4.140	4.114
PSL 6	3.042	2.883	2.859	2.923
PSL 4	2.078	2.020	2.029	2.002
PSL 2	0.947	0.950	0.929	0.922

Table 5.3: Table of nominal and measured radii from PSL 8, 6, 4 and 2 particle. All values are given in μm.

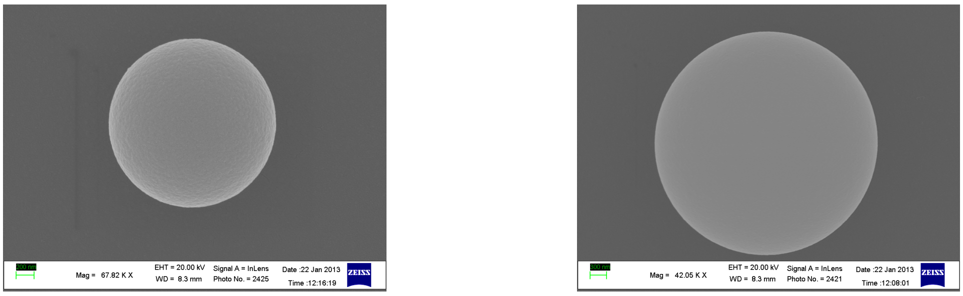

(a) SEM - PSL 2

(b) SEM - PSL 4

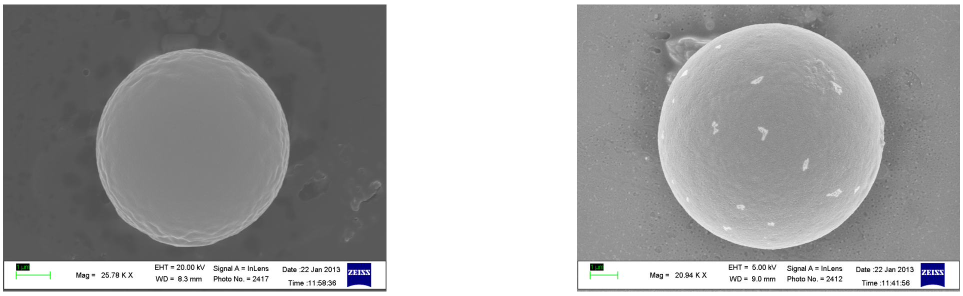

(c) SEM - PSL 6

(d) SEM - PSL 8

Figure 5.19: SEM images of PSL 2, 4, 6 and 8 particle. The electron beam uses different energies ranging from 5 to 20 keV.

5.4 Microgel measurements

Additional to quiescent measurements of PSL particles also microgel (**PNIPAM**[2]) solutions are characterized by the SALS apparatus. This results are preliminary results, which should give a possible future aspect of the SALS apparatus. The analysed microgel is temperature sensitive in size and therefore analysed at constant sample temperature of 24.5°.
The first microgel figure 5.20 show the scattering profile from one microgel size in four different particle concentrations, all measured ten minutes after the sample preparation. The microgel samples are measured with the same sample device (see section 3.3.1) used for quiescent measurements.

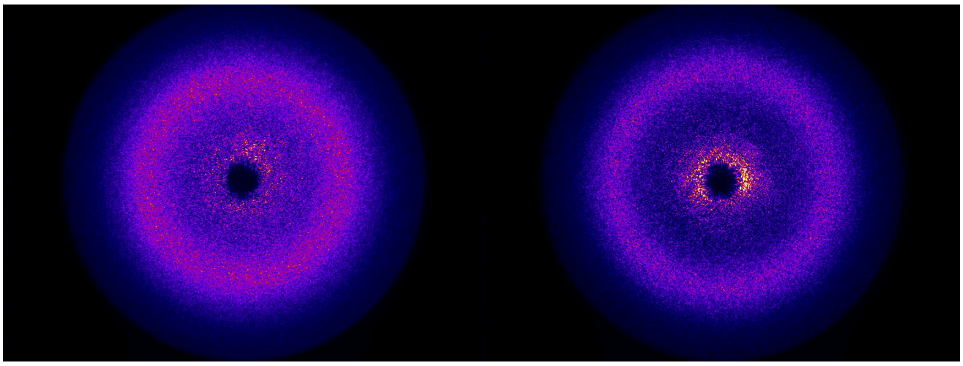

(a) Microgel - C1 (b) Microgel - C2

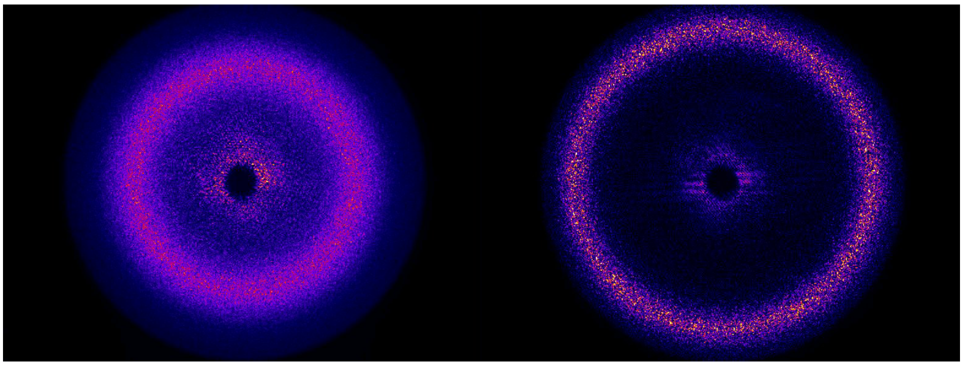

(c) Microgel - C3 (d) Microgel - C4

Figure 5.20: Four different PNIPAM microgel concentrations of one particle size are illustrated in quiescent measurement condition. The measurements highlight in colour the intensity distribution of the scattered light.

The camera used for this measurements is different to previous measurements. The sensor chip of this cooled CCD-camera (PRINCTON INSTRU-

---

[2] Poly N-isopropylacrylamide - is a temperature responsive polymer.

MENTS[3] - Micromax-1300YHS) allow maximum 782x582 pixel by a pixel pitch of 6.8 μm.

Moreover are small changes in the detection system, which do not influence the measurement itself. All in all is the scattering profile for the last microgel *C4* significant different with *C1*, *C2* or *C3*. This result corresponds with the given microgel by changing the particle concentration.

Measurement in-flow conditions are not yet realized. More precise measurements in quiescent conditions by changing ambient temperature over time are from significant interest to be measured.

Preliminary results of another PNIPAM microgel fraction over time showed further interesting results of **Bragg diffraction**[4]. The time period between the two measurements is 2 weeks, while the first measurement is proceeded directly after the sample preparation of the sample.

The scattering profiles shown in figure 5.21 demonstrate what can happen when ***face centred cubic lattice*** of particle is illuminated by the incident laser beam of the SALS apparatus. The measured scattering profiles are recorded at different sample positions.

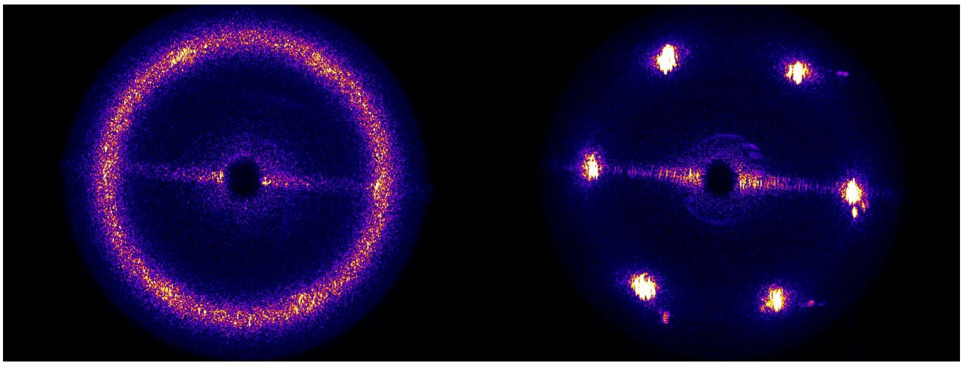

(a) Microgel - time 1

(b) Microgel - time 2

Figure 5.21: PNIPAM microgel measured at time 1 (day zero) and time 2 (day 14). The measurements highlight in colour the intensity distribution of the scattered light. Both samples are measured in quiescent conditions.

Measurement 5.21b is highlighted in colour to illustrate more effective the **bragg scattering peaks**. For more precise analyses of the measured microgel are further test necessary.

---

[3] Princton Instruments (Roper Industries, Inc.), Trenton (MA), USA

[4] Light wave fields interfere with each other either constructively or destructively, producing a diffraction pattern.

Chapter 6

FUTURE ASPECTS

This chapter gives a short outlook, about possible improvements for the SALS apparatus and reflects important properties which may influence the accuracy of the measurement. In particular the influence of alternating index of refraction and wavelength changes is discussed.
In fact the workability of the SALS apparatus described in this work is given. Now the optimization and implementation of additional features is considered.

6.1 Wavelength change

What happens with the scattering pattern of a particle if the incident wavelength changes? This questions is quite easy to answer. Out of formula 3.18 it is seen that the wavelength of the incident beam is the main parameter to influence the wave-vector of the scattering pattern. As a consequence figure 6.1 show, what happens when the incident wavelength is alternated.
The hereby chosen wavelengths are the most widely used in the field of light scattering experiments. Figure 6.1 is plotted for a range of ±40°. This way of plotting express more clear the difference of scattering patterns the SALS apparatus measure. The red curve (λ = 633 nm) corresponds to the used wavelength of the SALS apparatus. By reducing the incident wavelength to 532 nm more than the double of minima and maxima appear out of the scattering pattern. Additional reduction of the wavelength to 404 nm shows even more minima and maxima in scattering profile. Surprisingly illustrated the curve for a wavelength of 780 nm also more minima and maxima in the scattering profile.
In this perspective more minima or maxima of a scattering profile indicate more parameters to characterize a particle. Therefore is a change to a different (smaller) incident wavelength a possible future improvement to analyse even smaller particle sizes with the SALS apparatus.

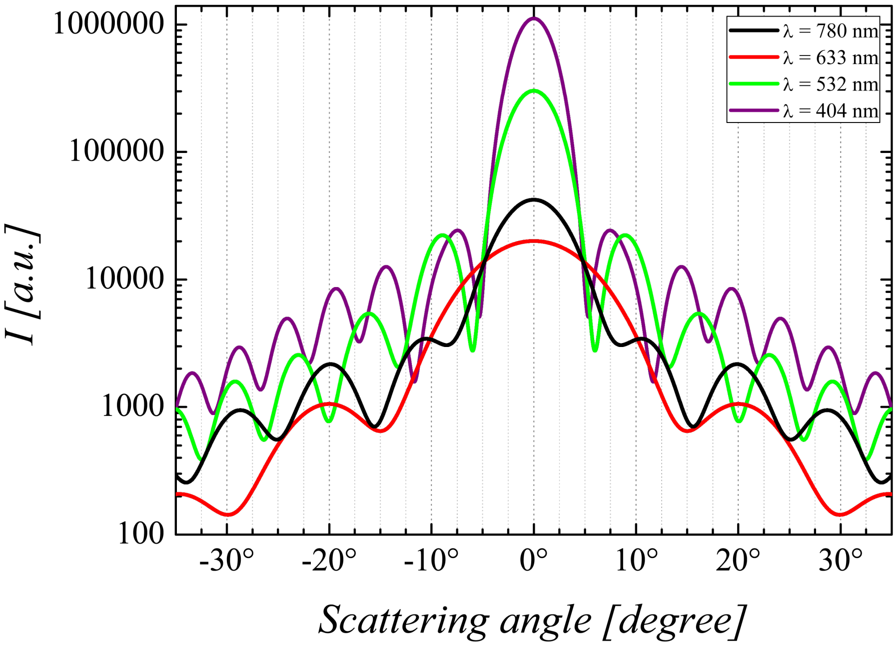

Figure 6.1: PSL 2 scattering patterns over scattering angle of the SALS apparatus is shown for different incident wavelengths.

6.2 Fluorescence implementation

The detection of fluorescence of single particle in-flow opens a new working field for the SALS apparatus. The binding of fluorescence markers is used to recognize target antibodies in a solution of particles. Moreover is the use of different fluorescence ratios at one particle useful to create a kind of bar-code system. Accurate analysis of the measured target particle requires therefore the simultaneously analysis of the fluorescence ratios.

Therefore is an implementation of a photomultiplier tube (PMT) from interest. By reflecting a defined amount of scattered light out of the detection system and the use of bandpass filter an accurate detection with the PMT is possible. The reflected light from the beam stop opens a simple way therefore, while the high ratio of incident light is problematic.

Additional is the implementation of a second PMT for the detection of fluctuations from the incident wavelength from significant interest. Indeed causes the fluctuation of the incident light additional background noise to the detection system. This information can be used to subtract background fluctuations of the scattered light.

6.3 Index of refraction change

The absorption of incident light by a particle, cause i.e.. fluorescence which is defined by the index of refraction. The more precise definition of the refractive index is mention in section 2.1. Figure 6.2 illustrate the influence of absorbing materials. A particle with radius 1 μm and two different material specifications are demonstrating the influence of the refractive index. The curves of figure 6.2 are based on theoretical predicted Lorenz-Mie calculations. The black curve is mentioning a PSL 2 particle without absorption. The corresponding absorption curve is illustrated in grey. A significant reduction of the overall intensity for the whole scattering profile is recognized, while the change of refractive index from 1.58722 for PSL to 1.37 for a biological particle[36] change the scattering profile. By absorption (red curve) a shifting of the minima is recognized. Moreover show the minima a significant more pronounced profile. Surprisingly scatters a particle with absorption at low scattering angles higher. Additionally change the position of the scattering profile minima.

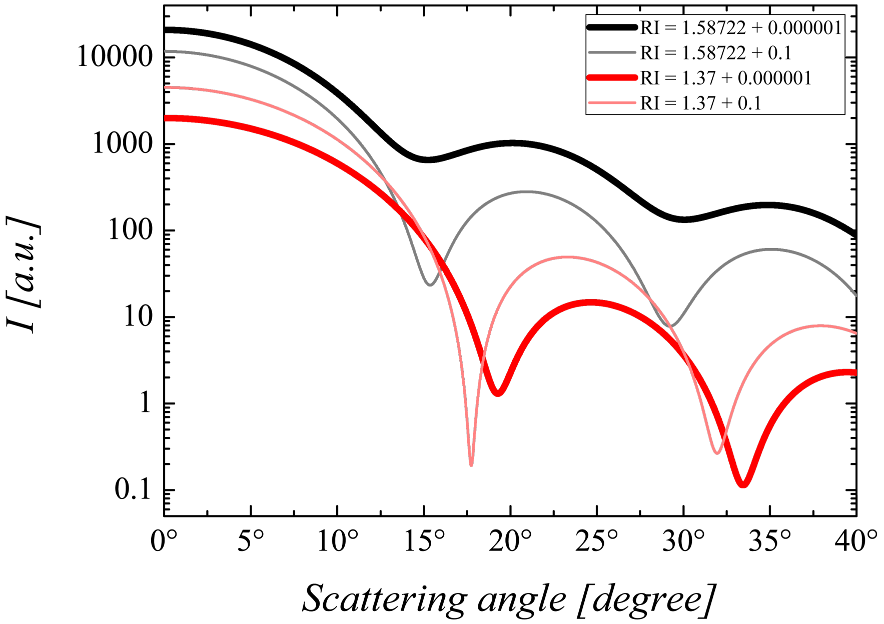

Figure 6.2: The influence of absorption on the scattering profile is demonstrated. Different index of refraction (RI) with and without absorption coefficient are compared. All calculations a based on the Lorenz-Mie theory.

In other words, the correct analysis of a scattering pattern without knowing the index of refraction is challenging. The more precise a SALS apparatus measure the scattering profile the better a particle can be characterized. In particular is the scattering profile for a PSL 6 particle highlighted in figure 6.3. The scattering pattern is changing dramatically according intensity and position of the scattered peaks due to the presence of absorption at the index of refraction.

The here illustrated scattering pattern in red is calculated for the nominal size of PSL 6 particle from the particle supplier. The scattering profile in green is the same particle with absorption. Due to the fact of absorption the scattering pattern is significant more difficult to recognize. Therefore is the correct characterization of this particle size from big interest for the workability of the SALS apparatus.

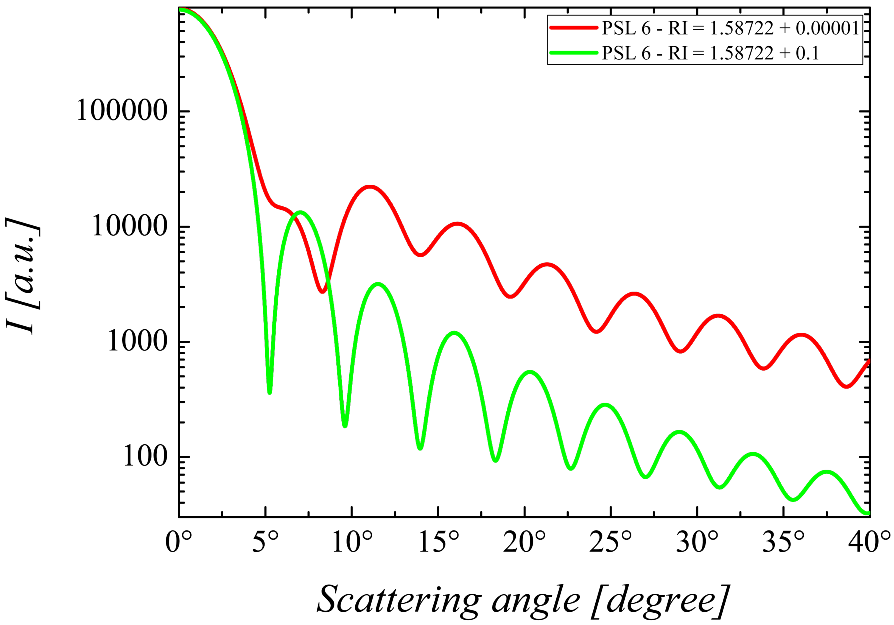

Figure 6.3: The scattering profile of a PSL 6 particle with and without absorption is plotted over the scattering angle of the SALS apparatus.

6.4 Polarization implementation

The intensity of scattered light from a particle depends on the polarizability of the particle. During the quiescent and in-flow measurements the scattering profile indicated possible polarization changes in the scattering profile. In general is polarization defined as the property of waves to oscillate with more than one orientation. Indeed the polarizability depends on the molec-

ular weight of a particle, while the orientation of a linearly polarized (HeNe laser used for the SALS apparatus) electromagnetic wave is thereby defined by the direction of the electric field vector. [4]
All Lorenz-Mie calculations are based on the scattering profile of un-polarized light (see section 2.4). The influence of different polarized incident light is not plotted in all previous graphs while figure 6.4 demonstrate this effect. The incident light is divided in three different polarizations stages; perpendicular, parallel and un-polarized.
The scattering profile of perpendicular polarized incident light change the position of the scattering peaks. Moreover alternate the amplitude of the scattering profile compared to parallel polarized light. The scattering pattern for un-polarized light is the average of both polarization. Figure 6.4 demonstrated the un-polarized scattering profile for a PSL 8 particle by the black curve.

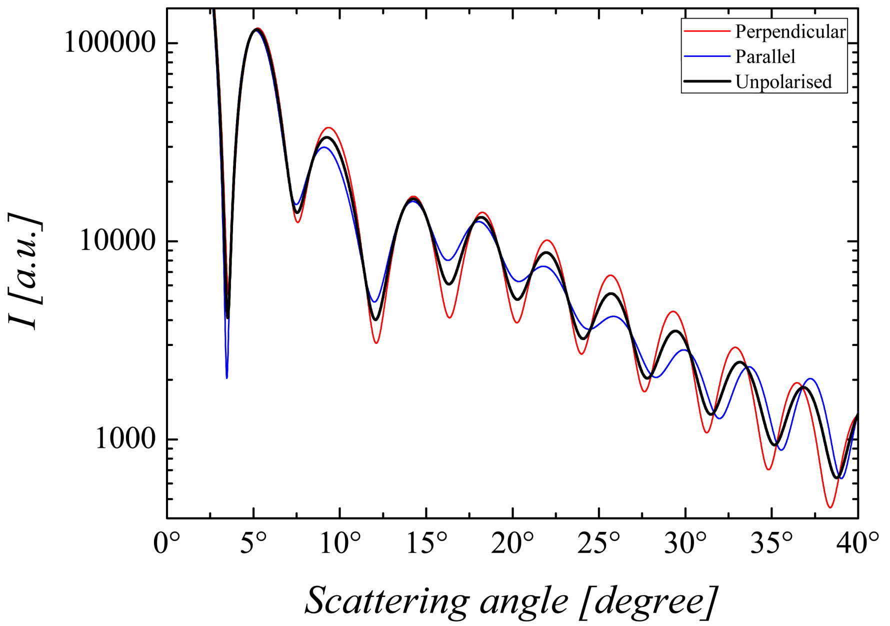

Figure 6.4: The polarization effect of scattered light is demonstrated on PSL 8 scattering profile for perpendicular, parallel and un-polarized incident light.

In conclusion, the accuracy of the SALS apparatus can be improved by the use of polarization filters. This kind of filter work like a band pass where only one specific polarization is passing through the filter. The implementation is simple to handle and economic to realize. No additional change of the acquisition system is necessary by an improved scattering profile measurement.

Chapter 7

CONCLUSION

In this study, a small angle light scattering apparatus has been constructed to measure single microscopic particles in quiescent and flow conditions. A cooled CCD-camera operating at -10°C is used as a detector to collect the scattering patterns of several different polystyrene latex particles ranging from 1 to 4 μm in radius. The optical layout of the apparatus allows to collect the scattered light from $5x10^{-1}$ to $6.8x10^{1}\mu m^{-1}$.

The calibration of the instrument is carried out by using pinholes of different radii from 5 and 10 μm. The collected light scattering patterns from the pinholes are analysed by a homemade Matlab routine to indicate possible dis-alignments of relevant optical parts. In could be proved that the scattering pattern of a spherical particle linearly increases with exposure time. Therefore all measurements in this analysis are measured with different exposure times and finally plotted with an exposure time of 1 ms for easier comparability.

Reliable results are obtained for both quiescent and in-flow measurements. Indeed, the measured scattering profiles are very well described in terms of the Lorenz-Mie theory. All particle sizes measured in quiescent conditions can be identified in-flow, thus opening the possibility to use this apparatus in real multiplex applications. Moreover the existence of an additional particle size in a stock solution from the supplier *Polyscience* could be determined. This finding in-flow conditions demonstrates further the multiplex application of this apparatus. Furthermore a solution of eight different PSL particle sizes was analysed and precisely recognized in-flow, demonstrating the multiplex ability of the apparatus. Systematic errors at low wave-vector ranges are attributed to the presence of stray light coming from the homemade beam stop.

Improvements of the collimation of the incident beam may allow the reduction of the beam stop size and thereby allow for the reaching of a smaller wave-vector range. Finally it is expected that more complex particle shapes, refractive indices as well as absorption coefficients can be characterized with this apparatus. Moreover, the effect of different flow conditions on the structure of single particles or particle assemblies can be determined.

The measurement of PNIPAM microgel particles in-flow condition by alternating the ambient temperature is of significant future interest. Additionally, the measurement of microgel over time with alternating temperature could be further analysed, along with further analysis of the effect of Bragg scattering peaks. The implementation of a fluorescence ratio detection stage as well as polarization filters are additional future tasks for this apparatus. The automation of data acquisition and real time comparison of the scattering profile with pre-calculated scattering intensity values stored in a table could speed up the read-out procedure.

In sum, the small angle light scattering apparatus is available for a wide range of different working fields. The diagnostic field of blood analysis is mentioned as an example as a possible field of work for this apparatus.

Bibliography

[1] Milton Abramowitz and Irene A. Stegun. *Handbook of mathematical functions: with formulas, graphs, and mathematical tables*, volume 55. Dover publications, 1965.

[2] Marcela Alexander and Ross F. Hallett. Small-angle light scattering: Instrumental design and application to particle sizing. *Appl. Opt.*, 38(19):4158–4163, Jul 1999.

[3] Michael Bass and Virendra N Mahajan. *Handbook of Optics: Geometrical and Physical Optics, Polarized Light, Components and Intruments.* McGraw-Hill, 2010.

[4] Craig F. Bohren and Donald R. Huffman. *Absorption and Scattering of Light by Small Particles.* WILEY-VCH Verlag GmbH & Co, 1983.

[5] G. Boyer and V. Sarafis. Two pinhole superresolution using spatial filters. *International Journal for Light and Electron Optics*, 112(4):177–179, 2001.

[6] M. Carpineti, F. Ferri, M. Giglio, E. Paganini, and U. Perini. Salt-induced fast aggregation of polystyrene latex. *The American Physical Society: Review A*, 42:7347–7354, Dec 1990.

[7] Lee W. Casperson, C. Yeh, and Wing F. Yeung. Single particle scattering with focused laser beams. *Appl. Opt.*, 16(4):1104–1107, 1977.

[8] Hyung-Su Chon, Gisung Park, Sang-Bum Lee, Seokchan Yoon, Jaisoon Kim, Jai-Hyung Lee, and Kyungwon An. Dependence of transverse and longitudinal resolutions on incident gaussian beam widths in the illumination part of optical scanning microscopy. *Optical Society of America*, 24(1):60–67, 2007.

[9] S. Chung, S. J. Park, J. K. Kim, C. Chung, D. C. Han, and J. K. Chang. Plastic microchip flow cytometer based on 2- and 3-dimensional hydrodynamic flow focusing. *Microsystem Technologies*, 9:525–533, 2003.

[10] Luca Cipelletti. Monte carlo multiple-scattering simulation and data correction in small-angle static light scattering. *The American Physical Society: Review E*, 55(6):7733–7740, 1997.

[11] Luca Cipelletti and D. A. Weitz. Ultralow-angle dynamic light scattering with a charge coupled device camera based multispeckle, multitau correlator. *American Institute of Physics: Review of Scientific Instruments*, 70(8):3214–3221, 1999.

[12] A. Clebsch. Ueber eine classe von gleichungen, welche nur reelle wurzeln besitzen. *Journal fuer die reine und angewandte Mathematik*, 62:232–245, 1863.

[13] Gaetano D'Avino, Giovanni Romeo, Massimiliano M. Villone, Francesco Greco, Paolo A. Netti, and Pier L. Maffettone. Single line particle focusing induced by viscoelasticity of the suspending liquid: theory, experiments and simulations to design a micropipe flow-focuser. *Lab Chip*, 12(9):1638–1645, 2012.

[14] R. Dorn, S. Quabis, and G. Leuchs. Sharper focus for a radially polarized light beam. *The American Physical Society: Review Letter*, 91(23):233901–4, 2003.

[15] Fabio Ferri. Use of a charge coupled device camera for low-angle elastic light scattering. *American Institute of Physics: Review of Scientific Instruments*, 68(6):2265–2274, jun 1997.

[16] Jess V. Ford, Bobby G. Sumpter, Donald W. Noid, Michael D. Barnes, Steven C. Hill, and David B. Hillis. Domain-size effects in optical diffraction from polymer/composite microparticles. *Physical Chemistry B*, 104(3):495–502, 2000.

[17] Marzio Giglio, Marina Carpineti, Alberto Vailati, and Doriano Brogioli. Near-field intensity correlations of scattered light. *Optical Society of America: Applied Optics*, 40(24):4036–4040, 2001.

[18] Frank T. Gucker and James J. Egan. Measurement of the angular variation of light scattered from single aerosol droplets. *Journal of Colloid Science*, 16(1):68 – 84, 1961.

[19] David W Hahn. Light scattering theory. Technical report, Department of Mechanical and Aerospace Engineering University of Florida, 2009.

[20] George M. Hale and Marvin R. Querry. Optical constants of water in the 200-nm to 200-nm wavelength region. *Appl. Opt.*, 12(3):555–563, Mar 1973.

[21] Pin Han and Hone-Ene Hwang. Far-field spectral intensity characteristics of a time-dependent gaussian pulse from a circular mask with a linear circular apertures array. *International Journal for Light and Electron Optics*, 115(11-12):499–506, 2004.

[22] E. Hecht. *Optics 4th edition*, volume 1. Addison Wesley, 2001.

[23] W. C. Hinds. *Aerosol technology: Properties, behavior, and measurement of airborne particles*, volume 2. Wiley-Interscience, 1999.

[24] H. H. Hopkins. Diffraction theory of laser read-out systems for optical video discs. *Optical Society of America*, 69(1):4–24, 1979.

[25] S. Izawa, A. Yamagishi, and H. Inaba. Analysis of wide-angle laser scattering intensity distribution for discriminating single microscopic particles. *Optics & Lasers in Engineering*, 2(1):57–66, 1981.

[26] Rimas Juskaitis. Measuring the real point spread function of high numerical aperture microscope objective lenses. In James B. Pawley, editor, *Handbook Of Biological Confocal Microscopy*, chapter 11, pages 239–250. Springer US, Boston, MA, 2006.

[27] A. Karlsson, Jiangping He, J. Swartling, and S. Andersson-Engels. Numerical simulations of light scattering by red blood cells. *IEEE Transactions on Biomedical Engineering*, 52(1):13–18, 2005.

[28] Stefka Nikolova Kasarova, Nina Georgieva Sultanova, Christo Dimitrov Ivanov, and Ivan Dechev Nikolov. Analysis of the dispersion of optical plastic materials. *Optical Materials*, 29(11):1481 – 1490, 2007.

[29] Wilbur Kaye and A. J. Havlik. Low angle laser light scattering-absolute calibration. *Optical Society of America: Applied Optics*, 12(3):541–550, 1973.

[30] Wilbur Kaye and J. B. McDaniel. Low-angle laser light scattering - rayleigh factors and depolarization ratios. *Optical Society of America: Applied Optics*, 13(8):1934–1937, 1974.

[31] Milton Kerker. *The scattering of light, and other electromagnetic radiation*, volume 16. Academic Press, New York, 1969.

[32] James B. Knight, Ashvin Vishwanath, James P. Brody, and Robert H. Austin. Hydrodynamic focusing on a silicon chip: Mixing nanoliters in microseconds. *The American Physical Society: Review Letter*, 80(17):3863–3866, 1998.

[33] David Lee Black, Mardson Q. McQuay, and Michel P. Bonin. Laser-based techniques for particle-size measurement: A review of sizing methods and their industrial applications. *Progress in Energy and Combustion Science*, 22(3):267–306, 1996.

[34] N. Lindlein, S. Quabis, U. Peschel, and G. Leuchs. High numerical aperture imaging with different polarization patterns. *Optical Society of America: Optical Express*, 15(9):5827–5842, 2007.

[35] Ximin Liu, Liren Liu, De'an Liu, and Lihua Bai. Design and application of three-zone annular filters. *International Journal for Light and Electron Optics*, 117(10):453–461, 2006.

[36] Valery A. Loiko, Gennady I. Ruban, Olga A. Gritsai, Alexey D. Gruzdev, Svetlana M. Kosmacheva, Natalia V. Goncharova, and Alexander A. Miskevich. Morphometric model of lymphocyte as applied to scanning flow cytometry. *Journal of Quantitative Spectroscopy and Radiative Transfer*, 102(1):73 – 84, 2006.

[37] Xiaole Mao, Sz-Chin S. Lin, Cheng Dong, and Tony J. Huang. Single-layer planar on-chip flow cytometer using microfluidic drifting based three-dimensional (3d) hydrodynamic focusing. *The Royal Society of Chemistry: Lab Chip*, 9(11):1583–1589, 2009.

[38] Francisco F. Medina, Jorge Garcia-Sucerquia, Roman Castaneda, and Giorgio Matteucci. Angular criterion to distinguish between fraunhofer and fresnel diffraction. *International Journal for Light and Electron Optics*, 115(11-12):547–552, 2004.

[39] Ralf Menzel and Martin Ostermeyer. Fundamental mode determination for guaranteeing diffraction limited beam quality of lasers with high output powers. *Optics Communications*, 149(4-6):321–325, 1998.

[40] K. Mielenz. Algorithms for fresnel diffraction at rectangular and circular apertures. *Journal of Research of the National Institute of Standards and Technology*, 103(5):497–509, 1998.

[41] K. Mielenz. On the diffraction limit for lensless imaging. *Journal of Research of the National Institute of Standards and Technology*, 104(5):479–485, 1999.

[42] Alexander I. Norman, Wenhua Zhang, Kathryn L. Beers, and Eric J. Amis. Microfluidic light scattering as a tool to study the structure of aqueous polymer solutions. *Journal of Colloid and Interface Science*, 299(2):580–588, 2006.

[43] Volker Oles. Shear-induced aggregation and breakup of polystyrene latex particles. *Journal of Colloid and Interface Science*, 154(2):351 – 358, 1992.

[44] Tao Peng, Jianlin Zhao, Liangping Xie, Zhijun Ye, Honghao Wei, Jingqin Su, and Junpu Zhao. Simulation analysis of the restraining effect of a spatial filter on a hot image. *Optical Society of America: Applied Optics*, 46(16):3205–3209, 2007.

[45] David T. Phillips, Philip J. Wyatt, and Richard M. Berkman. Measurement of the lorenz-mie scattering of a single particle: Polystyrene latex. *Journal of Colloid and Interface Science*, 34(1):159 – 162, 1970.

[46] V. T. Platonenko and V. V. Strelkov. Single attosecond soft-x-ray pulse generated with a limited laser beam. *Optical Society of America: Applied Optics*, 16(3):435–440, 1999.

[47] S. Quabis, R. Dorn, M. Eberler, O. Gloeckl, and G. Leuchs. Focusing light to a tighter spot. *Optics Communications*, 179(1-6):1–7, 2000.

[48] S. Quabis, R. Dorn, M. Eberler, O. Gloeckl, and G. Leuchs. The focus of light - theoretical calculation and experimental tomographic reconstruction. *Applied Physics B: Lasers and Optics*, 72:109–113, 2001.

[49] Arturo Quirantes, Rosario Plaza, and Angel Delgado. Static light scattering study of size parameters in core-shell colloidal systems. *Journal of Colloid and Interface Science*, 189(2):236–241, 1997.

[50] D'Avino G. Greco F. Netii P.A. Maffettone P.L. Romeo, G. Viscoelastic flow focusing in micorchannels: scalling properties of the particle radial distributions. *Lab on a Chip*, 2013. Accepted.

[51] F. Scheffold and R. Cerbino. New trends in light scattering. *Current Opinion in Colloid & Interface Science*, 12(1):50–57, 2007.

[52] Eric L. Shirley. Revised formulas for diffraction effects with point and extended sources. *Optical Society of America: Applied Optics*, 37(28):6581–6590, 1998.

[53] Kevin E. Spaulding and G. Michael Morris. Achromatic waveguide lenses. *Optical Society of America: Applied Optics*, 30(18):2558–2569, 1991.

[54] W. Szymanski and P.E. Wagner. Aerosol size distribution during a condensational growth process. measurements and comparison with theory. *Atmospheric Environment (1967)*, 17(11):2271 – 2276, 1983.

[55] Chien-Hsiung Tsai, Hui-Hsiung Hou, and Lung-Ming Fu. An optimal three-dimensional focusing technique for micro-flow cytometers. *Microfluidics and Nanofluidics*, 5:827–836, 2008.

[56] Hendrik Christoffel van de Hulst. *Light scattering by small particles.* Dover publications, 1981.

[57] Jan van Heiningen. *Ultra-small angle light scattering: Apparatus design optimization.* PhD thesis, McGill University (Canada), 2005.

[58] Peter N. Wild and Joshua Swithenbank. Beam stop and vignetting effects in particle size measurements by laser diffraction. *Optical Society of America: Applied Optics*, 25(19):3520–3526, 1986.

[59] A.P.Y. Wong and P. Wiltzius. Dynamic light scattering with a ccd camera. *The American Physical Society: Review of Scientific Instruments*, 64(9):2547–2549, 1993.

[60] Philip J. Wyatt. Differential light scattering: a physical method for identifying living bacterial cells. *Appl. Opt.*, 7(10):1879–1896, Oct 1968.

[61] Qinfeng Xu. Fourier treatment to the diffractive optical element composed of fresnel zone and pinholes. *International Journal for Light and Electron Optics*, 121(21):1941–1943, Nov 2010.

[62] Renliang Xu. *Particle characterization: light scattering methods*, volume 13. Springer, 2001.

[63] Ren Yang, Daniel L. Feeback, and Wanjun Wang. Microfabrication and test of a three-dimensional polymer hydro-focusing unit for flow cytometry applications. *Sensors and Actuators A: Physical*, 118(2):259–267, Feb 2005.

[64] Maojin Yun, Liren Liu, Jianfeng Sun, and De'an Liu. Three-dimensional superresolution by three-zone complex pupil filters. *Optical Society of America: Applied Optics*, 22(2):272–277, 2005.

[65] Guangpu Zhao, Xiaoling Ji, and Baida LÃij. Approximate analytical propagation equations of gaussian beams through hard-aperture optics. *International Journal for Light and Electron Optics*, 114(6):241–245, 2003.

List of Abbreviations

α	Half angle divergence of incident beam
Δ_p	Pressure gradient
$\dot{\gamma}$	Shear rate
η	Viscosity of microfluidic liquid
κ	Imaginary part of index of refraction
λ	Wavelength
λ_0	Wavelength in vacuum
λ_t	Relaxation time of a liquid
μ	Magnetic permeability of medium
μ_1	Magnetic permeability of a sphere
$\pi_n(\cos\theta)$	Angular scattering coefficient
Ψ_1	First normal stress difference coefficient
Ψ_2	Second normal stress difference coefficient
$\sigma\ SD$	Standard deviation
$\tau_n(\cos\theta)$	Angular scattering coefficient
θ	Scattering angle
θ_b	Incident beam divergence
θ_{max}	Maximum scattering angle arriving D
θ_{min}	Minimum scattering angle arriving D
A	Absorption coefficient
a	Particle radius
a_n	Scattering coefficient - external
b_n	Scattering coefficient - external
BS	Beam stop
c	Velocity of light
c_n	Scattering coefficient - internal
CA	Clear Aperture of a lens
CCD	Charged Couple Device
CT	Centre Thickness of a lens
D	Detector of the apparatus
D_0	Beam diameter at L4
D_1	Beam diameter at L5
D_{BS}	Beam diameter at BS
D_{L5}	Lens diameter of L5

d_n	Scattering coefficient - internal
DLS	Dynamic Light Scattering
EFL	Effective focal length
EFL_1	Effective focal length of L5
EFL_2	Effective focal length of L6
ELS	Elastic Light Scattering
ET	Edge Thickness of a lens
ET	Exposure Time
f	Frequency
FC	Ferrule Connector for single mode fibre
$GRIN$	Gradient Index
H	Principal plane of a lens
H_1	Principal plane of L5
H_2	Principal plane of L6
$h_n^{(1)}$	Spherical Hankel function of first kind
I_0	Incident light intensity
I_θ	Scattering intensity
$IELS$	In-Elastic Light Scattering
If_θ	Fitted scattering intensity
J_1	Bessel function of zero order
$j_n(z)$	Spherical Bessel function of first order
k	Wave-number
L	Microfluidic channel - length
$L1$	Lens of beam expander inlet
$L2$	Lens of beam expander outlet
$L3$	Lens for focusing incident beam
$L4$	Lens for collimation of incident beam
$L5$	Aspheric lens for collection of scattered light
$L6$	Plano-convex lens to map scattered light on D
l_b	Distance between L4 and S
l_{col}	Collimation length of the apparatus
m	Index of refraction
M_1	Magnification of L5
M_2	Magnification of L6
m_m	Index of refraction of ambient medium
m_r	Relative index of refraction
M_w	Molecular weight
MDa	Megadalton
n	Expansions index
n_r	Real part of index of refraction
NA	Numerical Aperture
$p1$	Front - effective focal length of L5
$P10$	Pinhole with aperture radius 10 μm

$p2$	Front - effective focal length of L6
$P5$	Pinhole with aperture radius 5 μm
PEO	Polyethylene oxide
PMT	Photomultiplier tube
$PNIPAM$	PolyN-isopropylacrlyamide
PSL	Microfluidic channel - blockage ratio
PSL	Polystyrene Latex
$PT1000$	Resistance Thermometer with 1000 Ohm
Q	Flow rate
q	Wave-vector
$q1$	Rear - effective focal length of L5
$q2$	Rear - effective focal length of L6
$QELS$	Quasi-Elastic Light Scattering
R	Distance between detector and particle
r'	Wave-vector position at beam stop
r_c	Microfluidic channel - inner radius
RI	Refractive Index
rs	Wave-vector radius on detector
S	Target particle plane
S_1	Complex scattering amplitude
S_2	Complex scattering amplitude
$SALS$	Small Angle Light Scattering
SEM	Scanning Electron Microscope
SLS	Static Light Scattering
TEM	Transverse Electro Magnetic
u	Position of first dark airy disk ring
V_m	Velocity in ambient material
V_p	Velocity in particle material
x	Size parameter
$y_n(z)$	Spherical Bessel function of first order
z	Coefficient for scattering coefficients

Appendix A

Equipment

Part (name)	Supplier	Cat. No.
Temperature module:		
Peltier Element	Eureca	TEC1R-17-22-9.5-23/78-B
Peltier Controller	Minco	TC0806-RS232
Thermistor (PT1000)	RS Components	362-9907
Sample device:		
Microslide	Vitrocom	W3520-050
Cappilary Tube	Unifibre (Molex)	TSP0475375
Ferrule	Nanoport	6-32 FB-360/510μm
Cameras:		
Camera - Setup	Hamamatsu	C11440-22CU
Camera - Microgel	Princton Instruments	Micromax-1300YHS
Camera - Beam Shape	Imperx	IGV-B0620
Calibration:		
Power and Energy Meter	Thorlabs	PM100D
Pinhole (P5)	Edmund Optics	NT56-276
Pinhole (P10)	Edmund Optics	NT56-279

Table A.1: SALS system equipment.

Part (name)	Supplier	Cat. No.	Items
Lenses:			
Achromatic Lens (L3)	Edmund Optics	NT47712-INK	1
GRIN Lens (L4)	Edmund Optics	NT64-515	1
Aspheric Lens (L5)	Edmund Optics	NT672-45	1
Plano-Convex Lens (L6)	Thorlabs	LA1951-A	1
Beam stop (BS):			
1/4 Wave N-BK7 Window	Edmund Optics	NT49-141	1
Rod Lens (BS)	Edmund Optics	NT54-092	1
Incident light:			
Laser Source	Melles Griot	05LHP151	1
Laser Mount	Thorlabs	C1502/M	1
Beam Expander (20x)	Edmund Optics	NT55-579	1
Optical Mirror	Thorlabs	KM200-E02	2
Optical fibre:			
Single Mode Fiber	Thorlabs	P1-630A-FC-1	1
FC/APC Fiber Adapter	Thorlabs	SM1FCA	1
SALS general:			
Breadboard	Melles Griot	07OBH509	1
XY-stage	Thorlabs	DT12XY/M	2
XY Translator	Thorlabs	ST1XY-S/M	1
Z-Axis Translation Mount	Thorlabs	SM1Z	2
Iris Diaphragm	Thorlabs	SM1D12	1
Absorptive ND Filter	Thorlabs	NE10B	1
Absorptive ND Filter	Thorlabs	NE20B	1
Kinematic Mount	Edmund Optics	NT58-872	2
Kinematic Mount	Thorlabs	KM100T	1
Translating Lens Mount	Thorlabs	LM1XY/M	1

Table A.2: SALS apparatus equipment. Not during this work mention auxiliary items of the SALS apparatus are not listed.

Appendix B

Manuscript - Optical Metrology - Munich 16-5-2013

Manuscript of SALS apparatus for oral speech at the **World of Photonics Congress** (12-16, 2013).

Section:
OPTICAL METROLOGY - organized by SPIE Europe Ltd.

Conference 8792:
Optical Methods for Inspection, Characterization and Imaging of Biomaterials

Sub-conference:
Optical Methods for Inspection, Characterization and Imaging of Biomaterials

Proceedings of SPIE:
Vol. 8792

Conference Chairs:
Pietro Ferraro, Istituto Nazionale di Ottica (Italy);
Monika Ritsch-Marte, Innsbruck Medical Univ. (Austria)

Small angle light scattering characterization of single micrometric particles in microfluidic flows

David Dannhauser[a], Giovanni Romeo[a], Filippo Causa[a], Paolo A. Netti[a]

[a]Center for Advanced Biomaterials for Healthcare@CRIB, Istituto Italiano di Tecnologia (IIT), Largo Barsanti e Matteucci 53, 80125 Naples, Italy & Interdisciplinary Research Centre on Biomaterials (CRIB), University Federico II, Piazzale Tecchio 80, 80125 Naples, Italy.

ABSTRACT

A CCD-camera based small angle light scattering (SALS) apparatus has been used to characterize single micrometric particles flowing in a micro-channel. The measured scattering vector spans the range $2x10^{-2} - 6.8x10^{1}\mu m^{-1}$. The incident laser light is collimated to a spot of about 50 μm in diameter at the sample position with a divergence lower than 0.045 rad. Such small collimated laser beam opens the possibility to perform on-line SALS of micron-sized particles flowing in micro-channels. By properly designing the micro-channel and using a viscoelastic liquid as suspending medium we are able to realize a precise 3D focusing of the target particles. The forward scattering emitted from the particle is collected by a lens with high numerical aperture. At the focal point of that lens a homemade beam stop is blocking the incident light. Finally, a second lens maps the scattered light on the CCD sensor, allowing to obtain far field images on short distances. Measurements with mono-disperse polystyrene particles, both in quiescent and in-flow conditions have been realized. Experiments in-flow allow to measure the single particle scattering. Results are validated by comparison with calculations based on the Lorenz-Mie theory. The quality of the measured intensity profiles confirms the possibility to use our apparatus in real multiplex applications, with particles down to 1 μm in radius.

Keywords: Small angle light scattering, multiplex, detection in-flow, micro-channel, single particle, Lorenz-Mie theory

1. INTRODUCTION

The most complete optical characterization of micrometric particle provides a distinct light scattering pattern, and light scattering is, thus, one of the most powerful tools to validate micrometric particles.

Today there are several well established and routinely used light scattering setups for the classification of micro- and nano-metric particles, which can be divided into static light scattering (SLS) products[1] and dynamic light scattering (DLS) ones.[2–4] These systems usually measure the scattering from an ensemble of particles. Scattering from single particle is required for counting and sizing in cytometry-like applications. In these applications flashes of light of gas-suspended particles flowing through a small illuminated aperture one at a time are measured at a fixed scattering angle. The light intensity contains informations about the refractive index and size of the particles.[5] A fundamental limitation of this technology is the need of *a-priori* knowledge of the refractive index of the measured particle.

The most direct and effective approach to improve such a light scattering system is the use of a multi-element sensor, such as the pixel array of a charged coupled device (CCD) camera, which is used to collect the signal at many different scattering angles simultaneously.[6,7] There has been a rapid development on small angle light scattering (SALS) techniques in recent years, which is essentially related to the progress in the CCD sensor technology.[8] Modern SALS devices can typically cover a range of scattering vectors going from $2x10^{-2}$ to $2x10^{1}\mu m^{-1}$ which corresponds a span from 0.1° to 10° for visible wavelengths of light.[8]

A SALS apparatus of *Norman* et al. has recently shown the formation and subsequent size distribution of multilamellar vescicles of diblock copolymers in a flow stream.[9] Also *Quirantes* and his co-workers showed the applicability of SLS to characterize spherical core shell particles.[10] In fact, a variety of techniques for focusing and collecting scattered light is present in literature.[11] However, collimating a laser beam in micro-channels with

---

Further author information: E-mail: david.dannhauser@iit.it, Telephone: +39 (081) 1993 3111.

diameters smaller than a few hundreds μm is a difficult task. As a consequence the implementation of SALS as a detection tool in microfluidic devices has been limited until now.[12]
In this work we overcome this issue, and describe a SALS system able to measure the scattering profile of single, micrometric particles flowing in a microfluidic-channel.

2. EXPERIMENTAL SETUP

The experimental setup schematically shown in figure 1 allows to measure the light scattered at different (small) angles by single micrometric particles flowing in a micro-channel. The scattering vector spans from $5x10^{-1}$ to $6.8x10^{1}\mu m^{-1}$, corresponding to scattering angles of 2° to 31°. The referring light source *(MELLES GRIOT - 05LHP151)* is a 5 mW polarized HeNe laser, operating at a wavelength of 632.8 nm with a beam waist diameter $1/e^2 = 0.80$ mm and full angle divergence $2\alpha = 1.00$ mrad. The output of the laser is directly aligned in a beam expander *(L1, L2 - EDMUND OPTICS - NT55-582)*, which enlarges the beam waist 20 times. A series of mirrors is used to adjust the expanded laser light, before an achromatic lens *(L3 - EDMUND OPTICS - 47712-INK)* with a focal length of 125 mm focuses the beam in a single mode fiber *(THORLABS - P1-630A-FC-1)*.

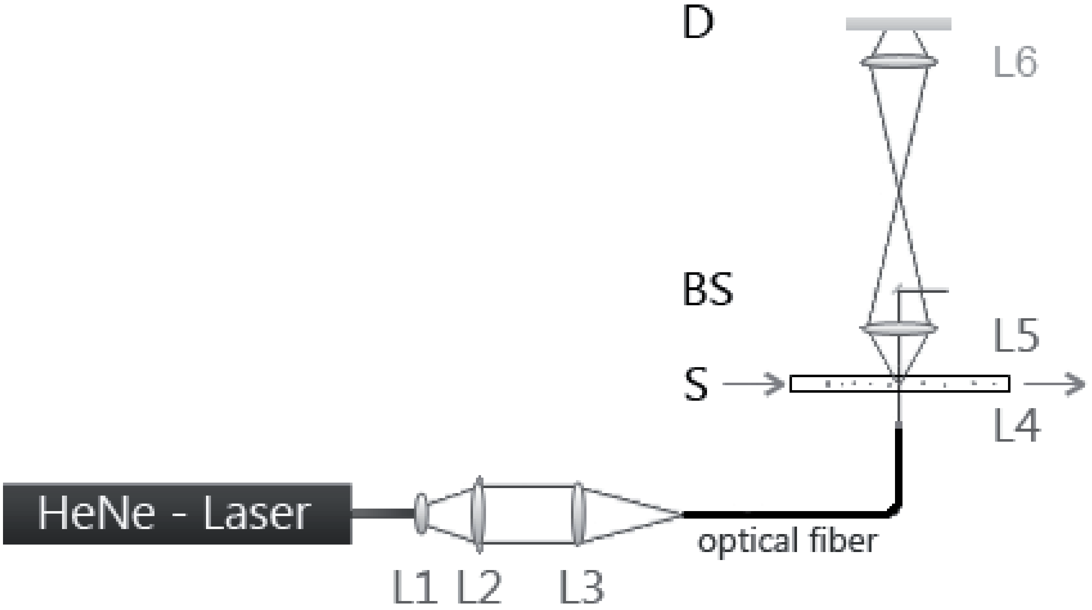

Figure 1: Schematic diagram of the experimental setup. *L1* & *L2* are lenses of the beam expander, while *L3* is focusing the incident laser light in the optical fibre. *L4* is indicating the collimation lens at the end of the optical fibre. *S* shows the position of the target sample. Furthermore, *L5* & *L6* are the lenses of the collimation stage, which collect and map the scattered laser light on the detector *D*. *BS* is indicating the homemade beam stop for the incident light.

The optical fibre transmits the incident laser light through a specially designed homemade microfluidic device, which ensures that the target particles are aligned in a single line when passing through the laser beam. To obtain a small and collimated beam size at the sample position we use a gradient-index (GRIN) lens *(L4 - EDMUND OPTICS - NT64-515)* with a working distance of zero, directly bond to the exit of the optical fibre, with a transparent UV cured adhesive *(NORLAND PRODUCTS - NOA61)*. A divergence of less than 0.045 rad, ensures the quasi collimation of the incident light to a waist diameter of maximal 50 μm at the target particle region *S*. Such collimated and small laser beam diameter at the target particle region distinguishes this SALS

apparatus from others in the literature.
The intensity distribution of the incident beam at different distances from the GRIN lens is shown in figure 2. Here the half beam shape starting from 0° (1 pixel) is represented. By calculating the beam divergence and knowing the sample to optical fibre exit distance, the spot size diameter in our homemade micro-channel can be calculated.

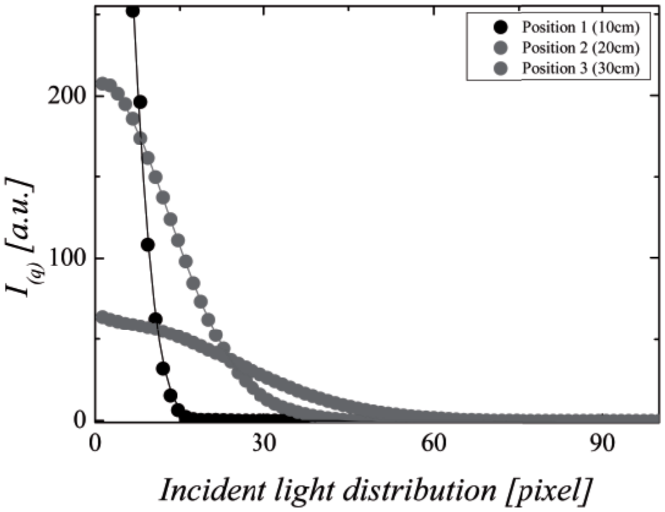

Figure 2: The Gaussian beam distribution of the incident laser beam at distances of 10, 20 and 30 cm after the optical fibre exit is plotted. The hereby used CCD-camera has a pixel pitch of 7.5 μm.

The micro-fluidic device is specifically designed to induce particle migration towards the central axis of the channel and hence to realize a precise 3D focusing of the target particle. To this aim we use a viscoelastic liquid (a solution of 0.4% polyethylene oxide (PEO*) in H_2O by weight) as the suspending medium. Indeed, due to the presence of normal stress differences, it is well-known that viscoelastic liquids induce particle migration in a certain range of shear rate.[13] We adjust the applied flow rate to get a shear rate of about 100 $\sec^{-1}$. We empirically tested that this shear rate gives the optimal particle focusing with this liquid.

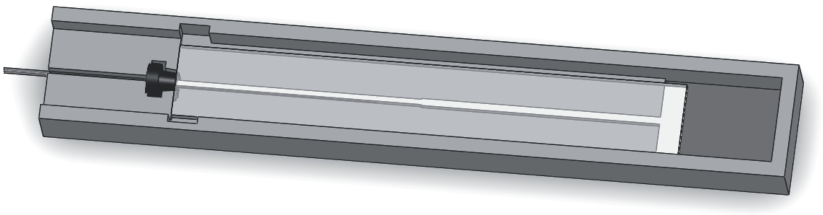

Figure 3: 3D view of our homemade microfluidic device. The tube entering the device on the left side is a glass capillary with inner diameter of 75 μm. A rubber conic ferrule holds this capillary in space and closes the channel to avoid liquid leakage. After the ferrule the microfluidic-channel has a width of 381 μm. The depth of the channel is held constant by around 400 μm. The top of the channel is closed by bonding with a cover-slide of PMMA with 0.5 mm.

---

*PEO with M_w = 4 MDA, from Sigma-Aldrich

The microfluidic device is made of a high quality Poly-methyl-methacrylate (PMMA *from GOODFELLOW CAMBRIDGE LTD.*), which provides high transparency. Figure 3 shows the design of the device which is realized by micro-milling. The device has an open groove on one side in which a round glass capillary *(UNIFIBRE - TSP075375)* with inner diameter of 75 μm is placed. The end of this capillary is hold in place with a ferrule *(NANOPORT - Ferrule 6-32 FB-360/510 μm)*; this ferrule additionally seals the microfluidic-channel. The channel has a rectangular shape with a width of 381 μm and height of 400 μm. The end of the capillary is placed in such a way that its centre coincides with the channel centre. At the end of the channel a reservoir is collecting all the out coming liquids. The microfluidic device is placed on a XY- and Z-stage *(THORLABS - DT12XY/M & SM1Z)* for accurate positioning of the target flow in the centre of the incident beam. The forward scattering emitted from a particle is collected by an aspheric lens *(L5 - EDMUND OPTICS - 67245)* with high numerical aperture. The limitation of the collecting scattering angle is mainly restricted by the numerical aperture of *L5* and its absolute distance to the target particle.

Near the focal plane of lens *L5*, a homemade beam stop *BS* reflects the incident light out of the collecting system. Concluding the collecting-system, a plano-convex lens *(L6 - THORLABS - LA1951-A)* after the beam stop maps the scattered light on the sensor D of a cooled CCD-camera *(PRINCETON INSTRUMENTS Micromax-1300YHS)*. The camera has a pixel pitch of 6.8 μm, a maximal sensor size of 582x782 pixel and is operating at a temperature of $-15°$C. The two lens system used here allows obtaining far field images on short distances. Each radial distance from the centre of the CCD sensor corresponds to one wave-vector $q \equiv |q|$; different azimuthal orientations are collected by one ring corresponding to the same wave-vector. The wave-vector is defined as $q = 4\pi\lambda^{-1}\sin(\theta/2)$, with θ the scattering angle, and λ the laser wavelength.[3,14]

The digitized images are saved and post-proceeded by a homemade Matlab *(The MathWorks, Inc., Natick (MA), USA)* routine. The calculation of the spot size on the detector area and its design optimization has been performed based on *van Heiningen*.[15]

3. ACQUISITION AND DATA PROCESSING

A calibration of the system with several different pinholes and measurements with particles in quiescent (multi-particle signal) and in-flow (single-particle signal) conditions are shown and compared with calculations based on the Lorenz-Mie theory.[16]

3.1 Calibration

Far-field patterns from different pinholes are compared with the Fraunhofer diffraction theory for a circular aperture.[16] The pinhole position is chosen exactly at the target particle plane of the microfluidic device. For a scattering angle θ the intensity I_θ of the Airy disk is:

$$I_\theta = I_0 \left[\frac{2J_1(ka\sin\theta)}{ka\sin\theta}\right]^2 \tag{1}$$

where J_1 is the Bessel function of zero order, $k = 2\pi/\lambda$ the wave number and a the radius of the pinhole.[17] To check the alignment of our apparatus, scattering patterns from pinholes with radii of 5 and 10 μm *(EDMUND OPTICS - NT56-276 & NT56-279)* are measured and compared with the theoretical prediction 1. Figure 4 shows the pattern scattered from a pinhole of 5 μm. The lowest measurable wave-vector $q \approx 1\mu m^{-1}$ is set by the beam stop dimension. The dynamic range of the CCD sensor sets the lowest measurable intensity. Indeed we are able to distinguish the first five maxima in the scattered pattern, while the intensity of higher order peaks is in the noise of the camera. The agreement between the measured maxima and minima with the theoretically predicted positions suggests the alignment of the system. The good agreement of the pattern scattered from a pinhole of radius 10 μm with theory, confirms the alignment of our apparatus.

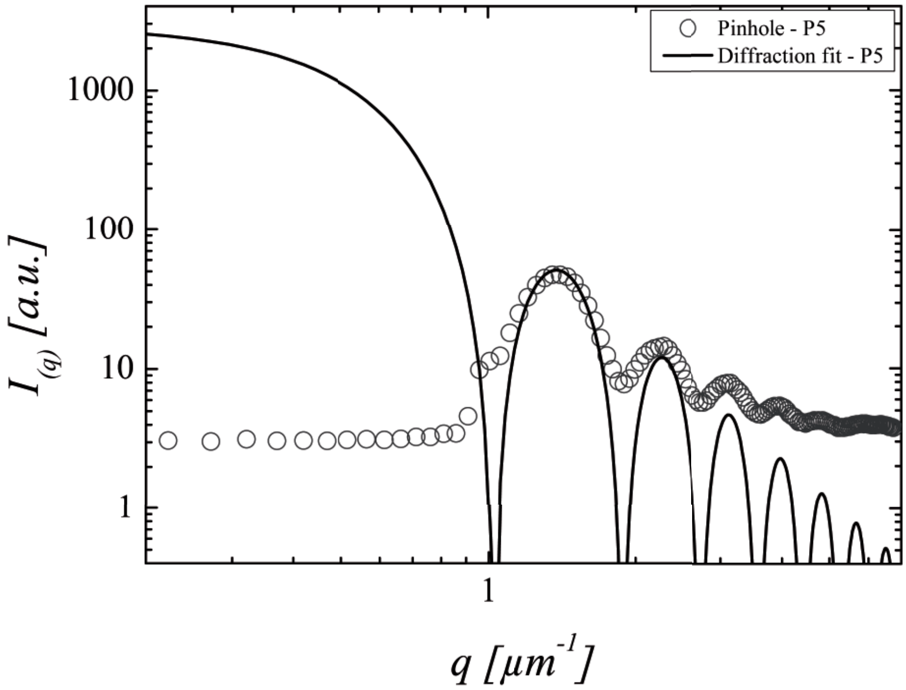

Figure 4: A pinhole with radius 5 μm has been used to calibrate the SALS apparatus. Its measured scattering pattern is shown with circles. Only one out of two data-points is shown for easier visualization. The theoretical diffraction pattern is illustrated by a line.

3.2 Particle characterization

To characterize the far-field patterns of micrometric PSL particles the Lorenz-Mie theory is used. The theoretical scattering amplitudes are calculated with a homemade Matlab routine. The scattering coefficients and amplitudes of the Lorenz-Mie theory are calculated on the basis of previously published Matlab code.[18]

The pattern of the intensity scattered by a particle can be described by the Lorenz-Mie solution for unpolarized incident light as:

$$I_s(\theta) = \frac{I_0(|S_1|^2 + |S_2|^2)}{2k^2r^2} \tag{2}$$

where r is the particle to sensor distance and I_0 the incident light intensity. The complex scattering amplitudes S_1 and S_2, which describe the scattering pattern of the particle are given by:

$$S_1(\cos\theta) = \sum_{n=1}^{\infty} \frac{2n+1}{n(n+1)}(a_n\pi_n + b_n\tau_n), \tag{3}$$

$$S_2(\cos\theta) = \sum_{n=1}^{\infty} \frac{2n+1}{n(n+1)}(a_n\tau_n + b_n\pi_n). \tag{4}$$

The coefficients a_n and b_n are called the scattering coefficients.[19] These are the observable quantities for the scattered field. Indeed, the interaction of the incident light with the sphere causes radiation of electromagnetic waves. These waves are not isotropic in general. By using vector spherical harmonics it is possible to expand the incident, scattered, and internal field of the homogeneous sphere. The coefficients of these expansion functions are chosen so that the tangential components of the electric and magnetic fields are continuous across the surface of the sphere. This scattering problem is formally identical to reflection and refraction with flat interfaces, although the sphere problem is more complicated because the scattered and internal fields are not plane waves. The expansion coefficients a_n and b_n, where n is the expansion index going from $n = 1$ to $n \to \infty$ are given by:

$$a_n = \frac{\mu m^2 j_n(mx)[xj_n(x)]' - \mu_1 j_n(x)[mxj_n(mx)]'}{\mu m^2 j_n(mx)[xh_n^{(1)}(x)]' - \mu_1 h_n^{(1)}(x)[mxj_n(mx)]'}, \tag{5}$$

$$b_n = \frac{\mu_1 j_n(mx)[xj_n(x)]' - \mu j_n(x)[mxj_n(mx)]'}{\mu_1 j_n(mx)[xh_n^{(1)}(x)]' - \mu h_n^{(1)}(x)[mxj_n(mx)]'}. \tag{6}$$

.

Here μ is the magnetic permeability of the medium and μ_1 of the sphere. The function $j_n(z)$ and $h_n^{(1)}(z)$ are spherical Bessel functions of first order ($n = 1$) and given arguments, $z = x$ or mx, respectively. Primes indicate derivatives with respect to the argument. The functions $\pi_n(\cos\theta)$ and $\tau_n(\cos\theta)$ describe the angular scattering patterns of the spherical harmonics.[16] The size parameter x and the relative refractive index m are given by:

$$x = ka = \frac{2\pi Na}{\lambda} \tag{7}$$

$$m = \frac{k_1}{k} = \frac{N_1}{N} \tag{8}$$

with a is the particle radius, and N_1 and N the refractive indices of particle and ambient medium respectively. By comparing the measured scattering pattern to the predictions from 2 it is in general possible to obtain both the particle size, a and refractive index m. Since for our polystyrene particles the refractive index m is known, m=1.58722 for $\lambda = 632.8$nm,[20] we only extract the particle size from the scattering pattern. For the medium, the refractive index of water is assumed.[21] The refractive index of the 0.4 % PEO solution was measured by a refractometer *(ANTON PAAR - Abbemat 200)* and showed similar values compared to H_2O. Indeed all calculations are proceeded with the refractive index of H_2O, $n = 1.33169$ as ambient medium.

3.3 Acquisition

Measurements of PSL particles in quiescent and flow conditions have been realized with our apparatus. In quiescent conditions, rectangular glass capillaries placed at the target particle plane are used. These microslides *(VITROCOM - W3520-050)* have an inner rectangular size of 0.2 times 4.0 mm.

For in-flow measurements an homemade microfluidic device has been used (shown in figure 3). A pressure pump *(DOLOMITE MICROFLUIDICS - Mitos P-pump)* supplies a flow rate of about 0.15 mm^3/min. Such flow rate allows to focus the particles in a round glass capillary *(UNIFIBRE - TSP075375)* with an inner diameter of 75 μm and length of 55 mm when the viscoelastic solution is used. The round capillary is thereby connected to the homemade microfluidic device (see in figure 3), where the particles kept on track in the centre until the end of the channel.

For each sample, we acquire 50 frames for quiescent conditions and 150 frames for in-flow conditions. Images are collected by keeping the exposure time between 1 and 5 ms with a delay of 10 ms between successive frames. For in-flow measurements the scattering profile depends on the position of the particle relatively to the laser-beam centre. The frame containing the scattering profile of a particle in the centre of the laser-beam, is determined as the frame with highest intensity among about 25 successive frames. Once the highest intensity frame is determined, to reduce thermal noise, we average the intensity of pixels over 3 successive frames. The background is measured over 50 frames both for the glass capillary and microfluidic device, both filled with ambient medium. The background intensity is then subtracted from the scattering profile. The wave-vector of the scattering pattern is calculated starting from $q = 0$ until the limit of the sensor size. For quiescent measurements strongly diluted mono-disperse solutions of PSL particles in water are used. Indeed strong dilution is minimizing the effect of multiple scattering. In-flow conditions scattering profiles are recorded from streams of mono-disperse particles in PEO solutions.

4. RESULTS

PSL particles (POLYSCIENCE & SIGMA-ALDRICH) of radii of 0.947, 2.078, 3.042 and 4.010 μm are analysed with our apparatus. All measurements show consistent intensity patterns which linearly shift up with increasing the exposure time. Therefore all measurements are vertically normalized to an exposure time of 1 ms.

Background subtraction is important for an appropriate signal analysis. Figure 5 shows, in the upper part, the pure scattering intensity *(PSL pure)* measured for a PSL 4 particle (nominal radius = 2.078 μm) and the corresponding background signal without particles *(H_2O)*. After background subtraction, the intensity profile reflects a much more defined scattering pattern over the whole wave-vector range. A comparison with the theoretical Lorenz-Mie calculation shown in figure 5 confirms the accuracy of our measurements in the entire meaningful wave-vector range.

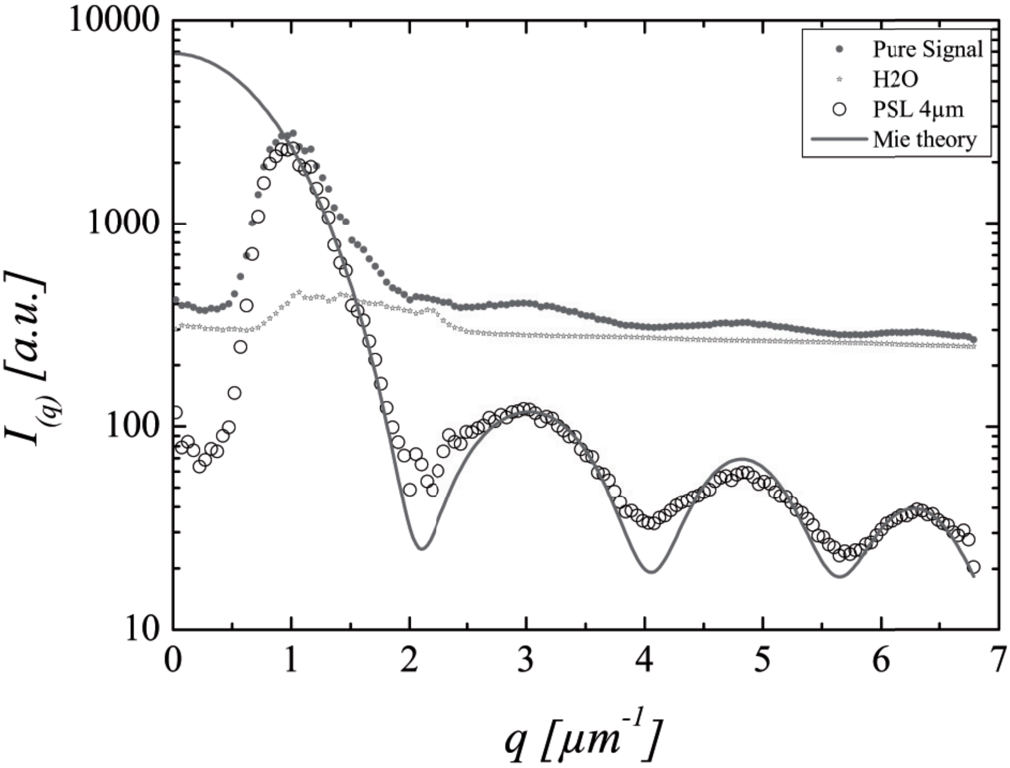

Figure 5: Intensity profiles as function of wave-vector. Small solid circles are the pure raw data *(Pure Signal)* from a polystyrene particle with a nominal radius of 2.078 μm. Under it the background signal *(H2O)* of a glass capillary filled with water is reported with small empty circles. By subtracting the background signal from the pure signal curve, the particle signal appears well-defined and is shown by big empty circles *(PSL 4 μm)*. The theoretical prediction from the Lorenz-Mie theory corresponding to a particle radius of 2 μm is shown by the solid curve *(Mie theory)*.

4.1 Quiescent measurements

Particles of different radii have been measured in quiescent conditions. Figure 6 shows the measured scattering patterns from particles of different radii and exposure times along with the related theoretical predictions. Particles with a nominal radius of 4.01 μm (PSL 8) show an extremely good agreement with the Lorenz-Mie theory. PSL 6 particles display a significantly different height of the first measured maximum with respect to theory. Such discrepancy may arise from small differences between the particle refractive index used in the calculation and the actual one. The scattering profile of PSL 4 particles shows good agreement with the Lorenz-Mie theory, with only small differences in the absolute value of the minima. Finally, figure 6 shows that also particles with a radius of 1 μm (PSL 2) can be measured quite accurately despite the maximum and the minimum are not quantitatively measured in height.

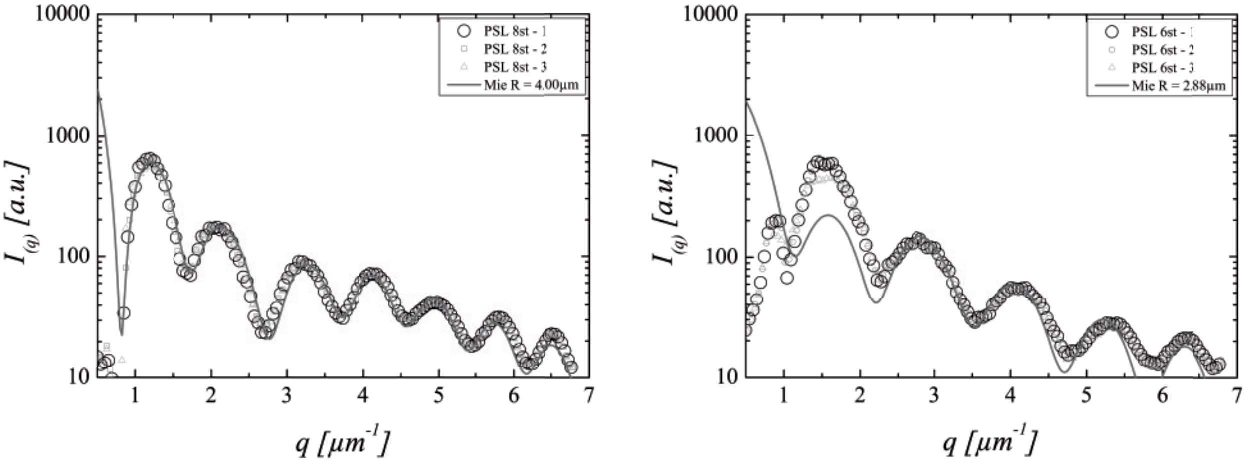

(a) PSL 8 quiescent

(b) PSL 6 quiescent

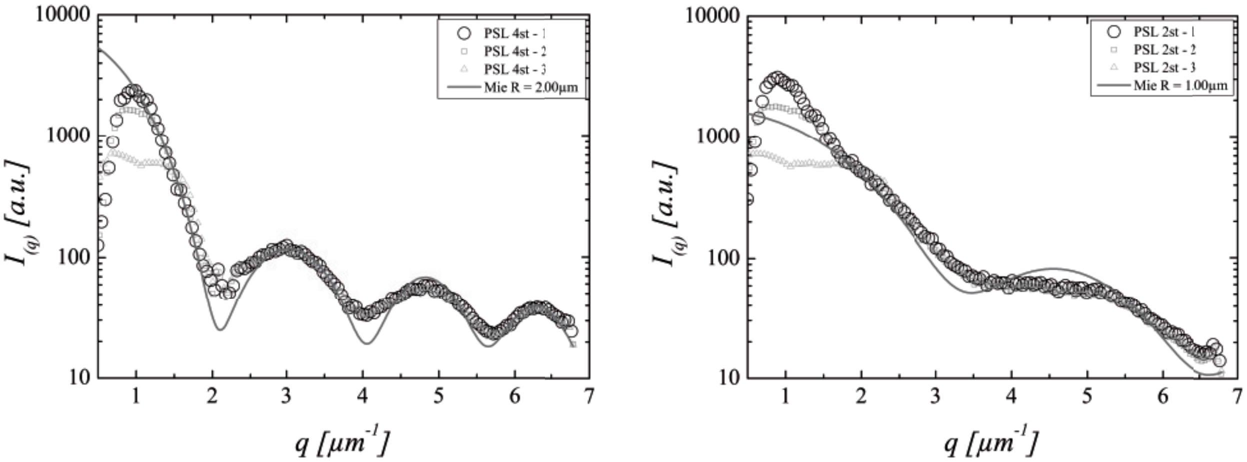

(c) PSL 4 quiescent

(d) PSL 2 quiescent

Figure 6: PSL particle measurements in quiescent condition: a) PSL 8 with nom. R = 4.01 μm & Mie theory for R = 4.00 μm, b) PSL 6 with nom. R = 3.04 μm & Mie theory for R = 2.88 μm, c) PSL 4 with nom. R = 2.08 μm & Mie theory for R = 2.00 μm, d) PSL 2 with nom. R = 0.95 μm & Mie theory for R = 1.00 μm. Circle are measurements of 1 ms, where rectangular symbols are used for 2 ms and triangles for exposure times of 5 ms. The measurements are normalized to an exposure time of 1 ms. Only one out of two data-points is shown for easier visualization.

4.2 In-flow measurements

In conditions of flow, the quality of the measurements is similar to that of quiescent conditions. Results of PSL 8 and PSL 2 measurements are reported in figure 7 to show this.

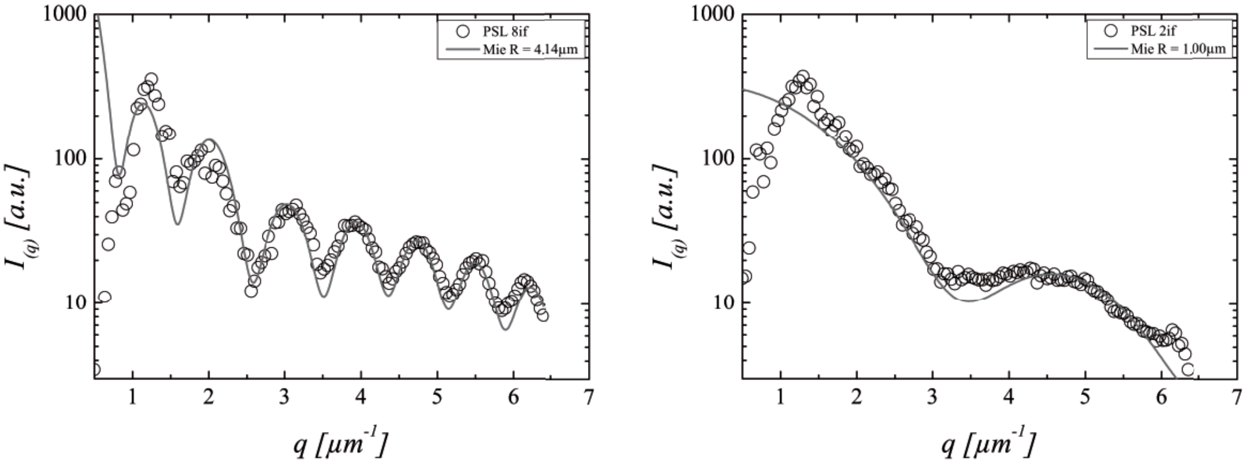

(a) PSL 8 in-flow (b) PSL 2 in-flow

Figure 7: PSL particles in-flow condition: a) PSL 8 with nom. R = 4.01 μm & Mie theory for R = 4.14 μm, b) PSL 2 with nom. R = 0.95 μm & Mie theory for R = 1.00 μm. The circle show measurements collected with an exposure time of 3 ms. All the measurements are normalized to an exposure time of 1 ms. Only one out of two data-points is shown for easier visualization.

Since in-flow we measure the scattering from a single particle, the scattering intensity is lower than in quiescent conditions. This makes the signal more noisy as can be seen from figure 7. Despite this, when compared to the Lorenz-Mie theory, both the peaks positions and peaks heights are well defined.

The in-flow measurements highlight the possibility to use our SALS system for real applications where detecting and distinguishing micrometric particles size in continuous microfluidic flows is required. In figure 8 we plot the sizes of the particles measured both in-quiescent and in-flow conditions along with their nominal values. We find very good agreement between the measured data and the nominal values with highest discrepancies not higher than 0.1 μm.

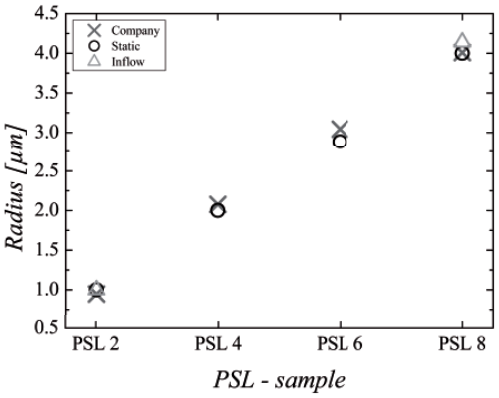

Figure 8: Comparison of quiescent, in-flow and nominal radii.

Thus, through the high sensitivity of our apparatus to size variations by constant refractive index, radial size changes of less then 0.1 μm are detectable. Finally, in table 1 we summarize all the measured radii with their standard deviations. Scanning electron microscope (SEM) measurements of all particles are also reported for additional comparison.

Particle	**Nom. r.**	*SD*	**Static - r.**	*SD*	**In-flow - r.**	*SD*	**SEM - r.**	*SD*
PSL 8	4.010	*0.049*	4.000	*0.050*	4.140	*0.050*	4.114	*0.029*
PSL 6	3.042	*0.041*	2.880	*0.100*			2.923	*0.012*
PSL 4	2.078	*0.031*	2.000	*0.050*			2.002	*0.028*
PSL 2	0.947	*0.022*	1.000	*0.050*	1.000	*0.050*	0.922	*0.008*

Table 1: Table of all nominal and measured radii. All values are given in μm.

All in all, the measured particle radii agree with the values from the seller as well as from the SEM measurements with an accuracy of 5 %.

5. CONCLUSIONS

An apparatus has built up to measure single microscopic particles flowing in micro-channels. A cooled CCD-camera operating at -15°C has been used as detector to collect the scattering patterns of several different PSL particles ranging from 1 to 4 μm in radius. Our small angle light scattering apparatus has been tested in quiescent and in-flow conditions. The optical layout of the apparatus allows to collect the scattered light from $5x10^{-1}$ to $6.8x10^{1}\mu m^{-1}$.

The calibration of the instrument has been carried out by using pinhole of several different radii ranging from 5 to 10 μm. The collected light scattering patterns from pinholes have been analysed by a homemade Matlab routine to indicate possible dis-alignments of relevant optical parts. The scattering patterns of spherical particles are linearly increase with exposure time. Reliable results are obtained for both quiescent and in-flow measurements. Indeed the measured scattering profiles are very well described in terms of the Lorenz-Mie theory. All particle sizes measured in quiescent conditions can be identified in-flow, thus opening the possibility to use this apparatus in real multiplex applications. Systematic errors at low wave-vector ranges are attributed to the presence of stray light coming from the homemade beam stop. Improvements of the collimation of the incident beam may allow to reduce the beam stop size and thus to reach a smaller wave-vector range.

Finally we expect that more complex particle shapes, different refractive indices as well as absorption coefficients, can be characterized with our apparatus. Moreover also the effect of different flow conditions on the structure of single particles or particle assemblies can be proved.

ACKNOWLEDGMENTS

REFERENCES

1. Oles, V., “Shear-induced aggregation and breakup of polystyrene latex particles,” *Journal of Colloid and Interface Science* **154**(2), 351 – 358 (1992).
2. Alexander, M. and Hallett, R. F., “Small-angle light scattering: Instrumental design and application to particle sizing,” *Appl. Opt.* **38**, 4158–4163 (Jul 1999).
3. Ferri, F., “Use of a charge coupled device camera for low-angle elastic light scattering,” *American Institute of Physics: Review of Scientific Instruments* **68**, 2265–2274 (jun 1997).
4. Carpineti, M., Ferri, F., Giglio, M., Paganini, E., and Perini, U., “Salt-induced fast aggregation of polystyrene latex,” *The American Physical Society: Review A* **42**, 7347–7354 (Dec 1990).
5. Casperson, L. W., Yeh, C., and Yeung, W. F., “Single particle scattering with focused laser beams,” *Appl. Opt.* **16**(4), 1104–1107 (1977).
6. Cipelletti, L. and Weitz, D. A., “Ultralow-angle dynamic light scattering with a charge coupled device camera based multispeckle, multitau correlator,” *American Institute of Physics: Review of Scientific Instruments* **70**(8), 3214–3221 (1999).
7. Wong, A. and Wiltzius, P., “Dynamic light scattering with a ccd camera,” *The American Physical Society: Review of Scientific Instruments* **64**(9), 2547–2549 (1993).
8. Scheffold, F. and Cerbino, R., “New trends in light scattering,” *Current Opinion in Colloid & Interface Science* **12**(1), 50–57 (2007).

9. Norman, A. I., Zhang, W., Beers, K. L., and Amis, E. J., "Microfluidic light scattering as a tool to study the structure of aqueous polymer solutions.," *Journal of Colloid and Interface Science* **299**(2), 580–588 (2006).
10. Quirantes, A., Plaza, R., and Delgado, A., "Static light scattering study of size parameters in core-shell colloidal systems," *Journal of Colloid and Interface Science* **189**(2), 236–241 (1997).
11. Lee Black, D., McQuay, M. Q., and Bonin, M. P., "Laser-based techniques for particle-size measurement: A review of sizing methods and their industrial applications," *Progress in Energy and Combustion Science* **22**(3), 267–306 (1996).
12. Quabis, S., Dorn, R., Eberler, M., Gloeckl, O., and Leuchs, G., "Focusing light to a tighter spot," *Optics Communications* **179**(1-6), 1–7 (2000).
13. D'Avino, G., Romeo, G., Villone, M. M., Greco, F., Netti, P. A., and Maffettone, P. L., "Single line particle focusing induced by viscoelasticity of the suspending liquid: theory, experiments and simulations to design a micropipe flow-focuser," *Lab Chip* **12**(9), 1638–1645 (2012).
14. Cipelletti, L., "Monte carlo multiple-scattering simulation and data correction in small-angle static light scattering," *The American Physical Society: Review E* **55**(6), 7733–7740 (1997).
15. van Heiningen, J., *Ultra-small angle light scattering: Apparatus design optimization*, PhD thesis, McGill University (Canada) (2005).
16. Bohren, C. F. and Huffman, D. R., [*Absorption and Scattering of Light by Small Particles*], WILEY-VCH Verlag GmbH & Co (1983).
17. Hecht, E., [*Optics 4th edition*], vol. 1, Addison Wesley (2001).
18. Maetzler, C., "Matlab function for mie scattering and absorption," tech. rep., University Bern (2002).
19. Bass, M. and Mahajan, V. N., [*Handbook of Optics: Geometrical and Physical Optics, Polarized Light, Components and Intruments*], McGraw-Hill (2010).
20. Kasarova, S. N., Sultanova, N. G., Ivanov, C. D., and Nikolov, I. D., "Analysis of the dispersion of optical plastic materials," *Optical Materials* **29**(11), 1481 – 1490 (2007).
21. Hale, G. M. and Querry, M. R., "Optical constants of water in the 200-nm to 200-nm wavelength region," *Appl. Opt.* **12**, 555–563 (Mar 1973).

Appendix C

Matlab code

List of Matlab routines used for the SALS apparatus:

C.1 Spot size calculation

1. Main file – SpotSizeCCDchip_MATLAB
(Figure file for the graphical interface is not included.)

C.2 Analysis software

1. Main file – Auswertungssoftware_MATLAB
(Figure file for the graphical interface is not included.)

2. Subfile – Airydisk_MATLAB
3. Subfile – Mie_ab_MATLAB
4. Subfile – Mie_pt_MATLAB
5. Subfile – Mie_S12_MATLAB

```
%%%%%%%%%%%%%%%%%%%%%%%%%%%%%%%%%%%%%%%%%%%%%%%%%%%%%%%%%%%%%%%%%%%%%%%%%%%
%%% SPOTSIZECCDCHIP.m - M-file for SpotSizeCCDchip.fig %%%%%%%%%%%%%%%%%%%%
%%% from Dannhauser David 2013 %%%%%%%%%%%%%%%%%%%%%%%%%%%%%%%%%%%%%%%%%%%%
%%%%%%%%%%%%%%%%%%%%%%%%%%%%%%%%%%%%%%%%%%%%%%%%%%%%%%%%%%%%%%%%%%%%%%%%%%%

function varargout = SpotSizeCCDchip(varargin)


gui_Singleton = 1;
gui_State = struct('gui_Name',       mfilename, ...
                   'gui_Singleton',  gui_Singleton, ...
                   'gui_OpeningFcn', @SpotSizeCCDchip_OpeningFcn, ...
                   'gui_OutputFcn',  @SpotSizeCCDchip_OutputFcn, ...
                   'gui_LayoutFcn',  [] , ...
                   'gui_Callback',   []);
if nargin && ischar(varargin{1})
    gui_State.gui_Callback = str2func(varargin{1});
end

if nargout
    [varargout{1:nargout}] = gui_mainfcn(gui_State, varargin{:});
else
    gui_mainfcn(gui_State, varargin{:});
end

function SpotSizeCCDchip_OpeningFcn(hObject, ~, handles, varargin)
handles.output = hObject;
guidata(hObject, handles);

function varargout = SpotSizeCCDchip_OutputFcn(~, ~, handles)
varargout{1} = handles.output;

    % Reading of the compartment picture
axes(handles.axes_Convex);      Picture1 = imread('Convex.JPG');
    % Imagining of the picture on the m-file, Show no axis and Calculate it
    % to the pixcel size
image(Picture1);     axis off;   axis image;
    % Reading of the compartment picture
axes(handles.axes_Setup);       Picture2 = imread('Setup2.JPG');
    % Imagining of the picture on the m-file, Show no axis and Calculate it
    % to the pixcel size
image(Picture2);     axis off;   axis image;
    % Reading of the compartment picture
axes(handles.axes_Formular_1);  Picture3 = imread('Formular_1.JPG');
    % Imagining of the picture on the m-file, Show no axis and Calculate it
    % to the pixcel size
image(Picture3);     axis off;   axis image;
    % Reading of the compartment picture
axes(handles.axes_Ferri);       Picture4 = imread('Ferri.JPG');
    %Imagining of the picture on the m-file, Show no axis and Calculate it
    % to the pixcel size
image(Picture4);     axis off;   axis image;

% -------------------------------------------------------------------------
% ___  refresh button _____________________________________________________
% -------------------------------------------------------------------------

function pushbutton_refresh_Callback(hObject, eventdata, handles)
global D1; global F1; global P1; global F2; global L; global Coll;
global P1Coll; global DL1; global DL2;
```

```
SET1 = get(handles.radiobutton_Set1,'Value');
SET2 = get(handles.radiobutton_Set2,'Value');
SET12 = get(handles.radiobutton_Set12,'Value');
CD1  = get(handles.radiobutton_CD1,'Value');
CD2  = get(handles.radiobutton_CD2,'Value');

L = str2double(get(handles.edit_Laser,'String'));
Tc1_ = get(handles.edit_Tc1,'String');      Tc1 = str2double(Tc1_);
Tc2_ = get(handles.edit_Tc2,'String');      Tc2 = str2double(Tc2_);
R1_ = get(handles.edit_R1,'String');        R1 = str2double(R1_);
R2_ = get(handles.edit_R2,'String');        R2 = str2double(R2_);
N1_ = get(handles.edit_N1,'String');        N1 = str2double(N1_);
N2_ = get(handles.edit_N2,'String');        N2 = str2double(N2_);
Fb1  = F1*(1-(Tc1*(N1-1))/(N1*R1));
Fb2  = F2*(1-(Tc2*(N2-1))/(N2*R2));
F1 = R1/(N1-1);
F2 = R2/(N2-1);
H1 = F1*(Tc1*(N1-1))/(N1*R1);
H2 = F2*(Tc2*(N2-1))/(N2*R2);
set(handles.edit_F1,'String',num2str(F1));
set(handles.edit_F2,'String',num2str(F2));
set(handles.edit_Fb1,'String',num2str(Fb1));
set(handles.edit_Fb2,'String',num2str(Fb2));
set(handles.edit_H1,'String',num2str(H1));
set(handles.edit_H2,'String',num2str(H2));

% Set 1
if CD1 == 1
    sd1_= get(handles.edit_SS1,'String');   sd1= str2double(sd1_);
    P1_ = get(handles.edit_P1,'String');    P1 = str2double(P1_);
    Q1 = (P1*F1)/(P1-F1);
    set(handles.edit_Q1,'String',num2str(Q1));
    M1  = Q1/P1;
    D1 = ((1.22*L*F1)*(1+M1))/sd1;
    set(handles.edit_D1,'String',num2str(D1));  % Diameter in first lens
else
    if SET1 == 1
        D1_ = get(handles.edit_D1,'String');    D1 = str2double(D1_);
        P1_ = get(handles.edit_P1,'String');    P1 = str2double(P1_);
        Q1 = (P1*F1)/(P1-F1);
        set(handles.edit_Q1,'String',num2str(Q1));
        M1  = Q1/P1;
        sd1 = (1.22*L)*(1+M1)*F1/D1;            % spot size sd1
    else
        if SET12 == 1
            D1_ = get(handles.edit_D1,'String');    D1 = str2double(D1_);
            P1_ = get(handles.edit_P1,'String');    P1 = str2double(P1_);
            Q1 = (P1*F1)/(P1-F1);
            set(handles.edit_Q1,'String',num2str(Q1));
            M1  = Q1/P1;
            sd1 = (1.22*L)*(1+M1)*F1/D1;        % spot size sd1
        else
            sd1 = 0;
            M1  = 0;
        end
    end
end
% Set 2
if CD2 == 1
```

```
    sd2_= get(handles.edit_SS2,'String');   sd2= str2double(sd2_);
    P2 = Q1 - F1;
    set(handles.edit_P2,'String',num2str(P2));
    Q2 = (P2*F2)/(P2-F2);
    set(handles.edit_Q2,'String',num2str(Q2));
    M2  = Q2/P2;
    D2 = ((1.22*L*F2)*(1+M2))/sd2;
    set(handles.edit_D2,'String',num2str(D2));  % Diameter in second lens
else
    if SET2 == 1
        D2_ = get(handles.edit_D2,'String');     D2 = str2double(D2_);
        P2 = Q1 - F1;
        set(handles.edit_P2,'String',num2str(P2));
        Q2 = (P2*F2)/(P2-F2);
        set(handles.edit_Q2,'String',num2str(Q2));
        M2  = Q2/P2;
        sd2 = (1.22*L)*(1+M2)*F2/D2;            % spot size sd2
    else
        if SET12 == 1
            P2 = Q1 - F1;
            set(handles.edit_P2,'String',num2str(P2));
            Q2 = (P2*F2)/(P2-F2);
            set(handles.edit_Q2,'String',num2str(Q2));
            M2  = Q2/P2;
            D2 = (P2/F1)*D1;
            set(handles.edit_D2,'String',num2str(D2));
            sd2 = (1.22*L)*(1+M2)*F2/D2;        % spot size sd2
        else
            sd2 = 0;
            M2  = 0;
        end
    end
end
sd12 = sd1 + sd2;
set(handles.edit_M1,'String',num2str(M1));
set(handles.edit_M2,'String',num2str(M2));
set(handles.edit_SS1,'String',num2str(sd1));
set(handles.edit_SS2,'String',num2str(sd2));
set(handles.edit_SS12,'String',num2str(sd12));
ParticleV = get(handles.popupmenu_ParticleSize,'Value');
P_S = get(handles.popupmenu_ParticleSize,'String');
P  = str2double(cell2mat(P_S(P_V)));

DL1_ = get(handles.edit_DL1,'String');      DL1 = str2double(DL1_);
DL2_ = get(handles.edit_DL2,'String');      DL2 = str2double(DL2_);
DBS_ = get(handles.edit_BeamStop,'String'); DBS = str2double(DBS_);
Thmin  = atan((DBS/2)/F1);                  ThminGrad  = Thmin *(180/pi);
set(handles.edit_ThetaMIN,'String',num2str(ThminGrad));
Thmax1 = atan((DL1/2)/P1);                  ThmaxGrad1 = Thmax1*(180/pi);
set(handles.edit_ThetaMAX,'String',num2str(ThmaxGrad1));
S = 2*(P*10^-3)^2/(L*10^-3);
set(handles.edit_FarField,'String',num2str(S));
CollLength = (P1+Q1+Q2)/10;
set(handles.edit_CollimationLength,'String',num2str(CollLength));

    RV = get(handles.popupmenu_R,'Value');
    RS = get(handles.popupmenu_R,'String');
    R  = (str2double(cell2mat(RS(RV)))/1000);
    ThetaR = (R/(F1*M2));
    ThetaRgrad = ThetaR*(180/pi);
```

```
    set(handles.edit_ThetaR,'String',num2str(ThetaRgrad));
    QR = round((((2*pi)/L)* ThetaR) * 10^4);
    set(handles.edit_QR,'String',num2str(QR));

    Rmin = (F1*M2)*tan(Thmin);
    Qmin = round((((4*pi)/(L*10^-4))* (Thmin/2)));
    set(handles.edit_Qmin,'String',num2str(Qmin));
    set(handles.edit_Rmin,'String',num2str(Rmin));
    RPmin = F1 * tan(Thmin);
    set(handles.edit_RPmin,'String',num2str(RPmin));
    Rmax = (F1*M2)*tan(Thmax1);
    Qmax = round((((4*pi)/(L*10^-4)))* (Thmax1/2));
    set(handles.edit_Qmax,'String',num2str(Qmax));
    set(handles.edit_Rmax,'String',num2str(Rmax));
    RPmax = F1 * tan(Thmax1);
    set(handles.edit_RPmax,'String',num2str(RPmax));

    CHOTheta = 1.22*(L/P);
    CHOR=round(((F1*F2*(-F1+P1)*tan(CHOTheta))/(F1*(F1+F2)-(F2*P1)))*1000);
    set(handles.edit_CHOR,'String',num2str(CHOR));
    CHOQ = round((((4*pi)/(L*10^-4)))* (CHOTheta/2));
    set(handles.edit_CHOQ,'String',num2str(CHOQ));
    PixelS = get(handles.edit_Pixel,'String');
    Pixel = (str2double(PixelS));
    PixelDist = round(CHOR/Pixel);
    set(handles.edit_PixelDist,'String',num2str(PixelDist));

    D1 = 2.5;
    M2 = 5.3;
    F1 = 80;
    Pinc = 0.001;                           % in mW
Idiff=(pi/2)*(Pinc)*(((P/10000)^4)/(((D1*10)^2)*(L/10000)^2))*((M2/(8))^2);



    if DBS/2 == RPmin   set(handles.edit_RPmin,'BackgroundColor','green');
    else                set (handles.edit_RPmin,'BackgroundColor','white');
    end
    if DL1/2 > RPmax    set(handles.edit_RPmax,'BackgroundColor','green');
    else                set (handles.edit_RPmax,'BackgroundColor','white');
    end
% -------------------------------------------------------------------------
% ___  save button ________________________________________________________
% -------------------------------------------------------------------------
function pushbutton_Save_Callback(hObject, eventdata, handles)
global D1; global F1; global P1; global F2; global L; global Coll;
global P1Coll; global DL1; global DL2;

[file,path] = uiputfile('SpotSizeCalculation - .mat','Save Spot size as');
save(file,'D1','F1','P1','L','F2','Coll','P1Coll','DL1','DL2'); % Saving

% -------------------------------------------------------------------------
% ___  load button ________________________________________________________
% -------------------------------------------------------------------------

function pushbutton_Load_Callback(hObject, eventdata, handles)

[fileLoad] = uigetfile('*.mat*','select a file');   % Select file for fit
load (fileLoad);
if Coll == 1
```

```
    set(handles.checkbox_Coll,'Value',1);
    set(handles.text_Coll,'Visible','on');
    set(handles.text_CollMM,'Visible','on');
    set(handles.edit_Coll,'Visible','on');
    set(handles.edit_Coll,'String',num2str(P1Coll));
end
set(handles.edit_DL1,'String',num2str(DL1));
set(handles.edit_DL2,'String',num2str(DL2));
set(handles.edit_Laser,'String',num2str(L));
set(handles.edit_D1,'String',num2str(D1));
set(handles.edit_F1,'String',num2str(F1));
set(handles.edit_P1,'String',num2str(P1));
Q1 = (P1*F1)/(P1-F1);   set(handles.edit_Q1,'String',num2str(Q1));
M1 = Q1/P1;             set(handles.edit_M1,'String',num2str(M1));
sd1= (1.22*L)*(1+M1)*F1/D1; set(handles.edit_SS1,'String',num2str(sd1));
set(handles.edit_F2,'String',num2str(F2));
P2 = Q1-F1;             set(handles.edit_P2,'String',num2str(P2));
D2 = (P2/F1)*D1;        set(handles.edit_D2,'String',num2str(D2));
Q2 = (P2*F2)/(P2-F2);   set(handles.edit_Q2,'String',num2str(Q2));
M2 = Q2/P2;     set(handles.edit_M2,'String',num2str(M2));
sd2= (1.22*L)*(1+M2)*F2/D2; set(handles.edit_SS2,'String',num2str(sd2));
sd12 = sd1 + sd2;       set(handles.edit_SS12,'String',num2str(sd12));
P_V = get(handles.popupmenu_ParticleSize,'Value');
P_S = get(handles.popupmenu_ParticleSize,'String');
P  = str2double(cell2mat(P_S(P_V)));

global D1; global F1; global P1; global F2; global L; global Coll;
global P1Coll; global DL1; global DL2;

% -------------------------------------------------------------------------
% ____ default button ______________________________________________________
% -------------------------------------------------------------------------

function pushbutton_Default_Callback(hObject, eventdata, handles)
global D1; global F1; global P1; global F2; global L; global Coll;
global P1Coll; global DL1; global DL2;

set(handles.checkbox_Coll,'Value',0);
set(handles.text_Coll,'Visible','off');
set(handles.text_CollMM,'Visible','off');
set(handles.edit_Coll,'Visible','off');
load('SpotSizeCalculation - Ferri (Giov).mat');
set(handles.edit_DL1,'String',num2str(DL1));
set(handles.edit_DL2,'String',num2str(DL2));
set(handles.edit_Laser,'String',num2str(L));
set(handles.edit_D1,'String',num2str(D1));
set(handles.edit_F1,'String',num2str(F1));
set(handles.edit_P1,'String',num2str(P1));
Q1 = (P1*F1)/(P1-F1);   set(handles.edit_Q1,'String',num2str(Q1));
M1 = Q1/P1;             set(handles.edit_M1,'String',num2str(M1));
sd1= (1.22*L)*(1+M1)*F1/D1; set(handles.edit_SS1,'String',num2str(sd1));
set(handles.edit_F2,'String',num2str(F2));
P2 = Q1-F1;             set(handles.edit_P2,'String',num2str(P2));
D2 = (P2/F1)*D1;        set(handles.edit_D2,'String',num2str(D2));
Q2 = (P2*F2)/(P2-F2);   set(handles.edit_Q2,'String',num2str(Q2));
M2 = Q2/P2;             set(handles.edit_M2,'String',num2str(M2));
sd2= (1.22*L)*(1+M2)*F2/D2; set(handles.edit_SS2,'String',num2str(sd2));
sd12 = sd1 + sd2;       set(handles.edit_SS12,'String',num2str(sd12));
P_V = get(handles.popupmenu_ParticleSize,'Value');
P_S = get(handles.popupmenu_ParticleSize,'String');
```

```
P  = str2double(cell2mat(P_S(P_V)));

% -------------------------------------------------------------------------
% ____ clear button _______________________________________________________
% -------------------------------------------------------------------------

function pushbutton_Clear_Callback(hObject, eventdata, handles)
set(handles.edit_D1,'String',0);        set(handles.edit_F1,'String',0);
set(handles.edit_P1,'String',0);        set(handles.edit_Q1,'String',0);
set(handles.edit_D2,'String',0);        set(handles.edit_F2,'String',0);
set(handles.edit_P2,'String',0);        set(handles.edit_Q2,'String',0);
set(handles.edit_M1,'String',0);        set(handles.edit_M2,'String',0);
set(handles.edit_FarField,'String',0);  set(handles.edit_SS1,'String',0);
set(handles.edit_SS2,'String',0);       set(handles.edit_SS12,'String',0);
set(handles.radiobutton_CSS1,'Value',1);
set(handles.radiobutton_CSS2,'Value',1);
set(handles.radiobutton_CD1,'Value',0);
set(handles.radiobutton_CD2,'Value',0);
set(handles.radiobutton_Set1,'Value',0);
set(handles.radiobutton_Set2,'Value',0);
set(handles.radiobutton_Set12,'Value',1);
set(handles.uipanel_Set1,'Visible','on');
set(handles.uipanel_Set2,'Visible','on');
set(handles.popupmenu_ParticleSize,'Value',3);
set(handles.text_Coll,'Visible','off');
set(handles.text_CollMM,'Visible','off');
set(handles.edit_Coll,'Visible','off');
set(handles.checkbox_Coll,'Value',0);
%% Radiobutton
function radiobutton_Set1_Callback(~, ~, handles)
set(handles.radiobutton_Set12,'Value',0);
set(handles.radiobutton_Set2,'Value',0);
set(handles.uipanel_Set2,'Visible','off');
set(handles.text_D2,'Visible','off');
set(handles.text_F2,'Visible','off');
set(handles.text_P2,'Visible','off');
set(handles.text_Q2,'Visible','off');
set(handles.uipanel_Set1,'Visible','on');
set(handles.text_D1,'Visible','on');
set(handles.text_F1,'Visible','on');
set(handles.text_P1,'Visible','on');
set(handles.text_Q1,'Visible','on');

function radiobutton_Set2_Callback(~, ~, handles)
set(handles.radiobutton_Set12,'Value',0);
set(handles.radiobutton_Set1,'Value',0);
set(handles.uipanel_Set1,'Visible','off');
set(handles.text_D1,'Visible','off');
set(handles.text_F1,'Visible','off');
set(handles.text_P1,'Visible','off');
set(handles.text_Q1,'Visible','off');
set(handles.uipanel_Set2,'Visible','on');
set(handles.text_D2,'Visible','on');
set(handles.text_F2,'Visible','on');
set(handles.text_P2,'Visible','on');
set(handles.text_Q2,'Visible','on');

function radiobutton_Set12_Callback(~, ~, handles)
set(handles.radiobutton_Set1,'Value',0);
set(handles.radiobutton_Set2,'Value',0);
```

```
set(handles.uipanel_Set2,'Visible','on');
set(handles.text_D2,'Visible','on');
set(handles.text_F2,'Visible','on');
set(handles.text_P2,'Visible','on');
set(handles.text_Q2,'Visible','on');
set(handles.uipanel_Set1,'Visible','on');
set(handles.text_D1,'Visible','on');
set(handles.text_F1,'Visible','on');
set(handles.text_P1,'Visible','on');
set(handles.text_Q1,'Visible','on');

function radiobutton_CSS1_Callback(~, ~, handles)
set(handles.radiobutton_CD1,'Value',0);
set(handles.radiobutton_CSS1,'Value',1);

function radiobutton_CSS2_Callback(~, ~, handles)
set(handles.radiobutton_CD2,'Value',0);
set(handles.radiobutton_CSS2,'Value',1);

function radiobutton_CD1_Callback(~, ~, handles)
set(handles.radiobutton_CSS1,'Value',0);
set(handles.radiobutton_CD1,'Value',1);

function radiobutton_CD2_Callback(~, ~, handles)
set(handles.radiobutton_CSS2,'Value',0);
set(handles.radiobutton_CD2,'Value',1);

%% Popup
function popupmenu_ParticleSize_Callback(~, ~, ~)
function popupmenu_ParticleSize_CreateFcn(hObject, ~ , ~)
    if ispc && isequal(get(hObject,'BackgroundColor'),
        get(0,'defaultUicontrolBackgroundColor'))
        set(hObject,'BackgroundColor','white');
    end

function popupmenu_R_Callback(~, ~, ~)
function popupmenu_R_CreateFcn(hObject, ~ , ~)
    if ispc && isequal(get(hObject,'BackgroundColor'),
        get(0,'defaultUicontrolBackgroundColor'))
        set(hObject,'BackgroundColor','white');
    end

%% Checkbox
function checkbox_Coll_Callback(~, ~, ~)
Coll = get(handles.checkbox_Coll,'Value');
if Coll == 1
        set(handles.text_Coll,'Visible','on');
        set(handles.text_CollMM,'Visible','on');
        set(handles.edit_Coll,'Visible','on');
    else
        set(handles.text_Coll,'Visible','off');
        set(handles.text_CollMM,'Visible','off');
        set(handles.edit_Coll,'Visible','off');
end

%% Edit
function edit_Laser_Callback(~, ~, ~)
function edit_Laser_CreateFcn(hObject, ~ , ~)
    if ispc && isequal(get(hObject,'BackgroundColor'),
        get(0,'defaultUicontrolBackgroundColor')),
```

```
        set(hObject,'BackgroundColor','white');
    end

function edit_M1_Callback(~, ~, ~)
function edit_M1_CreateFcn(hObject, ~ , ~)
    if ispc && isequal(get(hObject,'BackgroundColor'),
        get(0,'defaultUicontrolBackgroundColor')),
        set(hObject,'BackgroundColor','white');
    end

function edit_M2_Callback(~, ~, ~)
function edit_M2_CreateFcn(hObject, ~ , ~)
    if ispc && isequal(get(hObject,'BackgroundColor'),
        get(0,'defaultUicontrolBackgroundColor')),
        set(hObject,'BackgroundColor','white');
    end

function edit_SS1_Callback(~, ~, ~)
function edit_SS1_CreateFcn(hObject, ~ , ~)
    if ispc && isequal(get(hObject,'BackgroundColor'),
        get(0,'defaultUicontrolBackgroundColor')),
        set(hObject,'BackgroundColor','white');
    end

function edit_SS2_Callback(~, ~, ~)
function edit_SS2_CreateFcn(hObject, ~ , ~)
    if ispc && isequal(get(hObject,'BackgroundColor'),
        get(0,'defaultUicontrolBackgroundColor')),
        set(hObject,'BackgroundColor','white');
    end

function edit_SS12_Callback(~, ~, ~)
function edit_SS12_CreateFcn(hObject, ~ , ~)
    if ispc && isequal(get(hObject,'BackgroundColor'),
        get(0,'defaultUicontrolBackgroundColor')),
        set(hObject,'BackgroundColor','white');
    end

function edit_D1_Callback(~, ~, ~)
function edit_D1_CreateFcn(hObject, ~ , ~)
    if ispc && isequal(get(hObject,'BackgroundColor'),
        get(0,'defaultUicontrolBackgroundColor')),
        set(hObject,'BackgroundColor','white');
    end

function edit_F1_Callback(~, ~, ~)
function edit_F1_CreateFcn(hObject, ~ , ~)
    if ispc && isequal(get(hObject,'BackgroundColor'),
        get(0,'defaultUicontrolBackgroundColor')),
        set(hObject,'BackgroundColor','white');
    end

function edit_P1_Callback(~, ~, ~)
function edit_P1_CreateFcn(hObject, ~ , ~)
    if ispc && isequal(get(hObject,'BackgroundColor'),
        get(0,'defaultUicontrolBackgroundColor')),
        set(hObject,'BackgroundColor','white');
    end

function edit_Q1_Callback(~, ~, ~)
```

```
function edit_Q1_CreateFcn(hObject, ~ , ~)
    if ispc && isequal(get(hObject,'BackgroundColor'),
        get(0,'defaultUicontrolBackgroundColor')),
        set(hObject,'BackgroundColor','white');
    end

function edit_D2_Callback(~, ~, ~)
function edit_D2_CreateFcn(hObject, ~ , ~)
    if ispc && isequal(get(hObject,'BackgroundColor'),
        get(0,'defaultUicontrolBackgroundColor')),
        set(hObject,'BackgroundColor','white');
    end

function edit_F2_Callback(~, ~, ~)
function edit_F2_CreateFcn(hObject, ~ , ~)
    if ispc && isequal(get(hObject,'BackgroundColor'),
        get(0,'defaultUicontrolBackgroundColor')),
        set(hObject,'BackgroundColor','white');
    end

function edit_P2_Callback(~, ~, ~)
function edit_P2_CreateFcn(hObject, ~ , ~)
    if ispc && isequal(get(hObject,'BackgroundColor'),
        get(0,'defaultUicontrolBackgroundColor')),
        set(hObject,'BackgroundColor','white');
    end

function edit_Q2_Callback(~, ~, ~)
function edit_Q2_CreateFcn(hObject, ~ , ~)
    if ispc && isequal(get(hObject,'BackgroundColor'),
        get(0,'defaultUicontrolBackgroundColor')),
        set(hObject,'BackgroundColor','white');
    end


function edit_FarField_Callback(~, ~, ~)
function edit_FarField_CreateFcn(hObject, ~ , ~)
    if ispc && isequal(get(hObject,'BackgroundColor'),
        get(0,'defaultUicontrolBackgroundColor')),
        set(hObject,'BackgroundColor','white');
    end

function edit_Divergence_Callback(~, ~, ~)
function edit_Divergence_CreateFcn(hObject, ~ , ~)
    if ispc && isequal(get(hObject,'BackgroundColor'),
        get(0,'defaultUicontrolBackgroundColor')),
        set(hObject,'BackgroundColor','white');
    end

function edit_Coll_Callback(~, ~, ~)
function edit_Coll_CreateFcn(hObject, ~ , ~)
    if ispc && isequal(get(hObject,'BackgroundColor'),
        get(0,'defaultUicontrolBackgroundColor')),
        set(hObject,'BackgroundColor','white');
    end

function edit_CollimationLength_Callback(~, ~, ~)
function edit_CollimationLength_CreateFcn(hObject, ~ , ~)
    if ispc && isequal(get(hObject,'BackgroundColor'),
        get(0,'defaultUicontrolBackgroundColor')),
```

```
        set(hObject,'BackgroundColor','white');
    end

function edit_DL1_Callback(~, ~, ~)
function edit_DL1_CreateFcn(hObject, ~ , ~)
    if ispc && isequal(get(hObject,'BackgroundColor'),
        get(0,'defaultUicontrolBackgroundColor')),
        set(hObject,'BackgroundColor','white');
    end

function edit_DL2_Callback(~, ~, ~)
function edit_DL2_CreateFcn(hObject, ~ , ~)
    if ispc && isequal(get(hObject,'BackgroundColor'),
        get(0,'defaultUicontrolBackgroundColor')),
        set(hObject,'BackgroundColor','white');
    end

function edit_Qmin_Callback(~, ~, ~)
function edit_Qmin_CreateFcn(hObject, ~ , ~)
    if ispc && isequal(get(hObject,'BackgroundColor'),
        get(0,'defaultUicontrolBackgroundColor')),
        set(hObject,'BackgroundColor','white');
    end

function edit_Qmax_Callback(~, ~, ~)
function edit_Qmax_CreateFcn(hObject, ~ , ~)
    if ispc && isequal(get(hObject,'BackgroundColor'),
        get(0,'defaultUicontrolBackgroundColor')),
        set(hObject,'BackgroundColor','white');
    end

function edit_Rmin_Callback(~, ~, ~)
function edit_Rmin_CreateFcn(hObject, ~ , ~)
    if ispc && isequal(get(hObject,'BackgroundColor'),
        get(0,'defaultUicontrolBackgroundColor')),
        set(hObject,'BackgroundColor','white');
    end

function edit_RPmin_Callback(~, ~, ~)
function edit_RPmin_CreateFcn(hObject, ~ , ~)
    if ispc && isequal(get(hObject,'BackgroundColor'),
        get(0,'defaultUicontrolBackgroundColor')),
        set(hObject,'BackgroundColor','white');
    end

function edit_RPmax_Callback(~, ~, ~)
function edit_RPmax_CreateFcn(hObject, ~ , ~)
    if ispc && isequal(get(hObject,'BackgroundColor'),
        get(0,'defaultUicontrolBackgroundColor')),
        set(hObject,'BackgroundColor','white');
    end

function edit_Rmax_Callback(~, ~, ~)
function edit_Rmax_CreateFcn(hObject, ~ , ~)
    if ispc && isequal(get(hObject,'BackgroundColor'),
        get(0,'defaultUicontrolBackgroundColor')),
        set(hObject,'BackgroundColor','white');
    end

function edit_ThetaMAX_Callback(~, ~, ~)
```

```
function edit_ThetaMAX_CreateFcn(hObject, ~ , ~)
    if ispc && isequal(get(hObject,'BackgroundColor'),
        get(0,'defaultUicontrolBackgroundColor')),
        set(hObject,'BackgroundColor','white');
    end

function edit_ThetaMIN_Callback(~, ~, ~)
function edit_ThetaMIN_CreateFcn(hObject, ~ , ~)
    if ispc && isequal(get(hObject,'BackgroundColor'),
        get(0,'defaultUicontrolBackgroundColor')),
        set(hObject,'BackgroundColor','white');
    end

function edit_ThetaR_Callback(~, ~, ~)
function edit_ThetaR_CreateFcn(hObject, ~ , ~)
    if ispc && isequal(get(hObject,'BackgroundColor'),
        get(0,'defaultUicontrolBackgroundColor')),
        set(hObject,'BackgroundColor','white');
    end

function edit_QR_Callback(~, ~, ~)
function edit_QR_CreateFcn(hObject, ~ , ~)
    if ispc && isequal(get(hObject,'BackgroundColor'),
        get(0,'defaultUicontrolBackgroundColor')),
        set(hObject,'BackgroundColor','white');
    end

function edit_BeamStop_Callback(~, ~, ~)
function edit_BeamStop_CreateFcn(hObject, ~ , ~)
    if ispc && isequal(get(hObject,'BackgroundColor'),
        get(0,'defaultUicontrolBackgroundColor')),
        set(hObject,'BackgroundColor','white');
    end

function edit_CHOTheta_Callback(~, ~, ~)
function edit_CHOTheta_CreateFcn(hObject, ~ , ~)
    if ispc && isequal(get(hObject,'BackgroundColor'),
        get(0,'defaultUicontrolBackgroundColor')),
        set(hObject,'BackgroundColor','white');
    end

function edit_CHOR_Callback(~, ~, ~)
function edit_CHOR_CreateFcn(hObject, ~ , ~)
    if ispc && isequal(get(hObject,'BackgroundColor'),
        get(0,'defaultUicontrolBackgroundColor')),
        set(hObject,'BackgroundColor','white');
    end

function edit_CHOQ_Callback(~, ~, ~)
function edit_CHOQ_CreateFcn(hObject, ~ , ~)
    if ispc && isequal(get(hObject,'BackgroundColor'),
        get(0,'defaultUicontrolBackgroundColor')),
        set(hObject,'BackgroundColor','white');
    end

function edit_Pixel_Callback(~, ~, ~)
function edit_Pixel_CreateFcn(hObject, ~ , ~)
    if ispc && isequal(get(hObject,'BackgroundColor'),
        get(0,'defaultUicontrolBackgroundColor')),
        set(hObject,'BackgroundColor','white');
```

```
    end

function edit_PixelDist_Callback(~, ~, ~)
function edit_PixelDist_CreateFcn(hObject, ~ , ~)
    if ispc && isequal(get(hObject,'BackgroundColor'),
        get(0,'defaultUicontrolBackgroundColor')),
        set(hObject,'BackgroundColor','white');
    end

function edit_Fb1_Callback(~, ~, ~)
function edit_Fb1_CreateFcn(hObject, ~ , ~)
    if ispc && isequal(get(hObject,'BackgroundColor'),
        get(0,'defaultUicontrolBackgroundColor')),
        set(hObject,'BackgroundColor','white');
    end

function edit_H1_Callback(~, ~, ~)
function edit_H1_CreateFcn(hObject, ~ , ~)
    if ispc && isequal(get(hObject,'BackgroundColor'),
        get(0,'defaultUicontrolBackgroundColor')),
        set(hObject,'BackgroundColor','white');
    end

function edit_Ff1_Callback(~, ~, ~)
function edit_Ff1_CreateFcn(hObject, ~ , ~)
    if ispc && isequal(get(hObject,'BackgroundColor'),
        get(0,'defaultUicontrolBackgroundColor')),
        set(hObject,'BackgroundColor','white');
    end

function edit_Tc1_Callback(~, ~, ~)
function edit_Tc1_CreateFcn(hObject, ~ , ~)
    if ispc && isequal(get(hObject,'BackgroundColor'),
        get(0,'defaultUicontrolBackgroundColor')),
        set(hObject,'BackgroundColor','white');
    end

function edit_R1_Callback(~, ~, ~)
function edit_R1_CreateFcn(hObject, ~ , ~)
    if ispc && isequal(get(hObject,'BackgroundColor'),
        get(0,'defaultUicontrolBackgroundColor')),
        set(hObject,'BackgroundColor','white');
    end

function edit_Fb2_Callback(~, ~, ~)
function edit_Fb2_CreateFcn(hObject, ~ , ~)
    if ispc && isequal(get(hObject,'BackgroundColor'),
        get(0,'defaultUicontrolBackgroundColor')),
        set(hObject,'BackgroundColor','white');
    end

function edit_H2_Callback(~, ~, ~)
function edit_H2_CreateFcn(hObject, ~ , ~)
    if ispc && isequal(get(hObject,'BackgroundColor'),
        get(0,'defaultUicontrolBackgroundColor')),
        set(hObject,'BackgroundColor','white');
    end

function edit_Ff2_Callback(~, ~, ~)
function edit_Ff2_CreateFcn(hObject, ~ , ~)
```

```
    if ispc && isequal(get(hObject,'BackgroundColor'),
        get(0,'defaultUicontrolBackgroundColor')),
        set(hObject,'BackgroundColor','white');
    end

function edit_Tc2_Callback(~, ~, ~)
function edit_Tc2_CreateFcn(hObject, ~ , ~)
    if ispc && isequal(get(hObject,'BackgroundColor'),
        get(0,'defaultUicontrolBackgroundColor')),
        set(hObject,'BackgroundColor','white');
    end

function edit_R2_Callback(~, ~, ~)
function edit_R2_CreateFcn(hObject, ~ , ~)
    if ispc && isequal(get(hObject,'BackgroundColor'),
        get(0,'defaultUicontrolBackgroundColor')),
        set(hObject,'BackgroundColor','white');
    end

function edit_N1_Callback(~, ~, ~)
function edit_N1_CreateFcn(hObject, ~ , ~)
    if ispc && isequal(get(hObject,'BackgroundColor'),
        get(0,'defaultUicontrolBackgroundColor')),
        set(hObject,'BackgroundColor','white');
    end

function edit_N2_Callback(~, ~, ~)
function edit_N2_CreateFcn(hObject, ~ , ~)
    if ispc && isequal(get(hObject,'BackgroundColor'),
        get(0,'defaultUicontrolBackgroundColor')),
        set(hObject,'BackgroundColor','white');
    end

% - - - - - - - - - - - - - - - - - - - - - - - - - - - - - - - - - - - - -
% ___  keyboard enter _____________________________________________________
% - - - - - - - - - - - - - - - - - - - - - - - - - - - - - - - - - - - - -

function figure1_KeyPressFcn(~, ~, handles)
if eventdata.Key == 'f5'
    global D1; global F1; global P1; global Q1; global D2; global F2;
    global P2; global Q2; global L; global Coll; global P1Coll; global DL1;
    global DL2;

    SET1 = get(handles.radiobutton_Set1,'Value');
    SET2 = get(handles.radiobutton_Set2,'Value');
    SET12 = get(handles.radiobutton_Set12,'Value');
    CD1  = get(handles.radiobutton_CD1,'Value');
    CD2  = get(handles.radiobutton_CD2,'Value');

    L = str2double(get(handles.edit_Laser,'String'));
    % Set 1
    if CD1 == 1
        sd1_= get(handles.edit_SS1,'String');   sd1= str2double(sd1_);
        F1_ = get(handles.edit_F1,'String');    F1 = str2double(F1_);
        P1_ = get(handles.edit_P1,'String');    P1 = str2double(P1_);
        Q1_ = get(handles.edit_Q1,'String');    Q1 = str2double(Q1_);
        M1  = Q1/P1;
        D1 = ((1.22*L*F1)*(1+M1))/sd1;
        set(handles.edit_D1,'String',num2str(D1));
    else
```

```
    if SET1 == 1
        D1_ = get(handles.edit_D1,'String');    D1 = str2double(D1_);
        F1_ = get(handles.edit_F1,'String');    F1 = str2double(F1_);
        P1_ = get(handles.edit_P1,'String');    P1 = str2double(P1_);
        Q1_ = get(handles.edit_Q1,'String');    Q1 = str2double(Q1_);
        M1  = Q1/P1;
        sd1 = (1.22*L)*(1+M1)*F1/D1;
    else
        if SET12 == 1
            D1_ = get(handles.edit_D1,'String');  D1 = str2double(D1_);
            F1_ = get(handles.edit_F1,'String');  F1 = str2double(F1_);
            P1_ = get(handles.edit_P1,'String');  P1 = str2double(P1_);
            Q1_ = get(handles.edit_Q1,'String');  Q1 = str2double(Q1_);
            M1  = Q1/P1;
            sd1 = (1.22*L)*(1+M1)*F1/D1;
        else
            sd1 = 0;
            M1  = 0;
        end
    end
end
% Set 2
if CD2 == 1
    sd2_= get(handles.edit_SS2,'String');   sd2= str2double(sd2_);
    F2_ = get(handles.edit_F2,'String');    F2 = str2double(F2_);
    P2_ = get(handles.edit_P2,'String');    P2 = str2double(P2_);
    Q2_ = get(handles.edit_Q2,'String');    Q2 = str2double(Q2_);
    M2  = Q2/P2;
    D2 = ((1.22*L*F2)*(1+M2))/sd2;
    set(handles.edit_D2,'String',num2str(D2));
else
    if SET2 == 1
        D2_ = get(handles.edit_D2,'String');     D2 = str2double(D2_);
        F2_ = get(handles.edit_F2,'String');     F2 = str2double(F2_);
        P2_ = get(handles.edit_P2,'String');     P2 = str2double(P2_);
        Q2_ = get(handles.edit_Q2,'String');     Q2 = str2double(Q2_);
        M2  = Q2/P2;
        sd2 = (1.22*L)*(1+M2)*F2/D2;
    else
        if SET12 == 1
            F2_ = get(handles.edit_F2,'String');  F2 = str2double(F2_);
            P2_ = get(handles.edit_P2,'String');  P2 = str2double(P2_);
            Q2_ = get(handles.edit_Q2,'String');  Q2 = str2double(Q2_);
            M2  = Q2/P2;
            D2 = ((F2*(M2+1))/(M2*F1))*D1;
            set(handles.edit_D2,'String',num2str(D2));
            sd2 = (1.22*L)*(1+M2)*F2/D2;
        else
            sd2 = 0;
            M2  = 0;
        end
    end
end
sd12 = sd1 + sd2;
set(handles.edit_M1,'String',num2str(M1));
set(handles.edit_M2,'String',num2str(M2));
set(handles.edit_SS1,'String',num2str(sd1));
set(handles.edit_SS2,'String',num2str(sd2));
set(handles.edit_SS12,'String',num2str(sd12));
P_V = get(handles.popupmenu_ParticleSize,'Value');
```

```
    P_S = get(handles.popupmenu_ParticleSize,'String');
    P   = str2double(cell2mat(P_S(P_V)));

    if Coll == 1
        P1_ = get(handles.edit_Coll,'String');
        P1Coll = str2double(P1_);
        CollLength = (P1Coll+Q1+P2+Q2)/10;
        Div = (atan((D1/2)/P1Coll))*180/pi;
        DivMAX1 = (atan((DL1/2)/P1Coll))*180/pi;
    else
        CollLength = (P1+Q1+P2+Q2)/10;
        Div = (atan((D1/2)/P1))*180/pi;
        DivMAX1 = (atan((DL1/2)/P1))*180/pi;
    end
    S = 2*(P*10^-3)^2/(L*10^-3);
    set(handles.edit_FarField,'String',num2str(S));
    DL1_ = get(handles.edit_DL1,'String');      DL1 = str2double(DL1_);
    DL2_ = get(handles.edit_DL2,'String');      DL2 = str2double(DL2_);
    DivMAX2 = (atan((DL2/2)/P2))*180/pi;
    set(handles.edit_CollimationLength,'String',num2str(CollLength));
    if DivMAX1 >= DivMAX2
        DIV = [num2str(Div),' - ',num2str(DivMAX2)];
        set(handles.edit_Divergence,'String',DIV);
    else
        DIV = [num2str(Div),' - ',num2str(DivMAX1)];
        set(handles.edit_Divergence,'String',DIV);
    end
end
```

```matlab
%%%%%%%%%%%%%%%%%%%%%%%%%%%%%%%%%%%%%%%%%%%%%%%%%%%%%%%%%%%%%%%%%%%%%%%%%%
%%% AUSWERTUNGSSOFTWARE.m - MATLAB code for Auswertungssoftware.fig %%%%%%
%%% from Dannhauser David 2013 %%%%%%%%%%%%%%%%%%%%%%%%%%%%%%%%%%%%%%%%%%%
%%%%%%%%%%%%%%%%%%%%%%%%%%%%%%%%%%%%%%%%%%%%%%%%%%%%%%%%%%%%%%%%%%%%%%%%%%

function varargout = Auswertungssoftware(varargin)
%%%%%%%%%%%%%%%%%%%%%%%%%%%%%%%%%%%%%%%%%%%%%%%%%%%%%%%%%%%%%%%%%%%%%%%%%%
% Files used in this program:
    % Airydisk.m
    % Mie_ab.m
    % Mie_pt.m
    % Mie_s12.m
%%%%%%%%%%%%%%%%%%%%%%%%%%%%%%%%%%%%%%%%%%%%%%%%%%%%%%%%%%%%%%%%%%%%%%%%%%

gui_Singleton = 1;
gui_State = struct('gui_Name',      mfilename,...
                   'gui_Singleton', gui_Singleton,...
                   'gui_OpeningFcn',@Auswertungssoftware_OpeningFcn,...
                   'gui_OutputFcn', @Auswertungssoftware_OutputFcn,...
                   'gui_LayoutFcn', [],...
                   'gui_Callback',  []);
if nargin && ischar(varargin{1})
    gui_State.gui_Callback = str2func(varargin{1});
end

if nargout
    [varargout{1:nargout}] = gui_mainfcn(gui_State, varargin{:});
else
    gui_mainfcn(gui_State, varargin{:});
end

function Auswertungssoftware_OpeningFcn(hObject, ~, handles, varargin)
handles.output = hObject;
guidata(hObject, handles);

function varargout = Auswertungssoftware_OutputFcn(~, ~, handles)
varargout{1} = handles.output;
axes(handles.axes_Show);    axis off;   cla(handles.axes_Show,'reset');
set(handles.axes_Show,'Visible','off');
axes(handles.axes_3D);      axis off;   cla(handles.axes_3D,'reset');
set(handles.axes_3D,'Visible','off');
axes(handles.axes_Fit);     axis off;   cla(handles.axes_Fit,'reset');
set(handles.axes_Fit,'Visible','off');
axes(handles.axes_Debye);   axis off;   cla(handles.axes_Debye,'reset');
set(handles.axes_Debye,'Visible','off');
axes(handles.axes_Guinier); axis off;   cla(handles.axes_Guinier,'reset');
set(handles.axes_Guinier,'Visible','off');

% ------------------------------------------------------------------------
% ____  find center button _______________________________________________
% ------------------------------------------------------------------------

function pushbutton_Center_Callback(~, ~, handles)

NameF = get(handles.edit_NameF,'String');       M = load(NameF);
Ia = imadjust(uint16(M));
%%
If = bwmorph(imfill(ge(Ia,6.5535e4),'holes'),'majority',inf);
imshow(If)
%%
```

```
p = bwboundaries(If);                           P = p{1};
C = regionprops(If,'centroid');                 C = C.Centroid; C=round(C);
plot(P(:,2),P(:,1),'r.',C(1),C(2),'g.')
set(handles.edit_Row,'String',num2str(C(2)));
set(handles.edit_Colum,'String',num2str(C(1)));

% -------------------------------------------------------------------------
% ____  start button _______________________________________________________
% -------------------------------------------------------------------------

function pushbutton_Start_Callback(~, ~, handles)
global NameF;   global StartV;  global EndV;    global ThetaR;
global P1;      global D;       global Iplot;   global R;
global r;       global c;       global DATAsub; global DATAsub_Int;

axes(handles.axes_Show);                            cla reset;
DebyeOn = get(handles.radiobutton_Rayleigh,'Value');
MieOn = get(handles.radiobutton_Mie,'Value');
DegreeOn = get(handles.radiobutton_Degree,'Value');
GuinierOn = get(handles.radiobutton_Guinier,'Value');
NameF = get(handles.edit_NameF,'String');
IntRadius_= get(handles.edit_Radius,'String');
IntRadius = str2double(IntRadius_);
Laser_= get(handles.edit_Laser,'String');
Laser = str2double(Laser_);
Pixel_= get(handles.edit_Pixel,'String');
Pixel = str2double(Pixel_);
F1_= get(handles.edit_F1,'String');                 F1 = str2double(F1_);
F2_= get(handles.edit_F2,'String');                 F2 = str2double(F2_);
P1_= get(handles.edit_P1,'String');                 P1 = str2double(P1_);
nu_= get(handles.edit_Nu,'String');                 nu = str2double(nu_);
T_= get(handles.edit_T,'String');                   T = str2double(T_);
SelMAX_= get(handles.edit_SelsizeMAX,'String');
SelMAX = str2double(SelMAX_);
set(handles.edit_SelMAX,'String',num2str(SelMAX));
SelMIN_= get(handles.edit_SelsizeMIN,'String');
SelMIN = str2double(SelMIN_);
StartV_= get(handles.edit_StartV,'String'); StartV = str2double(StartV_);
EndV_= get(handles.edit_EndV,'String');     EndV = str2double(EndV_);
I0_= get(handles.edit_I0,'String');         I0_User = str2double(I0_);
mIMAG_ = [get(handles.edit_mIMAG,'String'),'i'];
mIMAG = str2double(mIMAG_);
    % PSL at 0.6328 µm = 1.58722, H2O at 0.6328 µm = 1.33169
mREAL1_= get(handles.edit_mREAL1,'String');
mREAL1 = str2double(mREAL1_);
mREAL2_= get(handles.edit_mREAL2,'String'); mREAL2 = str2double(mREAL2_);
Q1 = (P1*F1)/(P1-F1);       P2 = Q1-F1;         Q2 = (P2*F2)/(P2-F2);
M1 = Q1/P1;                 M2 = Q2/P2;     DEG = 180/pi;
Auto = get(handles.checkbox_Auto_I0,'Value');
%% - get centre -----------------------------------------------------------
M = load(NameF);                            % Load data
    DATA = M;
    MMM = size (DATA);      MX = MMM(2);    MY = MMM(1);
    % Getting pixel size of measured raw data
    Zmin = min(min(DATA));                  Zmax = max(max(DATA));
    % Calculate the minimum and maximum value of the raw data
if Zmax == 65535 %4095
    % overwrite all saturation values with the minimum value
    [rZ cZ] = find(DATA == Zmax);           DATA(rZ,cZ) = Zmax-1;
end
```

```
% --------------------------------------------------------------------------
%% --- subtract noise ------------------------------------------------------
    DATAsub_Int(1:MY,1:MX) = DATA - Zmin;
    % getting overall intensity of the raw data
    DATAsub(1:MY,1:MX) = DATA - (Zmin-1);
    % Subtracting the minimum value form the raw data
% --------------------------------------------------------------------------
%% --- select points -------------------------------------------------------
cla reset;
    XLim(handles.axes_Show,[SelMIN SelMAX]);
    set(gca,'XScale','linear');
    YLim(handles.axes_Show,[SelMIN SelMAX]);
    set(gca,'YScale','linear');
    contourf(mat2gray(DATAsub(SelMIN:SelMAX,SelMIN:SelMAX)));
    colorbar('location','eastoutside');
  contour3(handles.axes_3D,mat2gray(DATAsub(SelMIN:SelMAX,SelMIN:SelMAX)));
    Centre = get(handles.checkbox_Centre,'Value');
    if Centre == 1
        r_ = get(handles.edit_Row,'String');        r = str2double(r_);
        c_ = get(handles.edit_Colum,'String');      c = str2double(c_);
    else
        [c,r]=getpts;   c = SelMIN + round(c);      r = SelMIN + round(r);
    end;
% --------------------------------------------------------------------------
%% --- Airydiscs -----------------------------------------------------------
    % Get minimum distance to edge
if r >= (MY/2);     rrM = MY-r;   else    rrM = r;      end
    % Get minimum distance to edge
if c >= (MX/2);     ccM = MX-c;   else    ccM = c;      end
    V = rank(ccM,rrM);                    % Pixel size calculation
    % Take the smaller for the max Pixel size!
if V == 0;          Pix = ccM-1;  else    Pix = rrM-1;  end
if EndV >= Pix
    EndV = Pix;
    set(handles.edit_EndV,'String',num2str(EndV));
end
    PixFull= (2*Pix)+1;             Nbr = 1;
    PixCount = Pix*Pixel;           R = linspace(Pixel,PixCount,Pix)*10^-3;
    % *10^-3 to bring the µm from the pixel in mm
    ThetaR = (R/(F1*M2));           Teta_DEG = ThetaR * DEG;
    % ThetaR is in radians!!!
    Rsub = DATAsub(r-Pix:r+Pix,c-Pix:c+Pix);
    B0 = zeros(PixFull,PixFull);    B0(Pix+1,Pix+1) = 1;
    % Center point of the data
    D = zeros(Pix+1,1);             MZ = zeros(1,Pix+1);
    % Gerneration of empty array for speed optimization
    C = Rsub.*B0;                   D(1) = sum(sum(C));     MZ(1) = 1;
    % First data point
for a=1 : 1 : Pix+1
        A1 = Airydisk(PixFull,a-1,Nbr);  A2 = Airydisk(PixFull,a,Nbr);
        B = A2-A1;
        % eval(sprintf('B%i = B;',a));  % if you want to see the data rings
        C  = Rsub.*B;               Tresh = C(C>T);
        A3 = nonzeros(Tresh);       MZZ = size(A3);       MZ(a+1) = MZZ(1);
        % Saving of the average data for each ring
        D(a+1) = (sum(sum(Tresh)))/MZ(a+1);
end

Teta_Ray = linspace(min(ThetaR), max(ThetaR), length(R));   % 0.1° to 32°
Teta_Ray_DEG = Teta_Ray * DEG;
```

```
m12 = mREAL1/mREAL2;    m = [m12 + mIMAG];
k_Diff = (2*pi*mREAL2) ./ Laser .* sin(Teta_Ray);
x_Diff = k_Diff .* IntRadius;
    % Because Laser is given in µm also k (wave vector) is given in µm!!!

if DebyeOn == 1
    k_Deb = ((4*pi*mREAL2) ./ Laser) .* sin(Teta_Ray/2);
    % q_ = ((4*pi*mREAL2)/Laser) * sin(Teta_Ray/2);
    x_Deb = (k_Deb .* IntRadius);
    Iplot_Deb = (3.*((x_Deb.*cos(x_Deb)-sin(x_Deb))./(x_Deb.^3)).^2);
    Iplot_Debye = ((I0_User*20).*Iplot_Deb) ./ (P1^2);

%% Fitting Debye ----------------------------------------------------------
            set(handles.axes_Debye,'Visible','on');
            axes(handles.axes_Debye);
            cla(handles.axes_Debye,'reset');
            Data_Deb = log(D(StartV:EndV));
            q_Deb = k_Diff(StartV:EndV).';
    % --- Excluding values ------------------------------------------------
            Exclude_Deb = find(Data_Deb == max(Data_Deb));
            ex_Deb = false(length(Data_Deb),1);
            ex_Deb(1:Exclude_Deb) = 1;
            fo_Deb = fitoptions('method','NonlinearLeastSquares',...
                                'Lower',[1 0.1],'Upper',[100000 2]);
            st_Deb = [100 0.5];
            set(fo_Deb,'Startpoint',st_Deb);
            ok_Deb = isfinite(q_Deb) & isfinite(Data_Deb);
    % --- Fitting this model ----------------------------------------------
       ft_Deb = fittype('C*(3*((sin(q*a)-(q*a)*cos(q*a))/(q^3*a^3)))^2',...
                        'dependent',{'log(Data)'},'independent',{'q'},...
                        'coefficients',{'C', 'a'});
       cf_Deb = fit(q_Deb(ok_Deb),Data_Deb(ok_Deb),ft_Deb,'Exclude',...
                    ex_Deb(ok_Deb));
            COEFFvalues_Deb = coeffvalues(cf_Deb);
            a_Fit = abs(COEFFvalues_Deb(2));
    % --- Result of fit ---------------------------------------------------
            FI_Deb = ['FitDebye - R = ',num2str(a_Fit)];
            plot(q_Deb,Data_Deb,'bo');  hold on;    plot(cf_Deb,'g');
            legend('DataDebye',FI_Deb);
else
    Iplot_Debye = linspace(0, 0.001, length(R));
end
if MieOn == 1
        k_Mie = (2*pi*mREAL2) ./ Laser;
        x_Mie = k_Mie .* IntRadius;
                for j = 1 : length(Teta_Ray)
                    u = cos(Teta_Ray(j));
                    S12(:,j) = Mie_S12(m,x_Mie,u);
                    I1(j) = real(S12(1,j)'* S12(1,j));
                    I2(j) = real(S12(2,j)'* S12(2,j));
                    I12(j)= (I1(j) + I2(j)) / 2;
                end;
                if Auto == 1
                    D_FIT = max(D(StartV:EndV));    rI = find(D == D_FIT);
                    Iplot_Mie_rI = ((I1(rI) + I2(rI)) / (2*k_Mie^2*P1^2));
                    I0_FIT = D_FIT / Iplot_Mie_rI;
                    Iplot_Mie =((I0_FIT.*(I1 + I2))./(2.*k_Mie.^2.*P1.^2));
                else
                    Iplot_Mie=((I0_User.*(I1 + I2))./(2.*k_Mie.^2.*P1.^2));
                end;
```

```matlab
else
    Iplot_Mie = linspace(0, 0.001, length(R));
end
    k_Diff_ = (2*pi) ./ Laser;
    x_Diff_ = k_Diff_ .* IntRadius.* sin(Teta_Ray);
    R_Diff = round(Q1*M1*M2);
    P0 = 5;
    A_Diff = pi*(IntRadius^2);
    I0_Diff = (P0*A_Diff)/((Laser^2)*(R_Diff^2))*10^6;
    J1 = besselj(nu,x_Diff_);
    Iplot_Diff = I0_Diff *(2.*J1./x_Diff_).^2;

% --------------------------------------------------------------------------
%% --- Plot ----------------------------------------------------------------
if DegreeOn == 1
    axes(handles.axes_Show);
    semilogy(Teta_Ray_DEG(:,StartV:EndV),Iplot_Mie(:,StartV:EndV),'r');
    hold on;
    semilogy(Teta_Ray_DEG(:,StartV:EndV),Iplot_Debye(:,StartV:EndV),'g');
    semilogy(Teta_Ray_DEG(:,StartV:EndV),Iplot_Diff(:,StartV:EndV),'c');
    semilogy(Teta_Ray_DEG(:,StartV:EndV),D(StartV:EndV,:),'b');
    plot(1.5,1:10000,'g*');
    legend('Mie - in°','Debye - in°','Diffr - in°','Data - in °');
    MAXy = max(max(D))*2;       MINy = D(EndV)/5;
    set(gca,'XLim',[Teta_Ray_DEG(StartV) Teta_Ray_DEG(EndV)]);
    set(gca,'YLim',[MINy MAXy]);
    set(gca,'XScale','linear');
    set(gca,'YScale','log');
else
    axes(handles.axes_Show);
    loglog(k_Diff(:,StartV:EndV),Iplot_Mie(:,StartV:EndV),'r');
    hold on;
    loglog(k_Diff(:,StartV:EndV),Iplot_Debye(:,StartV:EndV),'g');
    loglog(k_Diff(:,StartV:EndV),Iplot_Diff(:,StartV:EndV),'c');
    loglog(k_Diff(:,StartV:EndV),D(StartV:EndV,:),'b');
    plot(0.695,1:10000,'g*');
    legend('Mie - in°','Debye - in°','Diffr - in°','Data - in °');
    MAXy = max(max(D))*5;       MINy = min(D)/5;
    set(gca,'XLim',[k_Diff(StartV) k_Diff(EndV)]);
    set(gca,'YLim',[MINy MAXy]);
    set(gca,'XScale','log');
    set(gca,'YScale','log');
end
title(['Average intensity vs. Wave vector/scattering angle - Radius = ',...
      num2str(IntRadius),' µm']);       % Plot the ring intensities as bars
    NameP = ['Pinhole - ',num2str(IntRadius),' µm - ',NameF(5:12)];
                                        % print('-djpeg',NameP);
    zoom on;

if Centre == 0
    set(handles.edit_Row,'String',num2str(r));
    set(handles.edit_Colum,'String',num2str(c));
end;

    if GuinierOn == 1
        set(handles.axes_Guinier,'Visible','on');
        axes(handles.axes_Guinier);
        cla(handles.axes_Guinier,'reset');
        Data_Gui = log(D(StartV:EndV));
        q_Gui = k_Diff(StartV:EndV).';
```

```
% --- Excluding values ----------------------------------------------------
    ExcludeV_Gui = find(Data_Gui == max(Data_Gui));
    ex_Gui = false(length(Data_Gui),1);
    ex_Gui(1:ExcludeV_Gui) = 1;
% --- Fitting this model --------------------------------------------------
        fo_Gui = fitoptions('method','NonlinearLeastSquares','Lower',...
                            [1 0.1],'Upper',[100000 2]);
        ft_Gui = fittype('A * exp(- ((q*R)^2) / 5)','dependent',...
                        {'log(Data)'},'independent',{'q'},...
                        'coefficients',{'A', 'R'});
        st_Gui = [100 0.5];
        set(fo_Gui,'Startpoint',st_Gui);
        ok_Gui = isfinite(q_Gui) & isfinite(Data_Gui);
        cf_Gui = fit(q_Gui(ok_Gui),Data_Gui(ok_Gui),ft_Gui,'Exclude',...
                     ex_Gui(ok_Gui));
% --- Result of fit -------------------------------------------------------
        COEFFvalues_Gui = coeffvalues(cf_Gui);
        FI_Gui = ['FitGuinier - R = ',num2str(abs(COEFFvalues_Gui(2)))];
        plot(q_Gui,Data_Gui,'bo');          hold on;
        plot(cf_Gui,'m');                   legend('DataGuinier',FI_Gui);
        NameSaveData = [NameP,' - Gui','.txt'];
        save(NameSaveData,'Data_Gui','-ascii');
        save('Q - Gui.txt','q_Gui','-ascii');
    end
% --- Saving --------------------------------------------------------------
NameSave = [NameP,'.mat'];
save(NameSave,'k_Diff','NameF','StartV','EndV','Teta_Ray',...
              'Teta_Ray_DEG','D','Iplot_Debye','Iplot_Diff','Iplot_Mie',...
              'R','r','c','DATA','DATAsub');    % Saving important values

% --------------------------------------------------------------------------
% ___  fit button _______________________________________________________
% --------------------------------------------------------------------------

function pushbutton_Fit_Callback(~, ~, handles)
global NameF;   global StartV;  global EndV;    global ThetaR;  global P1;
global D;       global Iplot;   global R;       global r;       global c;
global DATAsub; global DATAsub_Int;

set(handles.axes_Guinier,'Visible','off');
set(handles.axes_Debye,'Visible','off');
MieOn = get(handles.radiobutton_Mie,'Value');
DEG = 180/pi;           DegreeOn = get(handles.radiobutton_Degree,'Value');
Radius_= get(handles.edit_Radius,'String');
Radius_SV = str2double(Radius_);
Laser_= get(handles.edit_Laser,'String');    Laser_SV = str2double(Laser_);
I0_= get(handles.edit_I0,'String');          I0_SV = str2double(I0_);
    % Setting background color for P1 fit field
set(handles.edit_P1Fit,'BackgroundColor',[0.8 0.9 0.8]);
mIMAG_ = [get(handles.edit_mIMAG,'String'),'i'];
    % PSL at 0.6328 μm = 1.58722, H2O at 0.6328 μm = 1.33169
mIMAG = str2double(mIMAG_);
mREAL1_= get(handles.edit_mREAL1,'String');
mREAL1 = str2double(mREAL1_);
mREAL2_= get(handles.edit_mREAL2,'String');
mREAL2 = str2double(mREAL2_);
ThetaR_DEG = ThetaR .* DEG';
Average_Int = sum(sum(DATAsub_Int))/(length(DATAsub_Int(:,1))...
                  *length(DATAsub_Int(1,:)));
set(handles.edit_Int,'String',num2str(round((Average_Int*100))/100));
```

```
% --- Defining raw data ---
The_ = R(StartV:EndV).';                    % Getting X values (Theta, R)
Int_ = log(D(StartV:EndV,:));               % Getting Y values (Intensity)
% --- plotting raw data in 3D ---
    % Getting min selected distance for view of interest
SelMAX_= get(handles.edit_SelMAX,'String');    SelMAX = str2double(SelMAX_);
    % Getting max selected distance for view of interest
SelMIN_= get(handles.edit_SelMIN,'String');    SelMIN = str2double(SelMIN_);
    % Plotting 3D graph
contour3(handles.axes_3D,mat2gray(DATAsub(SelMIN:SelMAX,SelMIN:SelMAX)));
% --- plotting contour of raw data (LEFT) ---
    % Clear the Showing axes
axes(handles.axes_Show);    cla(handles.axes_Show,'reset');
    % Setting X scale and style
XLim(handles.axes_Show,[SelMIN SelMAX]);    set(gca,'XScale','linear');
    % Setting Y scale and style
YLim(handles.axes_Show,[SelMIN SelMAX]);    set(gca,'YScale','linear');
    % Plotting red lines of used center
plot(c-SelMIN,1:SelMAX-SelMIN,'r');         hold on;
plot(1:SelMAX-SelMIN,r-SelMIN,'r');
contour(mat2gray(DATAsub(SelMIN:SelMAX,SelMIN:SelMAX)));
% --- plotting raw data for fit (right) ---
    % Clear the Fiting axes
axes(handles.axes_Fit);                 cla(handles.axes_Fit,'reset');
if DegreeOn == 1
    % Plotting measured data
    semilogy(ThetaR_DEG(1,StartV:EndV),Int_,'bo');              hold on;
    set(gca,'XLim',[ThetaR_DEG(StartV) ThetaR_DEG(EndV)]);
    set(gca,'XScale','linear');         % Setting X scale and style
else
    loglog(The_,Int_,'bo');             hold on;
    legend('Measured');                 % Plotting measured data
    set(gca,'XLim',[R(StartV) R(EndV)]);
    set(gca,'XScale','log');            % Setting X scale and style
end
    set(gca,'YLim',[1 10]);
    set(gca,'YScale','log');            % Setting Y scale and style
% --- Mie plot & calculation ---
if MieOn == 1
    m12  = mREAL1/mREAL2;
    m = [m12 + mIMAG];
    Laser_Mie = Laser_SV/mREAL2;
    k_Mie = (2*pi)/Laser_Mie;
    Teta = linspace(min(ThetaR), max(ThetaR), length(R));
    x_t  = k_Mie.* Radius_SV;
    Teta_DEG = Teta * DEG;
        for j = 1 : length(Teta)
            u = cos(Teta(j));
            S12(:,j) = Mie_S12(m,x_t,u);
            I1(j) = real(S12(1,j)'* S12(1,j));
            I2(j) = real(S12(2,j)'* S12(2,j));
            I12(j)= (I1(j) + I2(j)) / 2;
        end;
    I_Mie = ((I0_SV.*(I1 + I2)) ./ (2.*k_Mie.^2.*(P1*M1*M2).^2));
        axes(handles.axes_Fit);
    if DegreeOn == 1
        semilogy(Teta_DEG(1,StartV:EndV),I_Mie(1,StartV:EndV),'r');
        legend('Measured','MIE-I');
    else
        loglog(The_,I_Mie(1,StartV:EndV),'r');
```

```
        legend('Measured','MIE-I');
    end
else
% --- Pinhole plot & calculation ---
% --- Exclude -------------------------------------------------------------
ExcludeV = find(max(Int_)==Int_)-1;
ex_ = false(length(The_),1);
ex_(1:ExcludeV) = 1;
    % Checking if arrays have the same length
ok_ = isfinite(The_) & isfinite(Int_);
% --- Load values ---------------------------------------------------------
    Prediction_On_Off=get(handles.checkbox_Prediction,'Value');
    AlgorithmV      = get(handles.popupmenu_Algorithm,'Value');
    AlgorithmS      = get(handles.popupmenu_Algorithm,'String');
    Algorithm       = cell2mat(AlgorithmS(AlgorithmV));
    MaxFunEvalsV    = get(handles.popupmenu_MaxFunEvals,'Value');
    MaxFunEvalsS    = get(handles.popupmenu_MaxFunEvals,'String');
    MaxFunEvals     = str2double(cell2mat(MaxFunEvalsS(MaxFunEvalsV)));
    MaxIterV        = get(handles.popupmenu_MaxIter,'Value');
    MaxIterS        = get(handles.popupmenu_MaxIter,'String');
    MaxIter         = str2double(cell2mat(MaxIterS(MaxIterV)));
    DiffMinChangeV  = get(handles.popupmenu_DiffMinChange,'Value');
    DiffMinChangeS  = get(handles.popupmenu_DiffMinChange,'String');
    DiffMinChange   = str2double(cell2mat(DiffMinChangeS(DiffMinChangeV)));
    DiffMaxChangeV  = get(handles.popupmenu_DiffMaxChange,'Value');
    DiffMaxChangeS  = get(handles.popupmenu_DiffMaxChange,'String');
    DiffMaxChange   = str2double(cell2mat(DiffMaxChangeS(DiffMaxChangeV)));
    RobustV         = get(handles.popupmenu_Robust,'Value');
    RobustS         = get(handles.popupmenu_Robust,'String');
    Robust          = cell2mat(RobustS(RobustV));
    NormalizeV      = get(handles.popupmenu_Normalize,'Value');
    NormalizeS      = get(handles.popupmenu_Normalize,'String');
    Normalize       = cell2mat(NormalizeS(NormalizeV));
    DisplayV        = get(handles.popupmenu_Display,'Value');
    DisplayS        = get(handles.popupmenu_Display,'String');
    Display         = cell2mat(DisplayS(DisplayV));
    TolFunV         = get(handles.popupmenu_TolFun,'Value');
    TolFunS         = get(handles.popupmenu_TolFun,'String');
    TolFun          = str2double(cell2mat(TolFunS(TolFunV)));
    TolXV           = get(handles.popupmenu_TolX,'Value');
    TolXS           = get(handles.popupmenu_TolX,'String');
    TolX            = str2double(cell2mat(TolXS(TolXV)));
    AccuracyV       = get(handles.popupmenu_Accuracy,'Value');
    AccuracyS       = get(handles.popupmenu_Accuracy,'String');
    Accuracy        = str2double(cell2mat(AccuracyS(AccuracyV)));
    PredictionV     = get(handles.popupmenu_Prediction,'Value');
    PredictionS     = get(handles.popupmenu_Prediction,'String');
    Prediction      = str2double(cell2mat(PredictionS(PredictionV)));
    PredictionTypeV = get(handles.popupmenu_PredictionType,'Value');
    PredictionTypeS = get(handles.popupmenu_PredictionType,'String');
    PredictionType  = cell2mat(PredictionTypeS(PredictionTypeV));

F1_= get(handles.edit_F1,'String');         F1_SV = str2double(F1_);
F2_= get(handles.edit_F2,'String');         F2_SV = str2double(F2_);
P1_= get(handles.edit_P1,'String');         P1_SV = str2double(P1_);
Back_SV = 1;                                K_SV = 2*pi/Laser_SV;
MIN_SV = 0.90;      MIN_SV_ = 0.99999;      MIN_SV__= 0.001;
MAX_SV = 1.10;      MAX_SV_ = 1.00001;      MAX_SV__= 10000;

Back_SV_MIN   = Back_SV * MIN_SV__;     Back_SV_MAX   = Back_SV * MAX_SV__;
```

```
I0_SV_MIN     = I0_SV * MIN_SV__;       I0_SV_MAX     = I0_SV * MAX_SV__;
P1_SV_MIN     = P1_SV * MIN_SV;         P1_SV_MAX     = P1_SV * MAX_SV;
F1_SV_MIN     = F1_SV * MIN_SV_;        F1_SV_MAX     = F1_SV * MAX_SV_;
F2_SV_MIN     = F2_SV * MIN_SV_;        F2_SV_MAX     = F2_SV * MAX_SV_;
K_SV_MIN      = K_SV  * MIN_SV_;        K_SV_MAX      = K_SV  * MAX_SV_;
Radius_SV_MIN = Radius_SV * MIN_SV_;    Radius_SV_MAX = Radius_SV *MAX_SV_;

% --- Fitting values -------------------------------------------------------
fo_ = fitoptions('method','NonlinearLeastSquares','Lower',...
                [F1_SV_MIN F2_SV_MIN P1_SV_MIN I0_SV_MIN Radius_SV_MIN...
                K_SV_MIN Back_SV_MIN],'Upper',[F1_SV_MAX F2_SV_MAX...
                P1_SV_MAX I0_SV_MAX Radius_SV_MAX K_SV_MAX Back_SV_MAX],...
                'Robust',Robust,'Display','iter','DiffMinChange',...
                DiffMinChange,'DiffMaxChange',DiffMaxChange,...
                'MaxFunEvals',MaxFunEvals,'MaxIter',MaxIter,'Normalize',...
                Normalize,'Display',Display,'TolFun',TolFun,'TolX',TolX);
st_ = [F1_SV F2_SV P1_SV I0_SV Radius_SV K_SV Back_SV];
set(fo_,'Startpoint',st_);      set(fo_,'Exclude',ex_(ok_));
ft_ = fittype('log((I0_SV * (( (2*(besselj(1,(K_SV*Radius_SV*sin(((F1_SV*(F1_SV+F2_SV)↙
- (F2_SV*P1_SV)) / (F1_SV*F2_SV*(-F1_SV+P1_SV)))*R))))) / (K_SV*Radius_SV*sin(((F1_SV*↙
(F1_SV+F2_SV) - (F2_SV*P1_SV)) / (F1_SV*F2_SV*(-F1_SV+P1_SV)))*R)) )^2)) +↙
Back_SV)','dependent',{'Intensity'},'independent',{'R'},'coefficients',{'F1_SV',↙
'F2_SV', 'P1_SV', 'I0_SV', 'Radius_SV', 'K_SV', 'Back_SV'});

% --- Fitting this model ---------------------------------------------------
[cf_Winview, gof_Winview] = fit(The_(ok_),Int_(ok_),ft_,fo_);
plot(cf_Winview,'g');                   % Fitting and plotting the result

% --- Result of fit --------------------------------------------------------
    % Getting the fitting result in a array
COEFFvalues_Winview = coeffvalues(cf_Winview);
F1_Fit = COEFFvalues_Winview(1);        F2_Fit = COEFFvalues_Winview(2);
P1_Fit = COEFFvalues_Winview(3);        I0_Fit = COEFFvalues_Winview(4);
Radius_Fit = COEFFvalues_Winview(5);    K_Fit = COEFFvalues_Winview(6);
Back_Fit = COEFFvalues_Winview(7);
set(handles.edit_F1Fit,'String',num2str(round((F1_Fit*10000))/10000));
set(handles.edit_F2Fit,'String',num2str(round((F2_Fit*10000))/10000));
set(handles.edit_I0Fit,'String',num2str(round(I0_Fit)));
set(handles.edit_RadiusFit,'String',...
    num2str(round((Radius_Fit*10000))/10000));
set(handles.edit_P1Fit,'String',num2str(P1_Fit));
set(handles.edit_BackFit,'String',num2str(round((Back_Fit*100))/100));

if round((P1_Fit*1000))/1000 == (P1_SV_MIN)
    set(handles.edit_P1Fit,'BackgroundColor','red');
end;
if round((P1_Fit*1000))/1000 == (P1_SV_MAX)
    set(handles.edit_P1Fit,'BackgroundColor','red');
end

% --- Prediction -----------------------------------------------------------
if Prediction_On_Off == 1
    predintCF = predint(cf_Winview,The_,Prediction,PredictionType,'on');
    plot(The_,predintCF,'y');
end

% --- Difference -----------------------------------------------------------
    % Clear the Showing axes
axes(handles.axes_Diff);            cla(handles.axes_Diff,'reset');
Theta = ((F1_Fit*(F1_Fit+F2_Fit) - (F2_Fit*P1_Fit)) / (F1_Fit*F2_Fit*...
```

```
        (-F1_Fit+P1_Fit)))*The_;   x_ = K_Fit*Radius_Fit*sin(Theta);
J1_ = besselj(1,x_);
    % Calculating intensity with values from fit
ycf = log((I0_Fit *(2.*J1_./x_).^2)+Back_Fit);
    % Getting difference between fit and raw data
for i = 1:length(Int_)  yDifference(i,1) = Int_(i) - ycf(i);    end;
bar(The_,abs(yDifference),'k');
set(gca,'XLim',[R(StartV) R(EndV)]);
set(gca,'XScale','log');
set(gca, 'XTick', []);                          % Plotting difference

% --- Saving --------------------------------------------------------------
save('Coeff.mat','COEFFvalues_Winview','NameF','StartV','EndV','ThetaR',...
    'D','Iplot','R','r','c','DATAsub');         % Saving important values

%% ------------------------------------------------------------------------
%% ------------------------------------------------------------------------
function checkbox_Fit_Callback(~ ,~ , handles)
    Fit = get(handles.checkbox_Fit,'Value');
    if Fit == 1                                 % Showing fit
        set(handles.axes_Fit,'Visible','on');
        set(handles.axes_Diff,'Visible','on');
        set(handles.pushbutton_Fit,'Visible','on');
        set(handles.checkbox_Prediction,'Visible','on');
        set(handles.popupmenu_PredictionType,'Visible','on');
        set(handles.edit_F1Fit,'Visible','on');
        set(handles.edit_F2Fit,'Visible','on');
        set(handles.edit_P1Fit,'Visible','on');
        set(handles.edit_RadiusFit,'Visible','on');
        set(handles.edit_I0Fit,'Visible','on');
        set(handles.edit_BackFit,'Visible','on');
        set(handles.edit_Int,'Visible','on');
        set(handles.popupmenu_Algorithm,'Visible','on');
        set(handles.popupmenu_MaxFunEvals,'Visible','on');
        set(handles.popupmenu_MaxIter,'Visible','on');
        set(handles.popupmenu_DiffMinChange,'Visible','on');
        set(handles.popupmenu_DiffMaxChange,'Visible','on');
        set(handles.popupmenu_Robust,'Visible','on');
        set(handles.popupmenu_Normalize,'Visible','on');
        set(handles.popupmenu_Display,'Visible','on');
        set(handles.popupmenu_TolFun,'Visible','on');
        set(handles.popupmenu_TolX,'Visible','on');
        set(handles.popupmenu_Accuracy,'Visible','on');
        set(handles.popupmenu_Prediction,'Visible','on');
        set(handles.text_DiffMinChange,'Visible','on');
        set(handles.text_Normalize,'Visible','on');
        set(handles.text_Prediction,'Visible','on');
        set(handles.text_TolX,'Visible','on');
        set(handles.text_Accuracy,'Visible','on');
        set(handles.text_Display,'Visible','on');
        set(handles.text_TolFun,'Visible','on');
        set(handles.text_Fit,'Visible','on');
        set(handles.text_Algorithm,'Visible','on');
        set(handles.text_MaxFunEvals,'Visible','on');
        set(handles.text_MaxIter,'Visible','on');
        set(handles.text_Robust,'Visible','on');
        set(handles.text_DiffMaxChange,'Visible','on');
        set(handles.text_Back,'Visible','on');
        set(handles.text_Int,'Visible','on');
    else                                        % Hiding fit
```

```
        cla(handles.axes_Fit,'reset');
        cla(handles.axes_Diff,'reset');
        set(handles.axes_Fit,'Visible','off');
        set(handles.axes_Diff,'Visible','off');
        set(handles.pushbutton_Fit,'Visible','off');
        set(handles.checkbox_Prediction,'Visible','off');
        set(handles.popupmenu_PredictionType,'Visible','off');
        set(handles.edit_F1Fit,'Visible','off');
        set(handles.edit_F2Fit,'Visible','off');
        set(handles.edit_P1Fit,'Visible','off');
        set(handles.edit_RadiusFit,'Visible','off');
        set(handles.edit_I0Fit,'Visible','off');
        set(handles.edit_BackFit,'Visible','off');
        set(handles.popupmenu_Algorithm,'Visible','off');
        set(handles.edit_Int,'Visible','off');
        set(handles.popupmenu_MaxFunEvals,'Visible','off');
        set(handles.popupmenu_MaxIter,'Visible','off');
        set(handles.popupmenu_DiffMinChange,'Visible','off');
        set(handles.popupmenu_DiffMaxChange,'Visible','off');
        set(handles.popupmenu_Robust,'Visible','off');
        set(handles.popupmenu_Normalize,'Visible','off');
        set(handles.popupmenu_Display,'Visible','off');
        set(handles.popupmenu_TolFun,'Visible','off');
        set(handles.popupmenu_TolX,'Visible','off');
        set(handles.popupmenu_Accuracy,'Visible','off');
        set(handles.popupmenu_Prediction,'Visible','off');
        set(handles.text_DiffMinChange,'Visible','off');
        set(handles.text_Normalize,'Visible','off');
        set(handles.text_Prediction,'Visible','off');
        set(handles.text_TolX,'Visible','off');
        set(handles.text_Accuracy,'Visible','off');
        set(handles.text_Display,'Visible','off');
        set(handles.text_TolFun,'Visible','off');
        set(handles.text_Fit,'Visible','off');
        set(handles.text_Algorithm,'Visible','off');
        set(handles.text_MaxFunEvals,'Visible','off');
        set(handles.text_MaxIter,'Visible','off');
        set(handles.text_Robust,'Visible','off');
        set(handles.text_DiffMaxChange,'Visible','off');
        set(handles.text_Back,'Visible','off');
        set(handles.text_Int,'Visible','off');
    end

function checkbox_Centre_Callback(~ ,~ , handles)
    Centre = get(handles.checkbox_Centre,'Value');
    if Centre == 1                              % Showing Centre manual values
        set(handles.text_Row,'Visible','on');
        set(handles.text_Colum,'Visible','on');
        set(handles.edit_Row,'Visible','on');
        set(handles.edit_Colum,'Visible','on');
    else
        set(handles.text_Row,'Visible','off');
        set(handles.text_Colum,'Visible','off');
        set(handles.edit_Row,'Visible','off');
        set(handles.edit_Colum,'Visible','off');
    end

function checkbox_Auto_I0_Callback(~ ,~ , handles)
    Auto = get(handles.checkbox_Auto_I0,'Value');
    if Auto == 1                                % Showing I0 values
```

```
        set(handles.edit_I0,'Visible','off');
    else
        set(handles.edit_I0,'Visible','on');
    end

function radiobutton_Rayleigh_Callback(~, ~, ~)
function radiobutton_Mie_Callback(~, ~, ~)
function radiobutton_Degree_Callback(~, ~, ~)
function radiobutton_Guinier_Callback(hObject, eventdata, handles)

function checkbox_Prediction_Callback(~, ~, ~)

function edit_NameF_Callback(~, ~, ~)
function edit_NameF_CreateFcn(hObject, ~, ~)
    if ispc && isequal(get(hObject,'BackgroundColor'),
        get(0,'defaultUicontrolBackgroundColor'))
        set(hObject,'BackgroundColor','white');
    end

function edit_Radius_Callback(~, ~, ~)
function edit_Radius_CreateFcn(hObject, ~, ~)
    if ispc && isequal(get(hObject,'BackgroundColor'),
        get(0,'defaultUicontrolBackgroundColor'))
        set(hObject,'BackgroundColor','white');
    end

function edit_Laser_Callback(~, ~, ~)
function edit_Laser_CreateFcn(hObject, ~, ~)
    if ispc && isequal(get(hObject,'BackgroundColor'),
        get(0,'defaultUicontrolBackgroundColor'))
        set(hObject,'BackgroundColor','white');
    end

function edit_Pixel_Callback(~, ~, ~)
function edit_Pixel_CreateFcn(hObject, ~, ~)
    if ispc && isequal(get(hObject,'BackgroundColor'),
        get(0,'defaultUicontrolBackgroundColor'))
        set(hObject,'BackgroundColor','white');
    end

function edit_F1_Callback(~, ~, ~)
function edit_F1_CreateFcn(hObject, ~, ~)
    if ispc && isequal(get(hObject,'BackgroundColor'),
        get(0,'defaultUicontrolBackgroundColor'))
        set(hObject,'BackgroundColor','white');
    end

function edit_F2_Callback(~, ~, ~)
function edit_F2_CreateFcn(hObject, ~, ~)
    if ispc && isequal(get(hObject,'BackgroundColor'),
        get(0,'defaultUicontrolBackgroundColor'))
        set(hObject,'BackgroundColor','white');
    end

function edit_P1_Callback(~, ~, ~)
function edit_P1_CreateFcn(hObject, ~, ~)
    if ispc && isequal(get(hObject,'BackgroundColor'),
        get(0,'defaultUicontrolBackgroundColor'))
        set(hObject,'BackgroundColor','white');
    end
```

```
function edit_Nu_Callback(~, ~, ~)
function edit_Nu_CreateFcn(hObject, ~, ~)
    if ispc && isequal(get(hObject,'BackgroundColor'),
        get(0,'defaultUicontrolBackgroundColor'))
        set(hObject,'BackgroundColor','white');
    end

function edit_I0_Callback(~, ~, ~)
function edit_I0_CreateFcn(hObject, ~, ~)
    if ispc && isequal(get(hObject,'BackgroundColor'),
        get(0,'defaultUicontrolBackgroundColor'))
        set(hObject,'BackgroundColor','white');
    end

function edit_T_Callback(~, ~, ~)
function edit_T_CreateFcn(hObject, ~, ~)
    if ispc && isequal(get(hObject,'BackgroundColor'),
        get(0,'defaultUicontrolBackgroundColor'))
        set(hObject,'BackgroundColor','white');
    end

function edit_SelMIN_Callback(~, ~, ~)
function edit_SelMIN_CreateFcn(hObject, ~, ~)
    if ispc && isequal(get(hObject,'BackgroundColor'),
        get(0,'defaultUicontrolBackgroundColor'))
        set(hObject,'BackgroundColor','white');
    end

function edit_SelMAX_Callback(~, ~, ~)
function edit_SelMAX_CreateFcn(hObject, ~, ~)
    if ispc && isequal(get(hObject,'BackgroundColor'),
        get(0,'defaultUicontrolBackgroundColor'))
        set(hObject,'BackgroundColor','white');
    end

function edit_StartV_Callback(~, ~, ~)
function edit_StartV_CreateFcn(hObject, ~, ~)
    if ispc && isequal(get(hObject,'BackgroundColor'),
        get(0,'defaultUicontrolBackgroundColor'))
        set(hObject,'BackgroundColor','white');
    end

function edit_EndV_Callback(~, ~, ~)
function edit_EndV_CreateFcn(hObject, ~, ~)
    if ispc && isequal(get(hObject,'BackgroundColor'),
        get(0,'defaultUicontrolBackgroundColor'))
        set(hObject,'BackgroundColor','white');
    end

function edit_P1Fit_Callback(~, ~, ~)
function edit_P1Fit_CreateFcn(hObject, ~, ~)
    if ispc && isequal(get(hObject,'BackgroundColor'),
        get(0,'defaultUicontrolBackgroundColor'))
        set(hObject,'BackgroundColor','white');
    end

function edit_RadiusFit_Callback(~, ~, ~)
function edit_RadiusFit_CreateFcn(hObject, ~, ~)
    if ispc && isequal(get(hObject,'BackgroundColor'),
```

```
        get(0,'defaultUicontrolBackgroundColor'))
        set(hObject,'BackgroundColor','white');
    end

function edit_F2Fit_Callback(~, ~, ~)
function edit_F2Fit_CreateFcn(hObject, ~, ~)
    if ispc && isequal(get(hObject,'BackgroundColor'),
        get(0,'defaultUicontrolBackgroundColor'))
        set(hObject,'BackgroundColor','white');
    end

function edit_F1Fit_Callback(~, ~, ~)
function edit_F1Fit_CreateFcn(hObject, ~, ~)
    if ispc && isequal(get(hObject,'BackgroundColor'),
        get(0,'defaultUicontrolBackgroundColor'))
        set(hObject,'BackgroundColor','white');
    end

function edit_I0Fit_Callback(~, ~, ~)
function edit_I0Fit_CreateFcn(hObject, ~, ~)
    if ispc && isequal(get(hObject,'BackgroundColor'),
        get(0,'defaultUicontrolBackgroundColor'))
        set(hObject,'BackgroundColor','white');
    end

function edit_BackFit_Callback(~, ~, ~)
function edit_BackFit_CreateFcn(hObject, ~, ~)
    if ispc && isequal(get(hObject,'BackgroundColor'),
        get(0,'defaultUicontrolBackgroundColor'))
        set(hObject,'BackgroundColor','white');
    end

function edit_Int_Callback(~, ~, ~)
function edit_Int_CreateFcn(hObject, ~, ~)
    if ispc && isequal(get(hObject,'BackgroundColor'),
        get(0,'defaultUicontrolBackgroundColor'))
        set(hObject,'BackgroundColor','white');
    end


function edit_mIMAG_Callback(~, ~, ~)
function edit_mIMAG_CreateFcn(hObject, ~, ~)
    if ispc && isequal(get(hObject,'BackgroundColor'),
        get(0,'defaultUicontrolBackgroundColor'))
        set(hObject,'BackgroundColor','white');
    end

function edit_mREAL1_Callback(~, ~, ~)
function edit_mREAL1_CreateFcn(hObject, ~, ~)
    if ispc && isequal(get(hObject,'BackgroundColor'),
        get(0,'defaultUicontrolBackgroundColor'))
        set(hObject,'BackgroundColor','white');
    end

function edit_mREAL2_Callback(~, ~, ~)
function edit_mREAL2_CreateFcn(hObject, ~, ~)
    if ispc && isequal(get(hObject,'BackgroundColor'),
        get(0,'defaultUicontrolBackgroundColor'))
        set(hObject,'BackgroundColor','white');
    end
```

```
function popupmenu_MaxFunEvals_Callback(~, ~, ~)
function popupmenu_MaxFunEvals_CreateFcn(hObject, ~, ~)
    if ispc && isequal(get(hObject,'BackgroundColor'),
        get(0,'defaultUicontrolBackgroundColor'))
        set(hObject,'BackgroundColor','white');
    end

function popupmenu_MaxIter_Callback(~, ~, ~)
function popupmenu_MaxIter_CreateFcn(hObject, ~, ~)
    if ispc && isequal(get(hObject,'BackgroundColor'),
        get(0,'defaultUicontrolBackgroundColor'))
        set(hObject,'BackgroundColor','white');
    end

function popupmenu_DiffMinChange_Callback(~, ~, ~)
function popupmenu_DiffMinChange_CreateFcn(hObject, ~, ~)
    if ispc && isequal(get(hObject,'BackgroundColor'),
        get(0,'defaultUicontrolBackgroundColor'))
        set(hObject,'BackgroundColor','white');
    end

function popupmenu_Robust_Callback(~, ~, ~)
function popupmenu_Robust_CreateFcn(hObject, ~, ~)
    if ispc && isequal(get(hObject,'BackgroundColor'),
        get(0,'defaultUicontrolBackgroundColor'))
        set(hObject,'BackgroundColor','white');
    end

function popupmenu_Normalize_Callback(~, ~, ~)
function popupmenu_Normalize_CreateFcn(hObject, ~, ~)
    if ispc && isequal(get(hObject,'BackgroundColor'),
        get(0,'defaultUicontrolBackgroundColor'))
        set(hObject,'BackgroundColor','white');
    end

function popupmenu_Display_Callback(~, ~, ~)
function popupmenu_Display_CreateFcn(hObject, ~, ~)
    if ispc && isequal(get(hObject,'BackgroundColor'),
        get(0,'defaultUicontrolBackgroundColor'))
        set(hObject,'BackgroundColor','white');
    end

function popupmenu_TolFun_Callback(~, ~, ~)
function popupmenu_TolFun_CreateFcn(hObject, ~, ~)
    if ispc && isequal(get(hObject,'BackgroundColor'),
        get(0,'defaultUicontrolBackgroundColor'))
        set(hObject,'BackgroundColor','white');
    end

function popupmenu_TolX_Callback(~, ~, ~)
function popupmenu_TolX_CreateFcn(hObject, ~, ~)
    if ispc && isequal(get(hObject,'BackgroundColor'),
        get(0,'defaultUicontrolBackgroundColor'))
        set(hObject,'BackgroundColor','white');
    end

function popupmenu_DiffMaxChange_Callback(~, ~, ~)
function popupmenu_DiffMaxChange_CreateFcn(hObject, ~, ~)
    if ispc && isequal(get(hObject,'BackgroundColor'),
```

```
        get(0,'defaultUicontrolBackgroundColor'))
        set(hObject,'BackgroundColor','white');
    end

function popupmenu_Accuracy_Callback(~, ~, ~)
function popupmenu_Accuracy_CreateFcn(hObject, ~, ~)
    if ispc && isequal(get(hObject,'BackgroundColor'),
        get(0,'defaultUicontrolBackgroundColor'))
        set(hObject,'BackgroundColor','white');
    end

function popupmenu_Algorithm_Callback(~, ~, ~)
function popupmenu_Algorithm_CreateFcn(hObject, ~, ~)
    if ispc && isequal(get(hObject,'BackgroundColor'),
        get(0,'defaultUicontrolBackgroundColor'))
        set(hObject,'BackgroundColor','white');
    end

function popupmenu_Prediction_Callback(~, ~, ~)
function popupmenu_Prediction_CreateFcn(hObject, ~, ~)
    if ispc && isequal(get(hObject,'BackgroundColor'),
        get(0,'defaultUicontrolBackgroundColor'))
        set(hObject,'BackgroundColor','white');
    end

function popupmenu_PredictionType_Callback(~, ~, ~)
function popupmenu_PredictionType_CreateFcn(hObject, ~, ~)
    if ispc && isequal(get(hObject,'BackgroundColor'),
        get(0,'defaultUicontrolBackgroundColor'))
        set(hObject,'BackgroundColor','white');
    end

function edit_Row_Callback(~, ~, ~)
function edit_Row_CreateFcn(hObject, ~, ~)
    if ispc && isequal(get(hObject,'BackgroundColor'),
        get(0,'defaultUicontrolBackgroundColor'))
        set(hObject,'BackgroundColor','white');
    end

function edit_Colum_Callback(~, ~, ~)
function edit_Colum_CreateFcn(hObject, ~, ~)
    if ispc && isequal(get(hObject,'BackgroundColor'),
        get(0,'defaultUicontrolBackgroundColor'))
        set(hObject,'BackgroundColor','white');
    end
```

```
%%%%%%%%%%%%%%%%%%%%%%%%%%%%%%%%%%%%%%%%%%%%%%%%%%%%%%%%%%%%%%%%%%%%%%%%%%%%
%%% AIRYDISK.m - Subfile for Auswertungssoftware.m %%%%%%%%%%%%%%%%%%%%%%%%%%
%%% from Dannhauser David 2013 %%%%%%%%%%%%%%%%%%%%%%%%%%%%%%%%%%%%%%%%%%%%%
%%%%%%%%%%%%%%%%%%%%%%%%%%%%%%%%%%%%%%%%%%%%%%%%%%%%%%%%%%%%%%%%%%%%%%%%%%%%

% This is a function to generate a circular disc.
% The function preforms a FT on the Circle and then displays the airy disc.

function img = Airydisk(dim,radius,mag,pos)

% img = Airydisk(dim,radius,mag,[pos])
% Generate a circular disk signal image with dimension 'dim',
% radius in pixels, and mag specifying the gray level value. 'pos' is an
% optional argument specigying the position of the center of the circ.
% The center of the image is set to be default.

if (length(dim) == 1)   dim = [dim dim];                      end
if (nargin == 3)        pos = fliplr((dim - [1 1]) / 2);     end
% Flip is used, because we use (x,y) coordinates!

x = 0:(dim(2)-1);       y = 0:(dim(1)-1);       [X,Y]=meshgrid(x,x);
r = sqrt( (X-pos(1) ).^2 + (Y-pos(2) ).^2);     img = mag * (r<=radius);
```

```
%%%%%%%%%%%%%%%%%%%%%%%%%%%%%%%%%%%%%%%%%%%%%%%%%%%%%%%%%%%%%%%%%%%%%%%%%%%
%%% MIE_AB.m - Subfile for Auswertungssoftware.m %%%%%%%%%%%%%%%%%%%%%%%%%%
%%% from Dannhauser David 2013 %%%%%%%%%%%%%%%%%%%%%%%%%%%%%%%%%%%%%%%%%%%%
%%%%%%%%%%%%%%%%%%%%%%%%%%%%%%%%%%%%%%%%%%%%%%%%%%%%%%%%%%%%%%%%%%%%%%%%%%%

function result = Mie_ab(m, x)
% Computes a matrix of Mie coefficients, a_n, b_n, of orders n=1 to nmax,
% complex refractive index m = m' + im", and size parameter x = k0 * a,
% where k0 = wave number in the ambient medium, a = sphere radius;
% p. 100, 477 in Bohren and Huffman(1983)
% -------------------------------------------------------------------------
% File origainally from C. Mätzler, (BEWI:TDD122), June 2002
% Modified by Dannhauser David, 2013
% -------------------------------------------------------------------------

nmax = round(2+x+4*x^(1/3));
    % All infinited series can be truncated after this max value!
n = (1:nmax);
    % Array from 1 to max order of Bessel function
nu = (n+0.5);
    % Order of Bessel function!
z  = m.*x;
    % The value z can be x or m the refractive index multiplied with x
m2 = m.*m;
    % ^2 of refractive index for Mie coefficient calculation
sqx = sqrt(0.5*pi./x);
    % Relationships between Bessel and spherical Bessel functions for x
sqz = sqrt(0.5*pi./z);
    % Relationships between Bessel and spherical Bessel functions for z
bx = besselj(nu, x).*sqx;           % First kind Bessel function of x
bz = besselj(nu, z).*sqz;           % First kind Bessel function of z
yx = bessely(nu, x).*sqx;           % Second kind Bessel function of x
hx = bx + i*yx;                     % Resulting Bessel function result

b1x = [sin(x)/x, bx(1:nmax-1)];
    % Starting value plus result of first kind bessel function for x
b1z = [sin(z)/z, bz(1:nmax-1)];
    % Starting value plus result of first kind bessel function for z
y1x = [-cos(x)/x,yx(1:nmax-1)];
    % Starting value plus result of second kind bessel function for x
h1x = b1x + i*y1x;
    % First type of spherical Hankel function

ax = x.*b1x-n.*bx;                  % Constant of the Mie coefficient
az = z.*b1z-n.*bz;                  % Constant of the Mie coefficient
ahx= x.*h1x-n.*hx;                  % Constant of the Mie coefficient
    an = (m2.*bz.*ax-bx.*az)./(m2.*bz.*ahx-hx.*az);
        % Calculation of Mie coefficient - an
    bn = (bz.*ax-bx.*az)./(bz.*ahx-hx.*az);
        % Calculation of Mie coefficient - bn
result = [an; bn];                  % Return result to Mie_S12 program
```

```
%%%%%%%%%%%%%%%%%%%%%%%%%%%%%%%%%%%%%%%%%%%%%%%%%%%%%%%%%%%%%%%%%%%%%%%%%%%
%%% MIE_PT.m - Subfile for Auswertungssoftware.m %%%%%%%%%%%%%%%%%%%%%%%%%%
%%% from Dannhauser David 2013 %%%%%%%%%%%%%%%%%%%%%%%%%%%%%%%%%%%%%%%%%%%%
%%%%%%%%%%%%%%%%%%%%%%%%%%%%%%%%%%%%%%%%%%%%%%%%%%%%%%%%%%%%%%%%%%%%%%%%%%%

function result = Mie_pt(u, nmax)
% pi_n and tau_n, -1 <= u= cos? <= 1, n1 integer from 1 to nmax angular
% functions used in Mie Theory
% Bohren and Huffman (1983), p. 94 - 95
% ---------------------------------------------------------------------------
% File origainally from C. Mätzler, (BEWI:TDD122), June 2002
% Modified by Dannhauser David, 2013
% ---------------------------------------------------------------------------

p(1) = 1;                               % Starting Value!
t(1) = u;                               % Starting Value! - u = cos(Theta)
p(2) = 3*u;                             % Starting Value!
t(2) = 3*cos(2*acos(u));                % Starting Value!

for n1 = 3 : nmax,
    p1 = (2*n1-1)./(n1-1).*p(n1-1).*u;  % First part of pi
    p2 = n1./(n1-1).*p(n1-2);           % Second part of pi
  p(n1)= p1-p2;                         % Formular for pi(n)
    t1 = n1*u.*p(n1);                   % First part of tau
    t2 = (n1+1).*p(n1-1);               % Second part of tau
  t(n1)= t1-t2;                         % Formular for tau(n)
end;

result=[p;t];                           % Return result to Mie_S12 program
```

```
%%%%%%%%%%%%%%%%%%%%%%%%%%%%%%%%%%%%%%%%%%%%%%%%%%%%%%%%%%%%%%%%%%%%%%%%%%%
%%% MIE_S12.m - Subfile for Auswertungssoftware.m %%%%%%%%%%%%%%%%%%%%%%%%%
%%% from Dannhauser David 2013 %%%%%%%%%%%%%%%%%%%%%%%%%%%%%%%%%%%%%%%%%%%%
%%%%%%%%%%%%%%%%%%%%%%%%%%%%%%%%%%%%%%%%%%%%%%%%%%%%%%%%%%%%%%%%%%%%%%%%%%%

function result = Mie_S12(m, x, u)
% Computation of Mie Scattering functions S1 and S2 for complex refractive
% index m = m'+im", size parameter x = k0*a, and u = cos(scattering angle),
% where k0 = vacuum wave number, a = sphere radius;
% s. p. 111-114, Bohren and Huffman (1983)
% -------------------------------------------------------------------------
% File origainally from C. Mätzler, (BEWI:TDD122), June 2002
% Modified by Dannhauser David, 2013
% -------------------------------------------------------------------------

nmax = round(2+x+4*x.^(1/3));
    % All infinited series can be truncated after this max value!

ab = Mie_ab(m,x);
    % Compute the Mie Coefficients an, bn, cn, dn
    an  = ab(1,:);                              % Saving Coefficient an
    bn  = ab(2,:);                              % Saving Coefficient bn

pt = Mie_pt(u,nmax);
    % Calculating pi and tau = angular scat. patterns of sph. harmonics
    pin = pt(1,:);                              % Saving pi(n)
    tin = pt(2,:);                              % Saving tau(n)

    n   = (1:nmax);                % Array from 1 to max calculation value
    n2  = (2*n+1)./(n.*(n+1));     % Costant for S1 & S2 calculation!
    pin = n2.*pin;                 % Multiply pi already with constant
    tin = n2.*tin;                 % Multiply tau already with constant

S1 = (an*pin'+bn*tin');        % Calculate complex scattering amplitudes S1
S2 = (an*tin'+bn*pin');        % Calculate complex scattering amplitudes S2

 result = [S1;S2];                 % Return result to other program
```